BIOGEOCHEMICAL MECHANISMS OF ARSENIC MOBILIZATION IN HAIWEE RESERVOIR SEDIMENTS

Thesis by

Kate Campbell

In Partial Fulfillment of the Requirements for the

degree of

Doctor of Philosophy

CALIFORNIA INSTITUTE OF TECHNOLOGY

Pasadena, California

2007

(Defended December 5, 2006)

Acknowledgements

I consider myself fortunate to have the chance to work with my advisor, Janet Hering, and would especially like to thank her for her patience, mentorship, and support throughout my time at Caltech. She has always impressed me with her intelligence and fortitude, and I am excited to see her career progress at EAWAG. I have learned so much from Janet by following her example. I would also like to thank Dianne Newman for her enthusiasm and help, especially as she taught a chemist biology. Mike Hoffmann and George Rossman have both helped to broaden my research perspective, and I appreciate their effort as members of my committee.

Davin Malasarn has made much of the work presented here possible, through his dedication and patience. I have enjoyed the hours of sampling bottles in a glove box because of his humor and positive attitude. His discussions on science have been invaluable, and I think he is a remarkable scientist and author.

Rob Root and Peggy O'Day have contributed to this work by collaborating in the field and introducing me to XAS. Rob especially made the long hours at the synchrotron interesting. I would also like to thank Nelson and Virginia for their help at the beam-lines.

The time in lab has been especially rewarding because of Janet's group over the years. I would especially like to thank Richard Wildman for his enthusiasm and friendship, and Megan Ferguson for her advice and friendship in lab and on the dance floor. Thanks to other members of the Hering group: Claire Farnsworth, Arthur Fitzmaurice, Diana Stefanescu, Azra Bilgin, Suvasis Dixit, Theresa Spano, Giehyeon Lee, and my SURF

students, Cory and Deepa. Nathan Dalleska is a genius with instruments and his knowledge, combined with a good dose of humor, has made my work possible. Thanks also to Mike Vondrus for drilling hundreds of little slots for the gel probe and doing it with a smile. Keck Lab has been a great place to work because of Linda, Fran, Cecilia, and Belinda.

Kiri Wagstaff has gone the distance for me, both as a friend and as a colleague. She has listened to most of my talks at least once, been my cheering section at conferences, read my dissertation in spite of being swamped with her own work, and always been a dear friend whether life has been going well or poorly. She is an inspiration to me, and she has never doubted my potential. Lisa Cowan has been a steady and motivating friend since Day 1 at Caltech. Her endless ideas and constant encouragement have been very important to me. I would also like to thank Heather Pinckett for her wonderful advice over the last 2+ years.

My parents, Anne and Gary Campbell, have been incredibly supportive throughout this entire process, and I could not have done this without them. They have always helped me keep a good perspective, rallied round me through the tough times, and celebrated with me when things went well. Finally, Larry Barber introduced me to a whole new world that made me realize how much I love science and appreciate the importance of doing environmental research. His mentorship over the years has been invaluable, and I believe that his work ethic and enthusiasm motivate me to this day to be the best scientist that I can be.

While from the bounded levels of our mind

Short views we take, nor see the lengths behind;

But more advanced behold with strange surprise

New distant scenes of endless science rise!

~Alexander Pope

Abstract

A natural geothermal source of arsenic (As) causes elevated concentrations in the Los Angeles Aqueduct, a major drinking water source for the City of Los Angeles. The As is removed by precipitating an amorphous iron (Fe) oxyhydroxide floc in the aqueduct waters. The floc is removed via sedimentation at Haiwee Reservoir, where the Fe- and As-rich sediments provide a unique field site for studying the mechanisms of As mobilization to sediment porewater.

In this study, a gel probe equilibrium sampler was developed to measure the porewater concentrations as well as the As sorption behavior in Haiwee Reservoir sediments. The gels consisted of a polyacrylamide polymer matrix and were 92% water. Undoped gels (clear gels) were used to determine porewater composition, and gels doped with hydrous ferric oxide (HFO) were used to measure *in situ* As adsorption chemistry. Gels were placed in a plastic holder, covered with a membrane filter, and allowed to equilibrate for 24 hours with the sediment porewaters. This study combined data from the gel probe samplers, gravity cores, and laboratory studies, to elucidate the biogeochemical processes governing As partitioning between the solid and aqueous phases. The gel probe device allowed for *in situ* observation of the effect of porewater chemistry on As adsorption, a unique contribution to the techniques available for field measurements.

Arsenic was reduced from As(V) to As(III) in the upper layers of the sediment, but the change in redox state did not cause As to be mobilized into the porewaters. Arsenic mobilization occurred as the Fe(III) oxides were reductively dissolved. Both As(V) and

Fe(III) reduction were most likely microbially mediated. Arsenic sorption onto the HFO-doped gels was inhibited at intermediate depths (10-20 cm), most likely due to competitive sorption by dissolved carbonate produced from the mineralization of organic carbon. The partitioning of As onto the solid phase in this region may be primarily controlled by porewater chemistry, rather than sorption site availability. Deeper in the sediment column, the Fe was partially transformed from amorphous Fe(III) oxyhydroxide to green rust, possibly sequestering dissolved carbonate. In this region, As adsorption onto HFO-doped gels was controlled by the presence of dissolved phosphate in the porewater. The accumulation of As in the porewater in this region may be due to lack of available surface adsorption sites on the sediment. Arsenic partitioning between solid and aqueous phases depends on microbially driven diagenetic processes, as well as porewater composition.

TABLE OF CONTENTS

LIST OF FIGURES

LIST OF TABLES

NOMENCLATURE

≡	A surface group on a solid, e.g., ≡FeOH
ω_{gel}	fraction of gel that is water
As(III)	Arsenite
As(V)	Arsenate
$C_{measured}$	Concentration of analyte in re-equilibrated solution
DET	Diffusive equilibrium in thin films
DGT	Diffusive gradient in thin films
ESEM	Environmental Scanning Electron Microscopy
EXAFS	Extended X-ray absorption fine spectra
FA	Fulvic acid
$H_2CO_3^*$	Sum of species: $CO_{2(aq)} + H_2CO_3$
HA	Humic acid
HFO	Hydrous ferric oxide
ICP-MS	Inductively coupled plasma mass spectrometry
K_D	Partition coefficient
LAA	Los Angeles Aqueduct
LADWP	Los Angeles Department of Water and Power
LC-ICP-MS	Liquid chromatography ICP-MS
M	mol/L
m_{gel}	mass of hydrated polyacrylamide gel

NOM	Natural organic matter
pK_a	acid dissociation constant
TEA	Terminal electron acceptor
V_{acid}	volume of acid added in re-equilibration
XANES	X-ray near edge spectra
XAS	X-ray absorption spectroscopy
XRD	X-ray diffraction
XRF	X-ray fluorescence

Chapter 1

Introduction and Motivation

1.1 Arsenic as a world-wide health concern

One of the most challenging environmental problems today is arsenic (As)-contaminated drinking water, which currently affects millions of people world-wide. The greatest exposure to As occurs through ingestion, which can lead to acute or chronic arsenic poisoning. Chronic As exposure can result in skin lesions, melanosis (skin discoloration), keratosis, cancer, and possible reproductive effects (Bhattacharyya et al. 2003; Ng et al. 2003). An estimated 41-57 million people are potentially exposed to elevated levels of arsenic, from 10 to 10,000 μg/L, especially in the Bengal Delta (Bangladesh and West Bengal, India), Taiwan, China, and parts of South America and Southeast Asia (Nordstrom 2002; Smedley and Kinniburgh 2002). The current drinking water standard in the United States is 10 μg/L, decreased from 50 μg/L in 2002 by the US Environmental Protection Agency (EPA). However, there is a greater challenge to find acceptable treatment options in less developed regions where the affected population is primarily rural and large scale treatment is prohibitively expensive.

Although there are some anthropogenic sources of arsenic to the environment through mining, pesticide application, wood preservation, and combustion of some coal deposits, elevated concentrations of As are often derived from natural sources. Arsenic occurs naturally in alluvial and deltaic sediments, as well as volcanic rocks and thermal

springs (Welch et al. 2000; Nordstrom 2002; Smedley and Kinniburgh 2002; Ng et al. 2003), and the weathering of such deposits can lead to mobilization of As. The situation in Bangladesh is an example of As occurring naturally in alluvial sediments that is being mobilized into the groundwater. A significant rural population relies upon this groundwater for its drinking water supply and consequently exhibits extreme health effects of chronic arsenic exposure (Bhattacharyya et al. 2003).

The causes of As mobilization are complex, and not well understood. In order to identify and treat the problem of elevated As concentrations in groundwater, it is necessary to understand the specific biogeochemical controls of As mobility in subsurface environments. By understanding the processes that govern mobilization, it may be possible to predict future problems of As contamination and design effective treatment methods. A field site in California (CA) has been selected to study the processes that influence arsenic release to groundwater.

1.2 Arsenic in the Los Angeles Aqueduct System

The City of Los Angeles imports water from several different sources, including the Sierra Nevada Mountains in Northern California. Approximately 70% of drinking water in the City of Los Angeles is delivered via the Los Angeles Aqueduct (LAA). The remaining 30% comes from the Colorado River Aqueduct, the California Aqueduct, and local groundwater wells. The main tributary to the LAA is the Owens River (Fig 1.1). Natural geothermal springs in Hot Creek, California, contribute large As loads to the LAA source waters, resulting in a long-term average As concentration in the LAA of 22 µg/L (yearly

averages from 1940-1991). Although the hot springs contribute <5% of the total water flow, they contribute >60% of the total As load to the LAA. The remaining As comes from smaller sources such as alkali lake discharge. The geothermal water has elevated concentrations of strontium (Sr), barium (Ba), zinc (Zn), manganese (Mn), aluminum (Al), and germanium (Ge) in addition to As, and significant amounts of chromium (Cr), copper (Cu), lead (Pb), molybdenum (Mo), tin (Sn), titanium (Ti), and vanadium (V). The As flux from the hot springs is relatively constant throughout the year, but changes in flow from snowmelt and aqueduct operations create seasonal fluctuations of As concentrations in the LAA (Willets et al. 1967; Stolarik and Christie 1999).

Pilot tests of optimizing coagulation treatment to remove As at the LAA filtration plant (LAAFP) in Sylmar, CA, resulted in early turbidity breakthrough and filter backwash solids requiring hazardous solid waste disposal and was, therefore, an unacceptable treatment option. The LA Department of Water and Power (LADWP) developed an interim management plan to remove arsenic from the LAA at Haiwee Reservoir, which went into effect in March, 1996 (Stolarik and Christie 1999). A better site for a treatment facility might be Hot Creek, which is close to the geothermal As source and upstream of dilution by the Owens River. However, construction of a facility in this location is not feasible. As an alternative, an existing treatment plant in the Owens Valley, the Cottonwood Treatment Plant, was modified to inject ferric chloride ($FeCl_3$) as a coagulant directly into the LAA about 27 km upstream of Haiwee reservoir (Figure 1.1). Cationic polymer (diallyldimethyl ammonium chloride, DADMAC) is also added as a flocculent aid to remove glacial silts that can clog filters at the LAAFP. The polymer dose does not affect As removal. The ferric chloride forms an amorphous iron (Fe) oxyhydroxide floc in the

aqueduct channel. Dissolved arsenic readily adsorbs and/or co-precipitates with the Fe floc, and is subsequently deposited in the inlet channel to Haiwee reservoir (see Figure 1.1 in Chapter 6 for a map of the study area). The treatment results in an average As concentration of 5.1 µg/L at the South Haiwee Reservoir outlet. Since the treatment removes ~67% of the incoming As in the LAA, occasionally the water downstream of Haiwee Reservoir has >10 µg/L As because of seasonal fluctuations. However, some of the remaining As is removed at the LAAFP. Another result of this treatment is substantial deposition of iron- and arsenic-rich sediments in the Haiwee Reservoir. These sediments are a natural laboratory for an investigation of biogeochemical controls on arsenic mobilization.

1.3 Research Scope and Objectives

The objective of this work is to answer the following questions:

1. What are the mechanisms controlling the partitioning of As and Fe between the sediments and porewaters?

2. What circumstances cause mobilization of As, Fe, and other elements into porewater?

3. What processes determine the fraction of the total As and Fe in the solid phase that is mobilized into the porewater?

These questions have been addressed by investigating the conversion of Fe- and As-bearing mineral phases, porewater chemistry, and the role of microbially-mediated redox transformations of As and Fe phases.

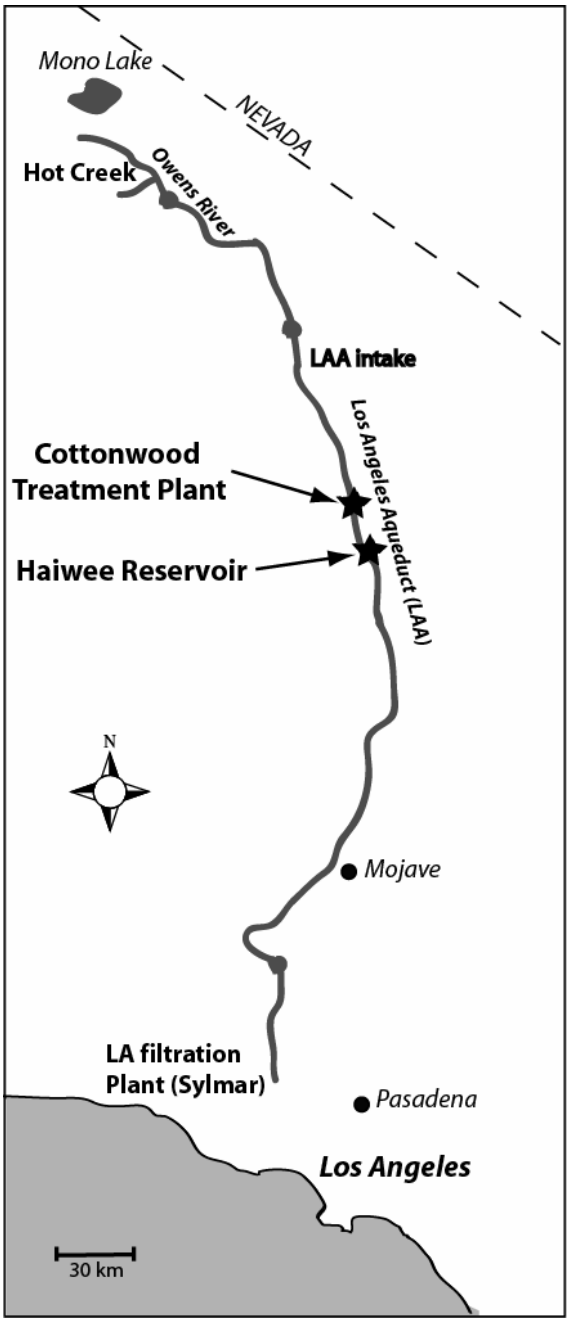

Figure 1.1. Map of the Los Angeles Aqueduct (LAA) system. Ferric chloride injections at Cottonwood Treatment plant result in Fe- and As- enriched sediment deposition at Haiwee Reservoir, the research site for this study.

1.4 Brief Overview of Chapters

A literature review and background information can be found in Chapter 2. A gel probe equilibrium sampler was developed for *in situ* measurement of porewater composition and As adsorption behavior by doping polyacrylamide gels with Fe(III) oxide. Laboratory development, gel properties, and As sorption performance in the presence and absence of competing ions are presented in Chapter 3. Chapter 3 also contains an X-ray absorption spectroscopy (XAS) calibration for quantifying As speciation on the Fe-doped gels. Gel probes were deployed at Haiwee reservoir on several dates. The results from the gel probe deployment and solid phase (core) analyses are discussed in Chapter 4. The field studies highlight how mineral transformation and porewater composition affect the accumulation of dissolved As in the sediment porewater. Microbiological studies of As(V) and Fe(III) reduction using an ambient bacterial population from Haiwee Reservoir sediments and a pure culture strain of bacteria are presented in Chapter 5. Further investigation into how the presence of adsorbed As affect bacterial Fe(III) reduction was performed by imaging the solid phase with light and electron microscopy as well as studying bacterial adhesion to surfaces (Chapter 6). Chapter 7 summarizes the information from the previous chapters and discusses the implications for Haiwee Reservoir sediment stability. Additional field and experimental data can be found in the appendices.

Chapter 2

Biogeochemical arsenic and iron cycling in freshwater sediments

2.1 Arsenic in the environment

2.1.1 Sources of Arsenic

With the relatively recent discovery that millions of people worldwide are affected by arsenic (As) contaminated drinking water, there has been a renewed interest in arsenic sources and biogeochemical processes that lead to As mobilization. Although there are both natural and anthropogenic inputs of As to the environment, elevated As concentrations in groundwater are often due to naturally-occurring As deposits. While the average abundance of As in the earth's crust is between 2 and 5 mg/kg, enrichment in igneous and sedimentary rocks, such as shale and coal deposits, is not uncommon (Cullen and Reimer 1989; Smedley and Kinniburgh 2002). Arsenic can co-occur with nickel (Ni), cobalt (Co), copper (Cu), and iron (Fe), as well as precious metals such as silver (Ag) and gold (Au), especially in sulfidic ores (Tamaki and Frankenberger 1992). Arsenic-containing pyrite (FeS) is probably the most common mineral source of As, although As is often found associated with more weathered phases (Nordstrom 2002). Mine tailings can contain substantial amounts of As, and the weathering of these deposits can liberate As into the surface- or groundwater, where numerous chemical and biological transformations can take place (Harrington et al. 1998; Cummings et al. 2000).

Arsenic can also be directly released into the aquatic environment through geothermal water, such as the hot springs in Hot Creek (Willets et al. 1967; Wilkie and Hering 1998). Anthropogenic sources of As include pesticide application, coal fly ash, smelting slag, feed additives, semiconductor chips, and As-treated wood, which can cause local water contamination.

High As concentrations in groundwater are not necessarily directly linked to geologic materials with high As content. Hering and Kneebone calculated that, in sediment with an As concentration of 1.8 mg/kg (crustal abundance), only a small fraction of the total As in the solid phase would be needed to account for a dissolved As concentration of ≥10 µg/L (Hering and Kneebone 2001). Therefore, As mobility is related not only to the amount of As in the geological source material, but also to the environmental conditions that control chemical and biological transformation of the material.

Iron-, aluminum (Al)-, and manganese (Mn)-rich minerals are an important sink for As in sediments, particularly through adsorption to mineral surfaces. Arsenic associated with Fe(III) oxide coatings on weathered alluvial sediments has been hypothesized to be the primary source of As in the Bengal delta aquifer, and release to groundwater occurs upon reductive dissolution of the Fe(III) oxide coating (Nickson et al. 1998; Nickson et al. 2000; Acharyya 2002; McArthur et al. 2004). Sedimentary biogeochemical processes are the focus of this work, with particular emphasis on Fe and As transformations.

2.1.2. Arsenic speciation

Arsenic is stable in several oxidation states (-III, 0, +III, +V), but the +III and +V states are the most common in natural systems. Arsine (-III), a compound with extremely high toxicity, can be formed under very reducing conditions, but its occurrence in nature is relatively rare. Both inorganic and organic species of As are present in the environment, although inorganic forms are typically more abundant in freshwater systems. Mobility and toxicity strongly depend on the oxidation state and structure. The inorganic species are more acutely toxic than organic species, and inorganic As(III) has a higher acute mammalian toxicity than As(V) (Ng et al. 2003). The effects of oxidation state on chronic toxicity are confounded by the redox conversion of As(III) and As(V) within human cells and tissues.

2.1.2.1 Inorganic As

Arsenite [As(III); $H_xAsO_3^{x-3}$, x=0-3] and arsenate [As(V); $H_xAsO_4^{x-3}$, x=0-3] are the two most environmentally-relevant inorganic forms of arsenic in freshwater systems. Arsenate is an anion at the pH of most natural waters ($H_2AsO_4^-$ and $HAsO_4^{2-}$), while arsenite is a neutral species (Table 2.1). The structure and chemistry of arsenate is similar to phosphate ($H_xPO_4^{x-3}$, x=0-3); this similarity has significant implications for sorption behavior and microbial metabolism. The toxicity of As(V) is due to its interference with oxidative phosphorylation in cells, by substituting for P in adenosine triphosphate (ATP) synthesis, essentially deactivating intracellular energy storage. As(III) toxicity is caused by a strong affinity for sulfhydryl groups, such as thiol groups in enzymes (NRC 1999).

As(V) is thermodynamically stable under oxic conditions, while As(III) is stable under more reducing conditions. However, As(V) and As(III) are often found to co-occur in both oxic and anoxic waters and sediments (Anderson and Bruland 1991) due to redox kinetics. For example, the oxidation of As(III) by O_2 is slow (on the order of several weeks), while bacterially-mediated redox reactions can be much faster (Cullen and Reimer 1989; Dowdle et al. 1996). The observed speciation of As in natural water depends on the local environmental conditions such as bacterial activity, sediment mineralogy, pH, and redox potential.

Table 2.1. Acidity constants for As(V) and As(III) at zero ionic strength from Nordstrom and Archer (Nordstrom and Archer 2003). The symbol "=" denotes chemical equilibrium.

Reactions	pK_a
Arsenate:	
$H_3AsO_4 = H_2AsO_4^- + H^+$	2.30
$H_2AsO_4^- = HAsO_4^{2-} + H^+$	6.99
$HAsO_4^{2-} = AsO_4^{3-} + H^+$	11.80
Arsenite:	
$H_3AsO_3 = H_2AsO_3^- + H^+$	9.17

2.1.2.2 Organic arsenic

Although there are many forms of organic As, the most common organic species are monomethylated and dimethylated As(III) and As(V). Organic As is less acutely toxic than the inorganic species, and methylation of inorganic As is one type of detoxification mechanism for some bacteria, fungi, phytoplankton, and higher level organisms such as humans. Methylation can also occur when organisms are stressed from nutrient limitation

(Cullen and Reimer 1989; Anderson and Bruland 1991; Ng et al. 2003). Organoarsenicals are typically direct metabolic products and should not be confused with inorganic As complexed with natural organic matter (NOM) (see section 2.4.2).

Both inorganic and organic As can be adsorbed onto mineral surfaces, a reaction which is strongly dependent on pH. Inorganic As adsorption will be discussed in greater depth in section 2.2.1. In adsorption studies with monomethylarsonic acid (MMAA) and dimethlyarsinic acid (DMAA), the affinity of the organoarsenic species for Fe oxides was observed to be less than that of As(V) and greater than that of As(III) below pH 7, but less than that of both inorganic forms of As above pH 7 (Xu et al. 1991; Bowell 1994). In sediment environments at circumneutral pH, organoarsenicals may be more mobile than inorganic forms.

Significant levels of organoarsenicals can be found seasonally in surface waters, but organoarsenicals generally contribute less than 10% of the total As in interstitial water except in isolated instances (Cullen and Reimer 1989; Anderson and Bruland 1991; Azcue and Nriagu 1994; NRC 1999; Newman 2000). Thus, inorganic As will be the focus of further discussion in this work.

2.2 Interactions of arsenic with iron

2.2.1 Adsorption of As onto Fe surfaces

Dissolved As concentrations can be controlled by precipitation or by sorption onto mineral phases such as Fe(III) oxyhydroxides, Fe(III) hydroxides, and Fe(III) oxides (hereafter collectively referred to as Fe(III) oxides) (Hering and Kneebone 2001).

Adsorption of As onto Fe oxides has been observed to be an important environmental process and is prevalent in many different sediment environments, including Haiwee Reservoir (Root et al. 2006).

2.2.1.1 Structure of HFO

Fe(III) oxides are ubiquitous in nature, and are often the result of aerobic weathering of magmatic rocks. Fe(III) is very insoluble at circumneutral pH and can precipitate as a number of different Fe(III) oxide minerals. Fe(III) oxides can form coatings on other mineral grains, making them chemically important substrates in the environment, even if they are not the dominant mineral by weight (Dzombak and Morel 1990). Amorphous Fe oxyhydroxide, also known as hydrous ferric oxide (HFO) or ferrihydrite, has the highest solubility of the Fe(III) oxides, and is often the first mineral type to precipitate upon hydrolysis of Fe(III) (Zachara et al. 2002). HFO has a very poorly ordered crystal structure with high surface area and is an excellent sorbent for a wide range of chemical species. Because of its amorphous structure and large water content, a molecular formula has not been established, and is often approximated by $Fe(OH)_3$, FeOOH, Fe_2O_3, or empirical formulae such as $Fe_5O_{12}H_9$ (Eggleton and Fitzpatrick 1988; Dzombak and Morel 1990; Cornell and Schwertmann 1996; Janney et al. 2000; Zachara et al. 2002). Depending on precipitation conditions, the degree of order can vary in both synthetic and natural HFO. Surface area measurements can be made by nitrogen gas adsorption (BET analysis), but it is often hard to reproduce the results due to the porous nature of HFO. A value of 600 m^2/g is accepted as an appropriate estimate of HFO surface area (Dzombak and Morel 1990). During precipitation, HFO initially forms spherical precipitates ranging from 30 to 100 Å in diameter, but will form larger

aggregates on the order of several microns within minutes to hours of precipitation (Eggleton and Fitzpatrick 1988; Cornell and Schwertmann 1996). Because of the disordered structure and large water content, HFO resembles a gel rather than a homogeneous solid phase (Dzombak and Morel 1990).

In general, HFO will tend to recrystallize into more thermodynamically stable Fe(III) oxides, such as hematite (Fe_2O_3), goethite (α-FeOOH), and lepidocrocite (γ-FeOOH) (Cornell and Schwertmann 1996; Zachara et al. 2002). HFO will primarily transform into goethite, although mixtures of several minerals can also form. Goethite formation requires local dissolution of the HFO followed by nucleation and re-crystallization. This process occurs over a period of weeks to months in the laboratory in the absence of adsorbing ions (Raven et al. 1998). Transformation to hematite is also possible through dehydration and rearrangement of the crystal structure and does not require the local dissolution of the HFO. The rates of transformation to goethite and/or hematite increase with increasing pH and temperature (Cornell and Schwertmann 1996; Makris et al. 2005), although hematite is preferentially formed at pH 7-8 and higher temperatures, while goethite is formed at higher pH values and lower temperatures (Baltpurvins et al. 1996). The presence of sorbed ions on the HFO surface also affects the rate of transformation. Numerous studies have found that nitrate, chloride, sulfate, silicate, phosphate, Al, titanium (Ti), Mn, organic matter, and various trace elements such as Cu, Ni, cadmium (Cd), vanadium (V), Co, zinc (Zn) and As retard the conversion of HFO (Waychunas et al. 1993; Baltpurvins et al. 1996; Cornell and Schwertmann 1996; Ford et al. 1997; Ford 2002; Makris et al. 2005). Adsorbed ions can stabilize natural ferrihydrite in soil environments by inhibiting internal reordering or dissolution.

Waychunas et al. observed that as the concentration of As(V) on the surface increased, the disorder of the HFO also increased (Waychunas et al. 1993). Adsorbed compounds such as organic carbon may also change the relative amounts of the transformation products (Cornell and Schwertmann 1996). The presence of Fe(II) can affect the transformation products substantially, and will be discussed in section 2.2.3.3.

As HFO transforms into more thermodynamically stable phases, it can either incorporate trace elements into the crystal structure or release them into the porewater as the surface area decreases during recrystallization (Ford et al. 1997). When Ford co-precipitated As(V) with HFO, As(V) was eventually incorporated into the hematite structure but not into goethite (Ford 2002). In natural sediments, As may be more permanently sequestered if it is incorporated into a mineral structure. However, if As is not incorporated, a decrease in available surface sites might release As into the porewaters. The fate of As also depends on the relative surface binding strengths of As onto the transformation products. Dixit and Hering found that the intrinsic surface complexation constant for As(V) on goethite was stronger than the corresponding constant for As(V) on HFO, implying that transformation to goethite will not necessarily release As(V), unless the total number of surface sites is substantially decreased (Dixit and Hering 2003).

2.2.1.2 As(V) and As(III) adsorption onto HFO

Sorption reactions at equilibrium satisfy a mass law equation, similar to aqueous equilibrium reactions. For surface reactions, the equilibrium constant is a product of an intrinsic term, corresponding to the chemical free energy of binding, and a coulombic term, which describes the effect of electrostatic charge at the surface.

Surface sites exhibit acid-base chemistry. Positive, negative, and neutral surface groups can be present depending on extent of protonation, and can be described by equations (2.1) and (2.2), where the symbol "≡" denotes a surface site and "=" signifies chemical equilibrium (Dzombak and Morel 1990).

$$\equiv FeOH = \equiv FeO^- + H^+ \quad (2.1)$$

$$\equiv FeOH_2^+ = \equiv FeOH + H^+ \quad (2.2)$$

Adsorption of As(V) and As(III) occurs via ligand exchange reactions with hydroxyl surface groups, also known as inner sphere complexation (Dzombak and Morel 1990). Neither the adsorption of As(III) nor As(V) is strongly affected by changes in ionic strength, which is indicative of inner sphere complexation (Pierce and Moore 1982; Hsia et al. 1994; Jain et al. 1999; Goldberg and Johnston 2001). Further evidence of specific adsorption has been obtained by spectroscopic data and is discussed in section 2.2.1.3.

Adsorbed As species are weak acids and can affect the surface charge due to proton exchange reactions. Whether As adsorbs as a mononuclear or binuclear complex has implications for the level of protonation of the surface species, illustrated in equations (2.3) and (2.4) with adsorbed As(III) species as an example. Binuclear complexes have fewer acidic protons due to the binding with the Fe oxide surface.

$$\equiv FeOH + H_3AsO_3 = \equiv FeH_xAsO_3^{x-2} + H_2O + (2-x)H^+ \quad \text{where } x=0\text{-}2 \quad (2.3)$$

$$(\equiv FeOH)_2 + H_3AsO_3 = (\equiv Fe)_2H_yAsO_3^{y-1} + 2H_2O + (1-y)H^+ \quad \text{where } y=0,1 \quad (2.4)$$

Adsorption isotherms (adsorbed As vs. dissolved As) and envelopes (adsorbed As vs. pH) have shown that As(V) and As(III) adsorption onto HFO depends strongly on pH and As concentration. Arsenate adsorption decreases with increasing pH, particularly above pH 7-8, and maximum sorption occurs at low pH values (pH 3-7) (Pierce and Moore 1982; Raven et al. 1998; Goldberg 2002; Dixit and Hering 2003). Arsenite has a broad maximum adsorption at circumneutral pH, and decreasing sorption at high and low pH values (Pierce and Moore 1982; Dixit and Hering 2003). Arsenite is often considered to be more mobile than As(V), but this generalization is not always true; the relative affinity for HFO depends strongly on pH as well as the presence of other adsorbed ions (Dixit and Hering 2003).

The initial rate of As adsorption is fast (~90% within 2 hours) onto pre-formed HFO, followed by a period of slower uptake (>100 hours) (Pierce and Moore 1982; Fuller et al. 1993; Raven et al. 1998). Fuller et al. accurately modeled this observation with As(V) diffusion into a sphere, with a subset of adsorption sites located in the interior requiring longer diffusion times than exterior surface sites (Fuller et al. 1993). Physically, this spherical model could correspond to an aggregate of HFO particles with surface sites in the interior requiring molecular diffusion of As into the aggregate. After aging the HFO for 6 days before As adsorption, the total amount of adsorbed As decreased by 20%, but the rates were unchanged (Fuller et al. 1993). Co-precipitated As(V) and HFO had significantly higher As adsorption initially but the As slowly desorbed as aggregation and aging occurred. The co-precipitated As(V) and HFO approached a steady-state concentration similar to As(V) adsorbed onto pre-synthesized HFO after >400 hours, indicating that the rate of As adorption/desorption onto HFO may

be diffusion controlled (Fuller et al. 1993). As(III) may have slightly faster adsorption kinetics, although this appears to be highly dependent on experimental conditions (Raven et al. 1998).

2.2.1.3 Molecular structure of adsorbed As onto Fe(III) oxide surfaces

X-ray absorption spectroscopy (XAS) is a synchrotron-based technique for probing element-specific local bonding structures and oxidation states. For a thorough reference on XAS, see the review by Brown et al. (Brown et al. 1988). An absorption edge is a sharp increase in absorption of X-rays that occurs over a narrow range of energy, which is due to excitation of an electron from a deep core state, such as a K-shell electron. The energy at which this excitation occurs depends on the element and its oxidation state. The spectrum near the absorption edge is called X-ray Absorption Near Edge Structure (XANES). The pre-edge region can contain features related to weak electronic transitions. At energies above the absorption edge, low-frequency oscillations due to weak backscattering with nearby atoms are observed. This region of the spectrum is referred to as Extended X-ray Absorption Fine Structure (EXAFS) (Figure 2.1). XANES edges can be used to determine oxidation state of the target element in certain cases because of differences in electronic shielding. Arsenite and arsenate have distinct edges at 11,871 eV and 11,875 eV, respectively, and these regions of the spectrum can be effectively used to determine As oxidation state in solid phases such as sediments. The EXAFS region can be used to identify local bonding structure, such as bond distances, coordination number, and the identity of nearest neighbor atoms. The EXAFS spectrum is extracted from the total spectrum and weighted to enhance the oscillations at higher energy. A Fourier transform is performed to de-convolute the signals from different

backscattering atoms. Bond distances and elemental information can be extracted from the Fourier transformed signal.

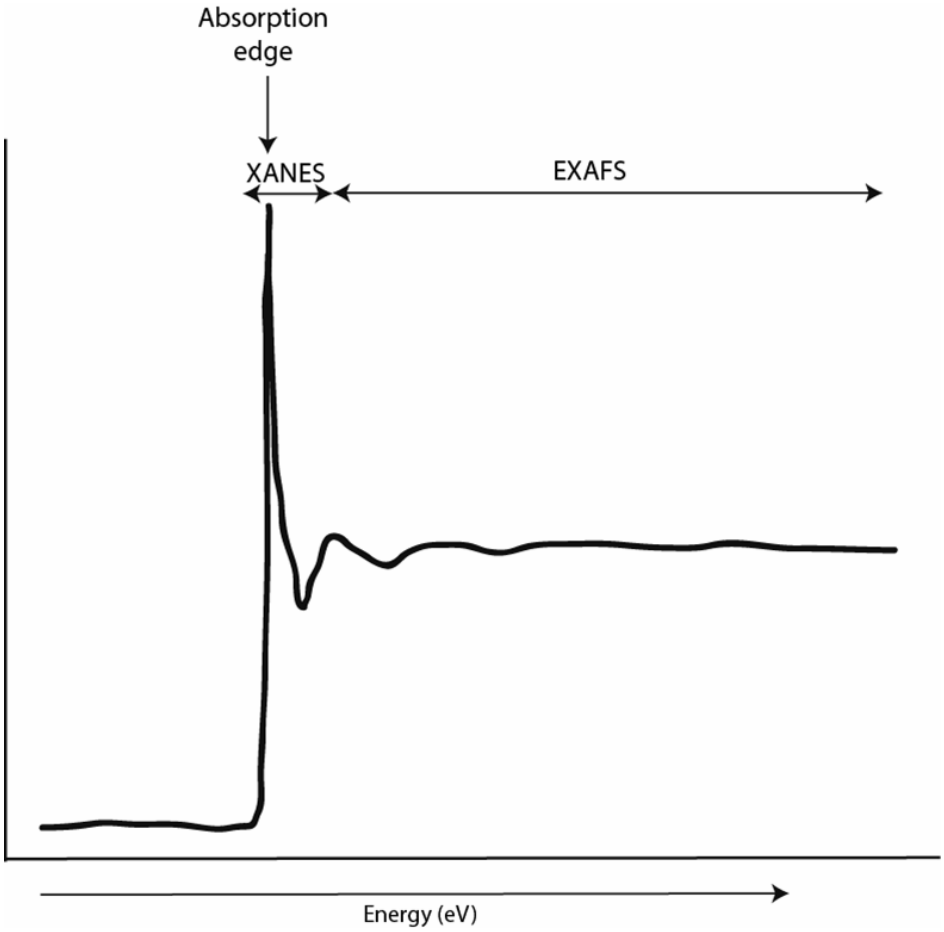

Figure 2.1. Schematic diagram of a normalized XAS spectrum, depicting the absorption edge and the XANES and EXAFS regions. The y-axis has arbitrary units for a normalized spectrum.

Many spectroscopic studies have been performed on As(III) and As(V) adsorbed onto HFO, and all confirm that inner sphere complexation is dominant. Local bonding environments of As(III) and As(V) have been determined by analyzing EXAFS spectra.

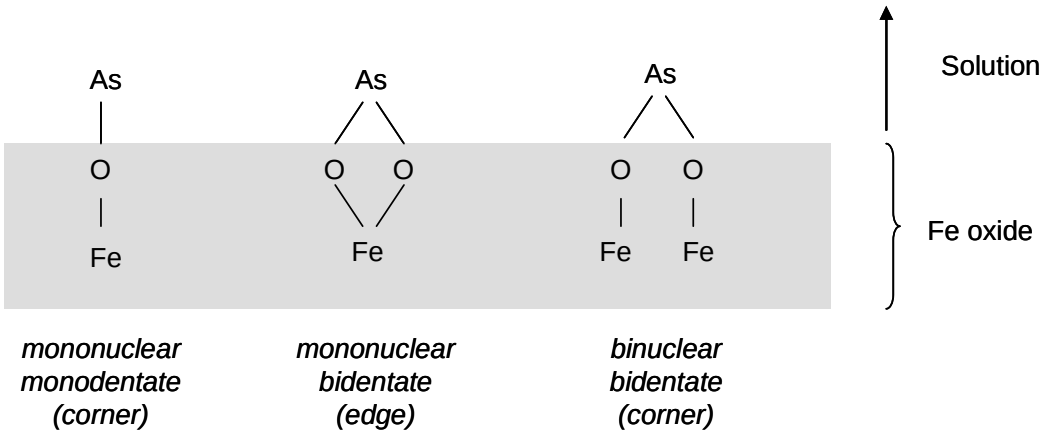

Figure 2.2. Schematic diagram of configurations of As adsorbed onto an Fe oxide surface. Adapted from Cornell and Schwertmann (Cornell and Schwertmann 1996).

There are several possible molecular configurations of As adsorption: mononuclear monodentate, mononuclear bidentate (edge-shared), and binuclear bidentate (corner-shared) (Figure 2.2, 2.3). EXAFS studies have shown that As(V) is primarily adsorbed as binuclear bidentate complexes, with average As-Fe bond lengths between 3.26 Å and 3.3 Å (Waychunas et al. 1993; Sherman and Randall 2003). Waychunas and co-workers proposed a monodentate mononuclear complex that became increasingly abundant as As surface coverage decreased (Waychunas et al. 1993). However, this surface species has been challenged on the basis of thermodynamic instability and crystal growth poisoning effects (Manceau 1995; Sherman and Randall 2003). A mononuclear bidentate complex has been hypothesized by Manceau (Manceau 1995), but this structure has also been questioned due to calculated thermodynamic instability (Waychunas et al. 1995; Sherman and Randall 2003). Arsenite is adsorbed predominantly as binuclear bidentate complexes with an average As-Fe bond length of 3.3 Å, although there is evidence for less-important mononuclear bidentate complexes (Manning et al. 1998;

Ona-Nguema et al. 2005). No mononuclear monodentate complex has been observed for As(III). Binuclear bonding for both As(III) and As(V) has been supported by FTIR studies (Sun and Doner 1996).

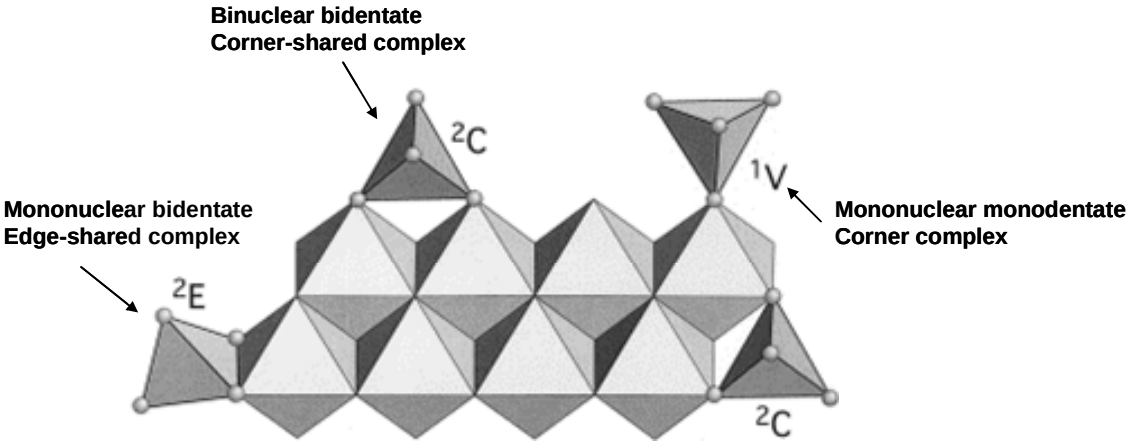

Figure 2.3. Diagram of molecular configurations of As adsorbed onto an Fe oxide surface showing a mononuclear bidentate edge complex (^{2}E), a binuclear bidentate corner complex (^{2}C), and a mononuclear monodentate corner complex (^{1}V). Figure from Sherman and Randall, 2003. Reprinted with permission from Elsevier.

2.2.1.4 Competitive effects on As adsorption

The presence of other adsorbing ions can significantly impact the adsorption of As onto HFO. Arsenic adsorption can be affected by electrostatic, steric, or competitive effects. Phosphate has the greatest effect on sorption of As, due to similarities in molecular structure and surface complexation chemistry. Phosphate competes directly with As for surface sites and effectively inhibits both As(III) and As(V) sorption (Liu et al. 2001; Dixit and Hering 2003) (Figure 2.4). Phosphate sorption is more pH dependent than As(V) sorption, and As(V) may be slightly more strongly adsorbed than

phosphate (Jain and Loeppert 2000; Hongshao and Stanforth 2001; Liu et al. 2001; Violante and Pigna 2002; Antelo et al. 2005). The order of sorbate addition affects the extent of sorption, particularly in the case of phosphate and As. The sorbate added first will adsorb to a greater extent than the competing sorbate (Hongshao and Stanforth 2001; Liu et al. 2001). Phosphate effects of As sorption will be discussed in more detail in Chapter 3.

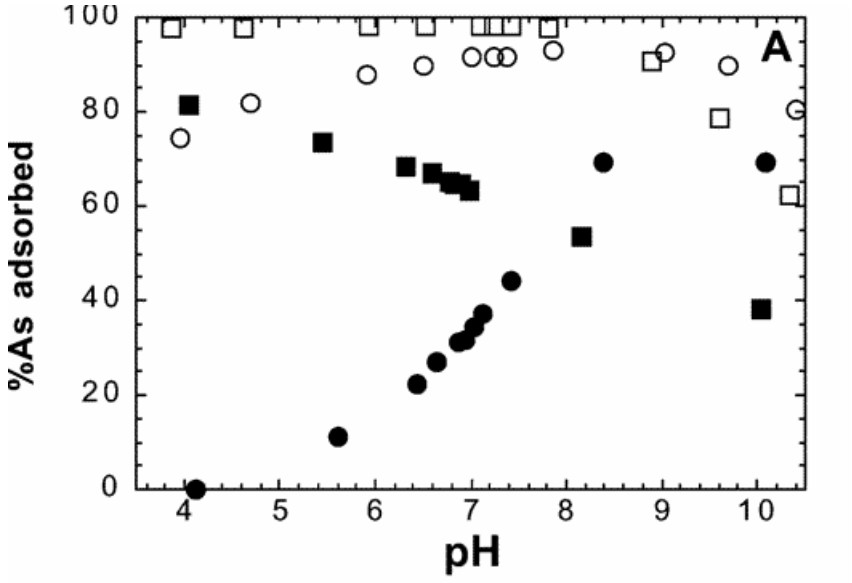

Figure 2.4. As(III) (circles) and As(V) (squares) adsorption envelopes on HFO (0.03 g/L) in the presence of 100 µM phosphate (shaded symbols) and absence of phosphate (open symbols). The total As concentration was 10 µM. Reprinted with permission from Dixit and Hering, 2003. Copyright 2003 American Chemical Society.

Sulfate (H_2SO_4) appears to adsorb to different HFO surface sites than As, and may not directly compete for surface sites in the same way as phosphate (Jain and Loeppert 2000). Sulfate has a very slight affect on As(V) adsorption, but can decrease

As(III) adsorption below pH 7.5 (Wilkie and Hering 1996; Jain and Loeppert 2000; Meng et al. 2000).

The adsorption edge of silicate (H_4SiO_4) is qualitatively similar to that of As(III), with broad maximum adsorption between pH 8-10 (Swedlund and Webster 1999). Silicate decreases As(III) and As(V) adsorption, with a greater effect on As(III) at high silicate concentrations and at pH>8. Silicate forms a polymer on the surface of HFO at high concentrations, resulting in large Si:Fe ratios (>0.1) (Swedlund and Webster 1999; Holm 2002). This surface polymer may inhibit As sorption through steric and/or electrostatic effects. In an experiment by Meng et al., Ca^{2+} or Mg^{2+} counteracted the effect of silicate on As sorption, indicating that a change in surface potential may be at least partially responsible for the inhibition of As adsorption by silicate (Meng et al. 2000). In another study by Wilkie and Hering, Ca^{2+} increased As(V) adsorption onto HFO, most likely due to electrostatic effects (Wilkie and Hering 1996). High concentrations of silicate can also form colloidal Si-Fe(III) polymers that can increase the Fe(III) mobility at high pH (Meng et al. 2000), but the relevance of this effect in natural systems in probably minimal.

The concentrations of carbonate (dissolved CO_2 as H_2CO_3 and its acid dissociation products) in groundwater can be elevated due to microbial respiration and carbonate mineral dissolution. The effect of carbonate concentrations due to atmospheric equilibration (~0.07 mM) on As adsorption is minimal (Fuller et al. 1993; Meng et al. 2000; Arai et al. 2004; Radu et al. 2005). However, higher concentrations (10% $CO_{2(g)}$ = 22 mM dissolved inorganic C) suppressed As(V) adsorption and caused significant amounts of As(III) to desorb in column studies with As(III) pre-equilibrated onto

goethite-coated sand (Radu et al. 2005). High concentrations of carbonate affected As(III) sorption more than As(V) (Radu et al. 2005), even though As(V) was hypothesized to be more affected based on surface charge effects (Appelo et al. 2002). Leaching of As from solids by the addition of bicarbonate salts was found to be dependent on both pH and carbonate concentration, with greatest leaching at high carbonate concentrations and at very low or very high pH values (Kim et al. 2000; Anawar et al. 2004). When directly compared to phosphate, carbonate was a much weaker inhibitor of As adsorption (Radu et al. 2005), although it may still be important in groundwater with high carbonate concentrations. Carbonate forms only a very weak complex with As(III) in solution, and As sorption inhibition is likely due to surface effects (Neuberger and Helz 2005).

Carbonate adsorption onto Fe(III) oxide surfaces is most likely a combination of inner and outer sphere complexes (van Geen et al. 1994, Su and Suarez 1997, Villalobos and Leckie 2000, Villalobos and Leckie 2001, Bargar et al. 2005). Arsenic adsorption inhibition is probably due to electrostatic effects from specifically adsorbed carbonate. Carbonate adsorption is highly dependent on pH with maximum sorption on goethite at pH 6 (van Geen et al. 1994). Bicarbonate (HCO_3^-) appears to have a greater affinity for surface complexation than $H_2CO_3^*$ or CO_3^{2-}. Ternary complexation with adsorbed carbonate may also be possible and can affect surface electrostatics (e.g., Na-CO_3-Fe oxide) (Villalobos and Leckie 2001).

Organic carbon may also affect surface complexation of As, and will be discussed in section 2.4.2.

2.2.2 As mineral phases

The partitioning of As between dissolved and solid phases can be controlled by As mineral precipitation as well as adsorption. Arsenite forms insoluble precipitates with sulfide, such as orpiment (As_2S_3), realgar (AsS), and arsenopyrite (FeAsS) in reducing environments (Cullen and Reimer 1989; Nordstrom and Archer 2003); precipitation can be microbially mediated (Newman et al. 1997; Nordstrom and Archer 2003). However, Haiwee Reservoir is non-sulfidogenic, and As-S-Fe mineral formation is unlikely. Scorodite ($FeAsO_4 \cdot 2H_2O$) precipitates only in very acidic environments such as acid mine drainage (Langmuir et al. 2006). Jia et al. observed a ferric arsenate precipitate that formed on the surface of HFO at low pH (pH 3-4), but sorption dominated the As-Fe association at circumneutral pH (Jia et al. 2006). Thus, sorption processes are dominant at Haiwee Reservoir.

2.2.3 Reductive Dissolution of Fe phases

There are four general pathways for Fe(III) dissolution: proton-assisted (acid), ligand-promoted acid, reductive, and ligand-promoted reductive dissolution (Afonso et al. 1990). Ligands such as oxalate can promote the dissolution (either reductive or non-reductive) of Fe(III) oxides. However, reductive dissolution is the most important pathway in the natural environment (Cornell and Schwertmann 1996). Reductive dissolution is driven by the reduction of Fe(III) in the solid phase to the more soluble Fe(II). The dissolution of the solid Fe(III) oxide can potentially release adsorbed trace elements into the porewaters. Reductive dissolution has been observed to release As into aquifers in Bangladesh (Nickson et al. 1998; Nickson et al. 2000; Acharyya 2002; Bose

and Sharma 2002; Swartz et al. 2004) and the United States (Peterson and Carpenter 1986; Welch and Lico 1998; Cummings et al. 2000; Welch et al. 2000; Kneebone et al. 2002), as well as into lake sediment porewaters in New Zealand (Aggett and O'Brien 1985) and Switzerland (Azcue and Nriagu 1994). The co-incident increase in dissolved As and Fe concentrations is a strong indicator that reductive dissolution of Fe(III) phases is a likely mechanism of As mobilization. Arsenic mobilization is controlled by the ability of Fe(III) oxides in the subsurface to re-adsorb As as reductive dissolution proceeds (Welch et al. 2000; Swartz et al. 2004; Pedersen et al. 2006) and by the presence of competing ions.

There are both abiotic and biotic pathways for the reductive dissolution of Fe(III). Lovely and co-workers compared the reduction of HFO by three strains of bacteria (a sediment isolate GS-15, *Clostridium pasteurianum*, and *Escherichia coli*) to chemical reduction by a number of different organic compounds, some of which are likely to be found in a natural sedimentary environment. Microbial reduction was faster and more extensive than chemical reduction at neutral pH, suggesting that microorganisms are primarily responsible for Fe(III) reduction in non-sulfidogenic sediments (Lovely et al. 1991). Roden noted that chemical reduction rates vary by three orders of magnitude while bacterial rates are more constant even between different strains, and extrapolation of laboratory chemical rates of compounds such as ascorbate to environmental conditions should be done with caution (Roden 2003). However, it is useful to compare the differences in mechanisms between chemical and biological reductive dissolution, noting that both pathways could be important under a variety of environmental conditions.

2.2.3.1 Chemical Mechanisms

Chemical reductants include H_2S and various organic compounds, such as ascorbate and humic acids (Hering and Stumm 1990; Schwertmann 1991; Rochette et al. 2000; Thamdrup 2000). Reductive dissolution is thought to occur through a series of reaction steps: adsorption of the reductant, electron transfer to the Fe(III), and release of Fe(II) from the lattice (usually the rate-limiting step). Fe(II) is more readily released from the crystal lattice because the binding energy is less for Fe(II) than Fe(III). In addition, surface protonation near the sorption site of the reductant can accelerate dissolution (Suter et al. 1991). Organic compounds that are not involved in electron transfer can either accelerate or inhibit reduction. If sorption of the organic compound polarizes the Fe bonds making the Fe(II) bond easier to break, reduction will occur at a faster rate. On the other hand, large organic compounds on the Fe(III) oxide surface may sterically hinder adsorption of the reductant, thus decreasing the reduction rate (Schwertmann 1991). The reaction pathway can be additionally complicated by catalysis of the dissolution and subsequent mineralogical transformations of the parent Fe(III) phase by Fe(II) (Zinder et al. 1986; Schwertmann 1991; Suter et al. 1991; Benner et al. 2002; Hansel et al. 2005; Pedersen et al. 2005; Pedersen et al. 2006). The effect of Fe(II) on secondary mineral formation will be discussed in more detail in section 2.2.3.3. Photoreduction has been observed for Fe(III) oxides, but is unlikely to be important in Haiwee Reservoir sediments, where iron reduction does not occur at the surface of the sediment.

Adsorbed oxyanions, such as As(V), have been shown to inhibit the reductive dissolution in laboratory studies with ascorbic acid as a reductant and in ligand-promoted

dissolution. This could be due to a decrease in surface protonation and/or reductant sorption because of steric or electrostatic effects at the oxide surface (Bondietti et al. 1993; Biber et al. 1994; Kraemer et al. 1998; Eick et al. 1999; Pedersen et al. 2006).

2.2.3.2 Biological Mechanisms

Bacterial Fe(III) reduction can be carried out by a genetically and metabolically diverse group of microorganisms. Bacteria can generally utilize many electron acceptors, usually coupled to organic carbon or H_2 oxidation. The sequence of electron acceptors follows decreasing pε: O_2, nitrate, Mn oxides, Fe(III) oxides, sulfate, and methane (fermentation) (Stumm and Morgan 1996). Fe(III) reduction may be responsible for a significant fraction of total organic carbon mineralization in sediments (Thamdrup 2000).

The mechanism of enzymatic reduction is not well known. Some organisms require direct contact with an Fe(III) oxide surface, while others may synthesize electron shuttle compounds or use naturally-occurring humic acids to transfer electrons between the cell and the Fe(III) oxide surface (Thamdrup 2000). Some cells may produce reactive oxygen species such as superoxide to mediate Fe(III) dissolution (Fujii et al. 2006). Natural Fe(III) chelators may also accelerate microbial Fe reduction without requiring direct cellular contact with the solid phase (Jones et al. 2000; Royer et al. 2002). Rates of bacterial Fe(III) reduction are highest with a poorly crystalline Fe(III) phase, and decrease with increasing crystallinity (Roden and Zachara 1996), confirming the observation that amorphous Fe(III) oxides are the most bioavailable.

2.2.3.3 Secondary mineral transformation

Fe(II) adsorption onto Fe(III) oxides is unique in that electron transfer into the Fe(III) oxide results in migration of the electron (and effectively the Fe(II)) into the bulk

mineral. This migration was observed by Mössbauer spectroscopy and isotopic exchange experiments (Williams and Scherer 2004; Pedersen et al. 2005). Fe(II) can destabilize the bulk mineral, allowing mineral transformations to take place more readily.

In the presence of Fe(II), HFO can transform to numerous other Fe(III) oxides such as goethite (α-FeOOH), lepidocrocite (γ-FeOOH), and hematite (Fe_2O_3), as well as other Fe(II) or mixed Fe(II)-Fe(III) minerals such as magnetite (Fe_3O_4), siderite ($FeCO_3$), vivianite ($Fe_3(PO_4)_2 \cdot 8H_2O$), and green rusts. The rate of transformation increases with increasing Fe(II) concentrations (Hansel et al. 2005; Pedersen et al. 2006). At low Fe(II) concentrations, goethite and lepidocrocite formation is catalyzed by increased local dissolution of the Fe(III) oxide because of Fe(II) destabilization of the Fe(III) oxide surface. Magnetite formation is more favorable at higher Fe(II) concentrations, and proceeds through solid state conversion or surface nucleation. At high rates of Fe(II) production, siderite can form if there is an adequate concentration of carbonate and vivianite with high concentrations of phosphate (Figure 2.5).

The mineralization process is complicated by the presence of anions, such as chloride, sulfate or carbonate (Figure 2.5). Phosphate, silicate, carbonate, Ni, Co, and Ca can favor the formation of green rusts and vivianite. While there are several forms of green rust, formation of carbonate green rust ($[Fe^{II}_4Fe^{III}_2(OH)_{12}]^{2+} \cdot [CO_3, nH_2O]$) is more favorable than the sulfate analogue (Ona-Nguema et al. 2004). The structure has layers of Fe(II) and Fe(III) octahedra, with water and anions such as carbonate intercalated in the interlayers. Green rusts have been observed as a microbially-induced biomineralization product of HFO in laboratory incubations (Fredrickson et al. 1998). Just as HFO is metastable with respect to the formation of goethite and hematite, green

rusts are metastable with respect to magnetite and siderite. Green rusts are formed in an early stage of biomineralization. Phosphate, As(V), silicate and Co stabilize green rusts by preventing re-crystallization into goethite, siderite, and magnetite (Zachara et al. 2002; Bocher et al. 2004).

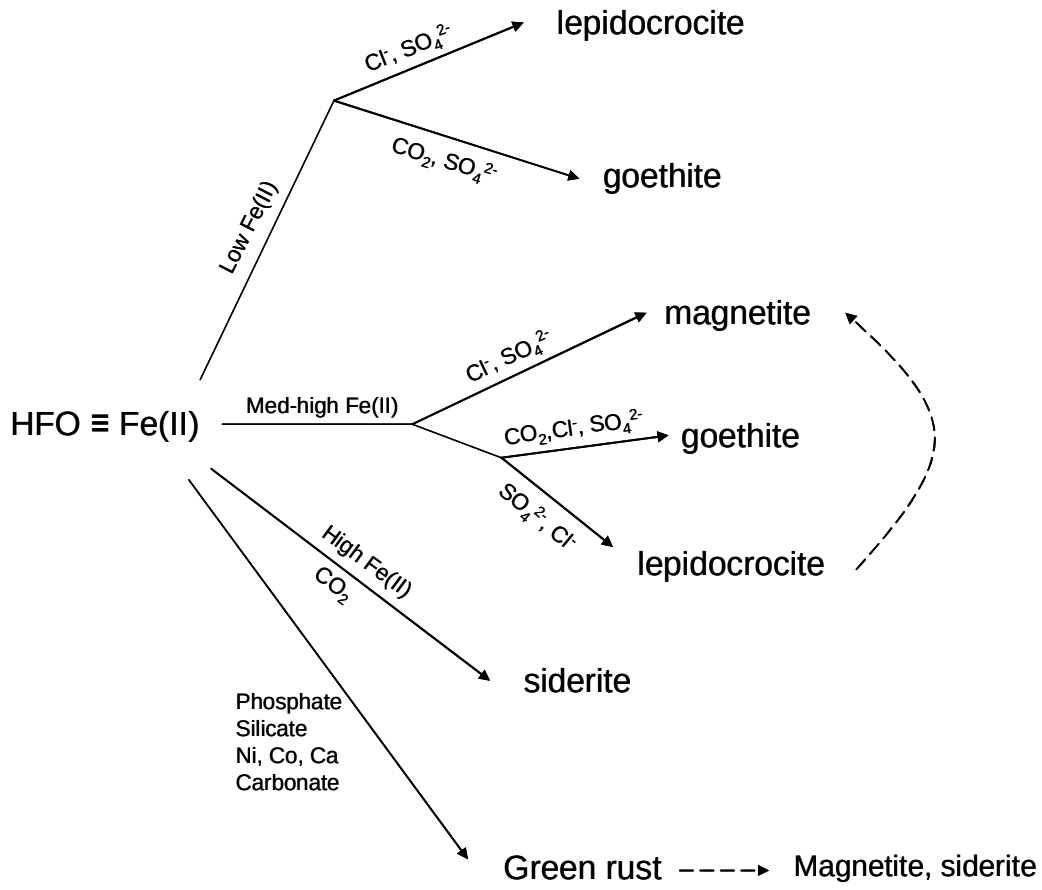

Figure 2.5. Secondary mineral transformations of HFO due to adsorbed Fe(II). Adapted from references: (Fredrickson et al. 1998; Benner et al. 2002; Zachara et al. 2002; Hansel et al. 2003; Hansel et al. 2005; Pedersen et al. 2005; Pedersen et al. 2006). The dashed lines indicate further mineral transformation that can occur spontaneously.

While Fe(II) can be produced by microbial processes, the role of bacteria in secondary mineral transformation is unclear. Many of the same secondary minerals are observed when Fe(II) is added abiotically. However, larger particles are formed in the abiotic Fe(II) reactions compared to biogenically produced Fe(II) transformation products (Hansel et al. 2003). In addition, complete conversion of Fe(III) in Fe(III) oxides to Fe(II) is rarely observed in biological experiments. Secondary mineral precipitation and Fe(II) adsorption may make the Fe(III) oxide less bioavailable for reduction (Urrutia et al. 1999; Hansel et al. 2004; Royer et al. 2004). While mineral transformation is primarily an abiotic reaction involving Fe(II), the rate and extent of Fe(II) production can be biologically controlled.

2.2.3.4 Implications for As mobility

Reductive Fe(III) oxide dissolution is controlled by a complex interplay of many different parameters, such as pH, redox state, mineralogy, biological activity, and solution chemistry. Biologically-mediated reduction depends strongly on the bacterial consortia present in the sediments, as well as substrate availability (e.g., organic carbon) and Fe oxide crystallinity. The rate of dissolution can, in turn, affect the mineral transformation products, which have the potential to sequester As in more crystalline lattice structures or release As to the porewaters as surface binding sites are lost.

2.3 Redox cycling of arsenic

2.3.1 Redox cycling of As by microbes

Bacteria may be one of the most important agents in As cycling in sediments. Both As(V) reduction and As(III) oxidation can be microbially mediated, and have been observed in the environment (Ahmann et al. 1997; Oremland et al. 2002).

The chemical similarity between As(V) and phosphate has important consequences for the biological cycling of arsenic. Bacteria have uptake systems to transport phosphate inside the cell. When there is an ample supply of phosphate, bacteria use the inorganic phosphate transport (Pit) uptake system, which is non-specific and allows As(V) inside the cell. When phosphate levels are low, the more phosphate specific transport (Pst) uptake system is used, which is less likely to transport As(V) inside the cell (Tamaki and Frankenberger 1992). Once As(V) has entered the cell, As(V) reduction can proceed via two different metabolic pathways: respiration and detoxification.

2.3.1.1 Respiratory As(V) reduction

Respiratory As(V) reduction couples the reduction of As(V) to the oxidation of a compound such as organic carbon, a process which conserves energy for the cell and allows for cell growth (Laverman et al. 1995; Newman et al. 1998). Bacteria capable of respiratory As(V) reduction have been isolated from many sediment and aquifer environments and represent a very genetically diverse group of organisms. Thus far, no obligate dissimilatory As(V) reducing bacteria have been found and all isolates are able to utilize other electron acceptors (Oremland and Stolz 2003). Unless the As concentrations are extremely high, such as in Mono Lake (17 mg/L), the contribution of

respiratory As(V) reduction is probably negligible with respect to the total mineralization of organic carbon (Oremland et al. 2000; Thamdrup 2000). However, this process can be significant for As redox transformations in sediment. The main pathway for dissimilatory As(V) reduction is the *arrA* pathway, named for the periplasmic ArrA reductase, and is well conserved among a diverse group of organisms (Saltikov and Newman 2003; Malasarn et al. 2004). Further discussion on respiratory As(V) reduction can be found in Chapter 5.

2.3.1.2 As(V) reduction for detoxification

Arsenic toxicity to bacteria cells has been mitigated by the evolution of several detoxification pathways. As mentioned in section 2.1.2.2, some bacteria methylate As to reduce its toxicity. Another pathway is As(V) reduction, which allows As(III) to be actively pumped out of the cell. This pathway, known as *arsC* for the cytoplasmic ArsC reductase, involves an As(III)-specific transporter that requires the consumption of ATP (Cervantes et al. 1994; Rosen 1996). Bacteria can have both the respiratory *arrA* and the *arsC* pathways. In *Shewanella* species strain ANA-3, the *arrA* pathway is activated at a much lower As(V) concentration than the *arsC* detoxification pathway (Saltikov et al. 2003; Saltikov et al. 2005). The rates of As(V) reduction via the detoxification pathway are less than the respiratory pathway, but As(V) reduction for detoxification may still be an environmentally relevant process under certain environmental conditions (Jones et al. 2000; Macur et al. 2004).

2.3.1.3 As(III) oxidation

As(III) oxidation can also be bacterially mediated (Oremland et al. 2002; Oremland and Stolz 2003). Macur et al. observed that microbial As(III) oxidation and

As(V) reduction can co-occur in unsaturated sediments under the same environmental conditions (Macur et al. 2004). In addition, bacterial As(III) oxidation has been shown to catalyze the oxidation of geothermal As(III) in Hot Creek (Wilkie and Hering 1998).

2.3.2 Abiotic As redox chemistry

Oxygen can oxidize As(III), although the kinetics of this reaction are slow except at high pH (>10) (Manning and Goldberg 1997; Swedlund and Webster 1999). Manganese oxides can quickly oxidize adsorbed As(III), and this has been shown to be an active pathway for several synthetic manganese oxides (manganite and birnessite) (Scott and Morgan 1995; Chiu and Hering 2000; Manning et al. 2002) and in natural sediments and clays (Manning and Goldberg 1997; Amirbahman et al. 2006). Green rust may also catalyze As(III) oxidation, although the importance of this reaction in biogenically formed green rust in sediment is unclear (Su and Puls 2004; Su and Wilkin 2005). As(V) reduction by green rust has not been observed (Randall et al. 2001; Ruby et al. 2006). In addition, natural organic carbon can either oxidize As(III) or reduce As(V), and will be discussed in section 2.4.2.

2.4 Effect of organic carbon on arsenic cycling

2.4.1 Source of organic carbon

Sedimentary organic matter is derived from decaying phytoplankton and other plant or animal material. As proteins, lipids, and other components decay, compounds such as melanins, humic acids, and fulvic acids are formed and are commonly found in

natural sediments (Stumm and Morgan 1996). Natural organic matter (NOM) is a mixture of many types of functional groups, including phenols, fatty acids, carbohydrates, sugars, and amino acids. NOM can also contain significant amounts of inorganic impurities, such as Fe, Mn, and Al. The organic carbon pool is a substrate for a range of microbial processes, including but not limited to As(V) and Fe(III) reduction.

2.4.2 Effect on As chemistry

There is some evidence that NOM has redox properties, and can catalyze the reduction of As(V) or the oxidation of As(III), particularly in the presence of a mineral surface such as hematite (Redman et al. 2002; Ko et al. 2004; Bauer and Blodau 2006). However, the redox activity of NOM is highly variable; Bauer et al. found that NOM extracted from peat promoted As(V) reduction, while NOM extracted from wetland sediment catalyzed As(III) oxidation (Bauer and Blodau 2006). It is, therefore, difficult to generalize the effect of organic matter on As redox chemistry, although it may be important in some sediment systems.

Organic carbon has been shown to promote As mobilization in laboratory studies, either due to sorption effects or aqueous complexation (Redman et al. 2002; Bauer and Blodau 2006). Humic and fulvic acids are capable of inhibiting As(III) and As(V) adsorption to Fe(III) oxide surfaces due to steric and/or electrostatic effects (Xu et al. 1991; Grafe et al. 2001; Grafe et al. 2002; Redman et al. 2002; Ko et al. 2004). Natural organic matter can adsorb onto Fe oxide surfaces through functional groups such as carboxylic acids, phenols, and amines or as outer-sphere complexes (Kaiser et al. 1997; Grafe et al. 2002; Buschmann et al. 2006). Organic carbon has also been shown to

complex As in solution, although the mechanism is most likely through inorganic impurities such as Fe(III) and Mn(III,IV). Fe(III) stabilized in NOM (dissolved Fe(III) or colloidal Fe(III) oxide particles) can form bridging complexes with As, for the same reasons that As adsorbs to the surface of Fe(III) minerals (Ko et al. 2004; Lin et al. 2004; Ritter et al. 2006). As(V) tends to form stronger complexes than As(III) on a variety of Fe(III)-containing organic substrates (Thanabalasingam and Pickering 1986; Warwick et al. 2005; Buschmann et al. 2006). Phosphate competes with As for NOM complexation, supporting the Fe(III) bridging mechanism (Thanabalasingam and Pickering 1986).

2.5 Early diagenesis in sediments

Sediment diagenetic processes are the biogenic and abiotic changes that occur to alter the sediment during and after deposition (Stumm and Morgan 1996). Diagenesis is driven primarily by the mineralization of organic carbon and the subsequent changes in redox potential with depth. As the sediments become more reducing, the redox equilibrium of various chemical species in the sediment shifts. However, it is important to recognize that the kinetics of these reactions are variable and sensitive to environmental parameters such as microbial activity (Hering and Kneebone 2001). Thus, it is common to observe As(III) and As(V) or Fe(III) and Fe(II) co-occurring under a variety of redox conditions due to kinetic factors.

Sediment diagenesis involves chemical, physical, and biological processes, including 1) deposition, 2) diffusion, 3) reductive dissolution (and other redox changes) and 4) secondary mineral precipitation. At Haiwee Reservoir, fresh, oxidized Fe- and

As- rich floc is deposited on the sediment surface. Organic matter is also deposited through the floc and by settling phytoplankton and plant matter. Organic matter deposition is seasonal, as primary productivity varies with nutrient input and temperature. In addition, sediment compaction decreases porosity with depth, possibly affecting molecular diffusion.

Oxygen is the most favorable electron acceptor, and the diffusion of O_2 into the sediments from the overlying water is balanced by microbial consumption. In many freshwater sediments, the transition from oxic or suboxic to anoxic can occur within a depth interval of millimeters to centimeters (Song and Muller 1999). In suboxic zones, Mn oxides and nitrate are reduced, releasing Mn(II) and nitrite or N_2. Reductive dissolution of Fe oxides and sulfate reduction occur in the more reducing anoxic zones, as discussed in section 2.2.3. Deeper in the sediment column, methane fermentation may occur under very reducing conditions. Trace elements, such as As, may also undergo redox transformations during this process, such as As(V) reduction, as discussed in section 2.3.

As the reductive dissolution of Fe(III) oxides releases Fe(II) and trace elements into the porewater, several chemical processes are possible. Dissolved organic carbon may form aqueous Fe and/or As complexes, or inhibit sorption onto mineral surfaces. Competitively sorbing compounds such as phosphate can be released from the dissolving solid phase or from mineralization of organic matter and affect the partitioning of As on the solid phase. Fe(II) may catalyze the formation of secondary minerals such as green rust, magnetite, and goethite, which can either sequester or mobilize As.

Dissolved Fe(II) and As are subject to molecular diffusion. If Fe(II) diffuses into the suboxic zone, it could be re-precipitated by reaction with O_2 or Mn oxides, resulting in fresh surface sites for As to be re-adsorbed.

The processes governing As mobilization and sequestration are a complex combination of biological, chemical, and physical parameters. The As- and Fe-rich sediment deposited at Haiwee reservoir provides a unique setting to study the biogenic and chemical diagenetic processes that control As partitioning between the solid and dissolved phases in the environment.

Chapter 3

A Gel Probe Equilibrium Sampler for Measuring Arsenic Porewater Profiles and Sorption Gradients in Sediments: Laboratory Development

3.1 Abstract

A gel probe equilibrium sampler has been developed to study arsenic (As) geochemistry and sorption behavior in sediment porewater. The gels consist of a hydrated polyacrylamide polymer, which has a 92% water content. Two types of gels were used in this study. Undoped (clear) gels were used to measure concentrations of As and other elements in sediment porewater. The polyacrylamide gel was also doped with hydrous ferric oxide (HFO), an amorphous iron (Fe) oxyhydroxide. When deployed in the field, HFO-doped gels introduce a fresh sorbent into the subsurface thus allowing assessment of *in situ* sorption. In this study, clear and HFO-doped gels were tested under laboratory conditions to constrain the gel behavior prior to field deployment. Both types of gels were allowed to equilibrate with solutions of varying composition and re-equilibrated in acid for analysis. Clear gels accurately measured solution concentrations, and As was completely recovered from HFO-doped gels. Arsenic speciation was determined in clear gels through chromatographic separation of the re-equilibrated solution. The relative amount of As(III) and As(V) adsorbed on HFO embedded in gel

was measured using X-ray absorption spectroscopy (XAS) based on calibration standards of known mixtures of HFO doped with As(III) and As(V); spectra were fit with a least-squares linear combination of As(III) and As(V) end-members. Sorption densities for As(III) and As(V) on HFO embedded in gel were obtained from sorption isotherms at pH 7.1. When As and phosphate were simultaneously equilibrated with HFO-doped gels, phosphate inhibited As sorption by up to 85% and had a stronger inhibitory effect on As(V) than As(III). Natural organic matter can also decrease As adsorption by up to 50%, but does not preferentially inhibit As(V) or As(III). The laboratory results provide a basis for interpreting results obtained by deploying the gel probe in the field and elucidating the mechanisms controlling As partitioning between solid and dissolved phases in the environment.

3.2 Introduction

Trace element concentrations in sediment porewaters are strongly affected by solid-solution interactions, especially associations with iron (Fe), aluminum (Al), and manganese (Mn) oxides (Smedley and Kinniburgh 2002). Sequestration and mobilization of trace elements depends on a complex interaction of mineralogy, sorption, precipitation, porewater composition, organic matter interactions, redox conditions, and microbially-controlled processes. One element of particular concern, because of its toxicity and prevalence, is arsenic (As), which affects drinking water quality around the world (Nordstrom 2002; Smedley and Kinniburgh 2002). Understanding the range of

geochemical conditions that contribute to the presence of As in porewaters may help predict and mitigate As contamination.

Arsenic is often found to be associated with Fe mineral phases through adsorption to mineral surfaces (Nickson et al. 2000; Smedley and Kinniburgh 2002). When Fe(III) (oxyhydr)oxides are reductively dissolved, As can be released to sediment porewaters. Since reductive dissolution of Fe (oxyhydr)oxides occurs in anoxic environments, collecting and processing sediment samples can be difficult. The ability to measure porewater composition and specific geochemical processes such as adsorption *in situ* circumvents many of these problems.

This study builds upon the concept of an *in situ* gel probe equilibrium sampler for measuring porewater composition first developed by Davison and co-workers. In previous studies, probes were constructed based on diffusive equilibration in a thin film (DET) to measure porewater concentrations of elements and compounds such as Fe, Mn, chloride, nitrate, sulfate, and ammonium in sediments where convection is limited (Davison et al. 1991; Davison et al. 1994; Krom et al. 1994). A thin sheet of polyacrylamide or agarose gel was placed into a plastic holder, covered with a permeable membrane, and allowed to equilibrate with sediment porewaters. The water inside the gel equilibrated with porewaters by solute diffusion through the membrane. Upon removal from the sediment, the gel was either chemically fixed or quickly sliced to preserve concentration gradients of target elements.

Gel probes have several advantages over other techniques for measuring porewater composition. Dialysis devices, also known as peepers, can require several weeks to reach equilibrium, while thin gels (several millimeters thick) equilibrate within

hours. Extracting porewaters from sediment cores requires substantial sample processing and has lower vertical resolution than gel probes, which can measure vertical gradients with several millimeters resolution (Davison et al. 1991).

The DET method was extended to trace metals by either using more sensitive detection techniques or incorporating a resin with a large capacity for binding metals as a preconcentration step, known as diffusive gradients in thin films (DGT) (Zhang and Davison 1995; Zhang et al. 1995; Zhang et al. 1998; Kneebone 2000; Docekalova et al. 2002). Porewater concentrations of certain trace metals can be calculated from DGT probes by measuring the flux onto resin embedded in the gel. An alternate approach for measuring concentrations of sulfide in marine sediments was to dope a polymer with lead acetate and measure the amount of insoluble lead sulfide formed in the gel (Reeburgh and Ericson 1982). Modifications of the gel probe design have been made for other applications. The extent of Mn oxide dissolution in sediments was observed by doping agarose gel with amorphous MnO_2 and measuring the extent of clearing after deployment as solid Mn(IV) was reduced to soluble Mn(II) (Edenborn 2002; Edenborn and Brickett 2002). A novel method of hazardous waste treatment was created by embedding uranium-reducing bacteria into a gel probe (Tucker et al. 1998).

In this study, the gel probe was adapted to study As sorption behavior by incorporating with two types of gels in a single probe device. One type of gel is a clear polyacrylamide gel, similar to the gels used in DET probes. The second type of gel is polyacrylamide doped with hydrous ferric oxide (HFO), an amorphous iron oxyhydroxide. The HFO-doped gels were designed to measure the amount of As adsorbed upon equilibration with sediment porewaters. Both types of gels were precut

into slabs and seated into slots etched into a plastic ladder-like holder; this constrained gel probe configuration eliminates the necessity of chemical fixing or cutting in the field, but limits resolution based on the separation and width of the gel slabs. The gel probe has two parallel columns of gels, allowing for simultaneous measurement of porewater concentrations (clear gels) and sorption profiles (HFO-doped gels) as a function of depth in sediments (for field results and probe design details, see Chapter 4).

The purpose of this study was to develop and validate a method for measuring As porewater and adsorption profiles using a constrained gel probe equilibrium sampler. Chapter 3 presents laboratory validation of the clear and HFO-doped gels, establishing a baseline for behavior in simplified chemical systems. Chapter 4 demonstrates field application in a series of deployments at Haiwee Reservoir (Olancha, CA), a field site with Fe- and As-rich sediments where elevated As concentrations have been observed in sediment porewaters.

3.3 Materials and Methods

3.3.1 Reagents

All chemicals used were reagent grade and used without further purification unless otherwise noted. All water used was 18 MΩ-cm deionized water (Elix/Milli-Q, Millipore). Solutions were stored in plastic containers that had been acid-washed in 2-5% hydrochloric acid. Experiments were performed in trace metal-free plastic tubes. All nitric acid solutions were made with trace metal grade HNO_3 (EM Science, Omnipure, 70%). As(V) stock solutions were made from Na_2HAsO_4 (Sigma). As(III) stock

solutions were made from $NaAsO_2$ (Baker), and used before any oxidation could occur (<2 weeks).

3.3.2 HFO synthesis

HFO was prepared by the drop-wise addition of 0.5 M NaOH to 150 mL of 0.05 M $Fe(NO_3)_3$ until the solution stabilized at pH 8 (Schwertmann and Cornell 1991). The suspension was equilibrated for 4 h under constant stirring, adjusting any pH drift as necessary with 0.5 M NaOH. The HFO was then washed three times with water. The solid was resuspended in 150 mL water to yield a 4.5 g/L stock solution. The crystallinity of a concentrated hydrated HFO slurry was analyzed by X-ray diffraction (XRD) on a Phillips X'Pert PRO with a Cu-Kα X-ray source. HFO stock solutions were used within 10 days to minimize changes in crystallinity (Ford et al. 1997; Raven et al. 1998).

3.3.3 Gel Casting

Gel slabs were made by modifying the methods of Tanaka (Tanaka 1981), Davison, et al. (Davison et al. 1994; Krom et al. 1994), and Kneebone et al. (Kneebone 2000; Kneebone et al. 2002). Gels were made by dissolving 3.75 g acrylamide (C_3H_5NO, Omnipure, EM Science) and 0.075 g N-N'-methylene-bis-acrylamide ($(CH_2CHCONH)_2CH_2$, Omnipure, EM Science) in 25 mL water for clear gels or HFO stock diluted with water for HFO-doped gels. In experiments where the amount of HFO in the gels was held constant at 2×10^{-6} mol Fe/gel slab, 7.5 mL of HFO stock was diluted with 12.5 mL water. In experiments with variable amounts of HFO per gel, the

amount of HFO stock solution was adjusted accordingly, and water was added to a total volume of 25 mL. The acrylamide solution was deoxygenated by bubbling with compressed nitrogen or argon for 30-45 minutes. Polymerization was initiated by the simultaneous addition of 150 µL of 1 g/L sodium persulfate (EM Science, Omnipure) and 25 µL of tetramethylethylenediamine (TEMED, Omnipure, EM Science). The solution was mixed and quickly poured into a heated, acid-washed, glass Petri dish to increase the polymerization rate. The gel was allowed to completely solidify (~5 min) before removing the dish from the heat. After the gel cooled to room temperature, it was gently extracted from the Petri dish with a flexible plastic spatula and transferred directly into a container with 1-2 L of water. The gel was hydrated for ≥12 hours and increased in size by approximately 30% when fully hydrated (Tanaka 1981). The gel was cut into slabs 2 cm × 0.5 cm × 0.2 cm by aligning the gel over a template and cutting it with a plastic, acid-washed blade. The gel slabs were placed into water and gently shaken to remove any excess reagents or loose HFO. Gel slabs were stored in water for up to one week to prevent dehydration.

3.3.4 Gel re-equilibration

Once a gel slab was equilibrated with a solution, target analytes were measured by re-equilibrating the gel slab in 1.25 mL of 1% nitric acid (clear gels) or 1.25 mL of 5% nitric acid (HFO gels) for at least 12 hours. At these acid concentrations, the polyacrylamide gel was unaffected, and the HFO dissolved completely out of the gel slabs. Re-equilibrated gel solutions were analyzed for total As (As(III) + As(V)) and phosphorous (P) by inductively coupled plasma mass spectrometry (ICP-MS, HP 4500).

Iron was measured by the phenanthroline colorimetric method with hydroxylamine (Standard Methods 1995). For HFO gels, analyte concentrations were normalized to the measured amount of Fe per gel slab (mol analyte/mol Fe). For the clear gels, the original concentration was calculated from the concentration in the re-equilibrated solution by the equation:

$$C = \frac{C_{measured}\left(m_{gel}\omega_{gel} + V_{acid}\right)}{m_{gel}\omega_{gel}} \qquad (3.1)$$

where $C_{measured}$ is the concentration in the re-equilibration solution, m_{gel} is the mass of the gel, ω_{gel} is the fraction of the gel mass that is water, and V_{acid} is the volume of acid added for re-equilibration (Kneebone 2000).

3.3.5 Arsenic speciation

Arsenic speciation was measured in the experiments described below by separating As(III) and As(V) on a liquid chromatography (LC) column (Agilent AS-11 column) with a 3 mM phosphate mobile phase at 0.9 mL/min flow rate. Arsenic was measured directly by ICP-MS in series with the LC outflow. This method will be referred to as LC-ICP-MS. For As speciation in the clear gels, the gels were re-equilibrated in 25 mM H_3PO_4 and analyzed within 24 hours to prevent oxidation of As(III).

Arsenic speciation was measured on the HFO gels using X-ray absorption near edge spectroscopy (XANES) by utilizing the K-edges of As(III) (11871 eV) and As(V) (11875 eV). In order to quantify the relative amount of As(III) and As(V) adsorbed onto the HFO gels, a series of gel slabs was equilibrated with appropriate solutions to obtain varying ratios of adsorbed As(III) and As(V). The gel slabs for the XANES calibration

contained 3.3 times more Fe than typical HFO gels since 25 mL of HFO stock solution was used without dilution in the gel casting step. Each gel slab was equilibrated for 24 hours with 20 mL of an As(III) and As(V) solution adjusted to pH 7 in 25mM HEPES buffer (Omnipure, EM Science). The amount of As(III) and As(V) adsorbed onto the gel slab after equilibration was determined by removing the gel slab and measuring the total As concentration (ICP-MS) and speciation (LC-ICP-MS) in the remaining solution. The gel slabs were immediately frozen upon removal from the solution, and remained frozen until loaded into an acid-washed Teflon holder and secured with Kapton tape. The mounted gel slabs were then refrozen in liquid nitrogen until loaded into a cryostat maintained at 4 K.

Arsenic K-edge spectra were collected at the Stanford Synchrotron Radiation Laboratory (SSRL) (Menlo Park, CA) on wiggler beamline 11-2 at a beam energy of 80-100 mA, using a 30-element Ge detector and a Si(220) monochromator crystal. Energy was calibrated using an As foil where the energy of first inflection of the absorption was set to 11867 eV, and a sodium arsenate reference (Sigma) was analyzed to verify calibration with maximum As(V) absorption at 11875 eV. Scans were averaged and background subtracted using the SIXPACK software package. Background subtraction was done with a linear fit through the pre-edge region and extrapolation into the EXAFS region. Spectra were normalized using the height of the edge step just above the absorption maximum. Normalized XANES spectra were fit to a binary reference set by linear combination using the program DATFIT with a least-squares linear combination. Fits were calibrated and verified to be linear by fitting end-member and known mixtures of As(III) and As(V) with DATFIT.

3.3.6 Laboratory Experiments

The following experiments were performed in 25 mM HEPES buffer (Omnipure, EM Science) and 5 mM $NaNO_3$ (Fisher). The pH was adjusted with 0.5 M NaOH or 0.2 M HNO_3. One gel slab was directly added to 20 mL of solution and allowed to equilibrate for 24 hours unless otherwise noted.

3.3.6.1 Recovery Experiments

To verify the accuracy of the concentration obtained from re-equilibrated clear gel slabs, a gel slab was added to a buffered solution (pH 8) with As(III) concentrations comparable to field values (0-35 µM As). The original solution concentration was calculated from the re-equilibrated solution using equation (1) and compared to the actual solution concentration. A similar experiment was performed for the HFO-doped gels with an HFO loading of 2×10^{-6} mol Fe/slab. The recovery of As(III) adsorbed onto the HFO-doped gel at pH 8 was determined by comparing the amount of As lost from solution after equilibration with the HFO gel and the amount of As released from the gel slab after re-equilibration in acid.

3.3.6.2 Iron loading in HFO-doped gels

The optimal amount of Fe loading per gel slab was determined by varying the amount of Fe from 1×10^{-6} to 8×10^{-6} mol Fe/slab. Each gel slab was added to 20 mL of 10 µM As(III) at pH 8 and allowed to equilibrate for 24 h. The amount of As adsorbed onto HFO in the gel was measured by re-equilibration in acid. The amount of Fe in subsequent experiments was 2×10^{-6} mol Fe/slab unless otherwise noted.

3.3.6.3 MINEQL modeling

The amount of As adsorbed on the HFO embedded into a gel was modeled using the surface complexation model, MINEQL+ (Schecher and McAvoy 1998). The diffuse double layer model was used to account for surface electrostatics. The specific surface area for HFO was assumed to be 600 m^2/g (Dzombak and Morel 1990), and the surface site density for HFO in the gels was determined from the sorption isotherms. Only ferrihydrite was allowed to precipitate in the model. The ionic strength was set to 0.01 M. Intrinsic surface complexation constants from the Dzomback and Morel database were used in the model (Dzombak and Morel 1990). Activity coefficients were calculated using the Davies equation correction for ionic strength.

3.3.6.4 Adsorption Time Series

The rate of As adsorption onto HFO gels was measured by adding an HFO-doped gel slab to a 10 µM As(III) solution at pH 8. Aliquots of solution were removed at each time point, acidified in nitric acid, and analyzed for As by ICP-MS. The effect of phosphate on the rate of As adsorption was measured under similar conditions with the addition of 50 µM phosphate (EM Science). Arsenic and P were analyzed at each time point by ICP-MS.

3.3.6.5 Adsorption Isotherms

Arsenic adsorption onto HFO-doped gels as a function of As concentration was measured for As(III) and As(V) at pH 7.1. Arsenic concentrations were varied from 0 to 200 µM. An additional isotherm was done for As(III) at pH 8.

3.3.6.6 Competitive effects of phosphate on As adsorption

The effects of phosphate on As(III) and As(V) adsorption onto HFO embedded in a gel were investigated by holding the As concentration constant and varying the phosphate concentration between 0 and 500 µM. One HFO-doped gel slab was equilibrated in a buffered solution at pH 7.1 at a given As and P concentration. Ten µM As was added as either all As(III), all As(V), or a 1:1 mixture of As(III) and As(V). After equilibration, each gel slab was removed from the solution, re-equilibration in acid, and analyzed for As and P. Phosphate concentrations were sufficiently large to require correction for the dissolved P in the HFO-doped gels. The amount of dissolved P was calculated using equation (1), and subtracted from the total P measurement, the difference being the amount of P adsorbed to the HFO surface.

3.3.6.7 Competitive effects of organic matter on As adsorption

The effect of organic matter on As adsorption onto HFO gels was investigated in solutions of As(III) or As(V) at pH 7.1. Two types of natural organic compounds were used: Soil humic acid (Soil HA, IHSS #1S102H) and Suwannee River natural organic matter (SR-NOM, IHSS #1N101). The As concentration was held constant at 10 µM and the organic carbon concentration was varied from 0 to 500 ppm.

3.4 Results and Discussion

3.4.1 Properties of clear and HFO-doped gels

The polyacrylamide gels are composed of 92% water (ω_{gel} = 0.92) and the mass of each gel (m_{gel}) is equal to 0.286 g. The gel was not affected by nitric acid, even at

concentrations greater than 35%. The XRD of HFO was consistent with an amorphous iron oxyhydroxide, and the solid was readily dissolved in 5% nitric acid.

For both clear and HFO-doped gels, As recovery was >95% (Figure 3.1 A, B). The variation in Fe concentration in HFO-doped gel slabs was less than 10%. The amount of As adsorbed was found to vary between 20% and 80% as the amount of Fe per gel slab was varied between 1×10^{-6} to 8×10^{-6} mol Fe/slab (Figure 3.2). All loadings of HFO were sufficient to ensure that the amount of adsorbed As to the HFO in the gel is in excess of the dissolved As in the solution phase in the gel, and that the contribution of dissolved As can be neglected in the HFO-doped gels. Since high Fe loadings have a greater probability of perturbing a natural sediment system and may require extended equilibration times, an intermediate Fe loading of 2×10^{-6} mol Fe/slab was used in laboratory experiments and in field deployments (Chapter 4).

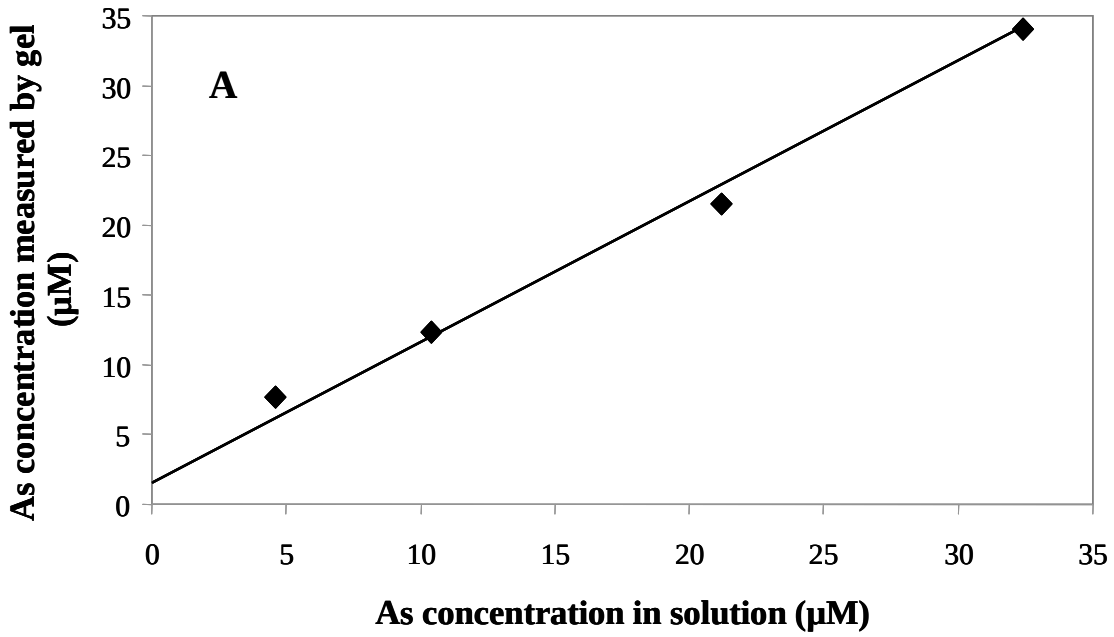

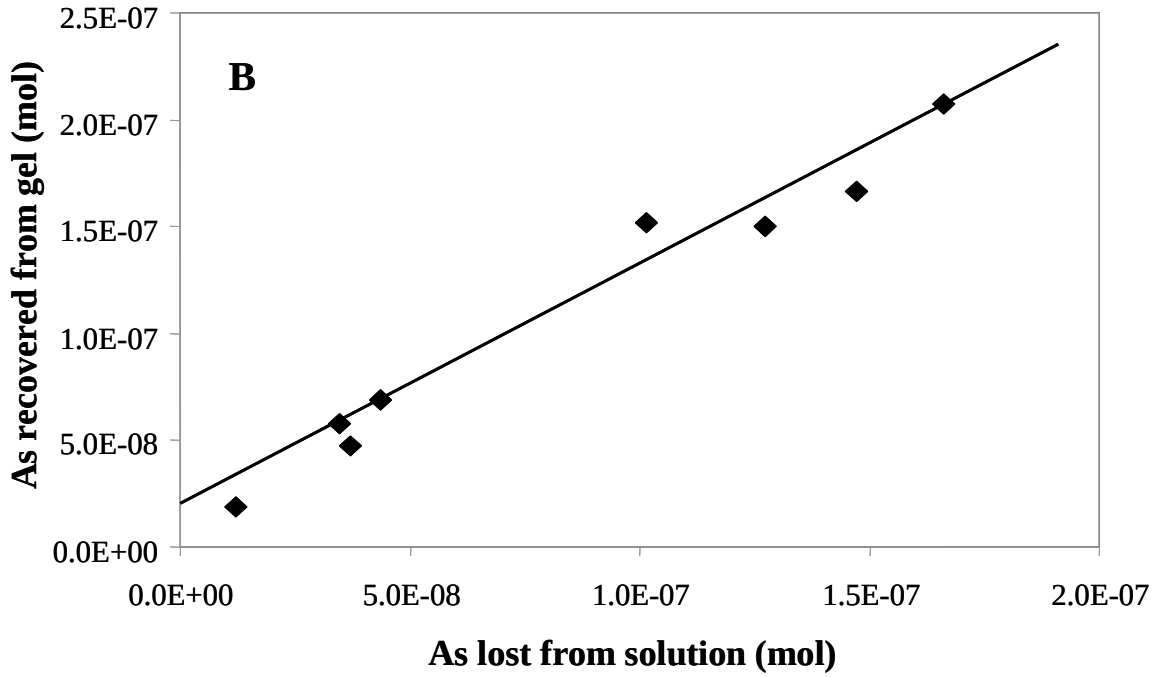

Figure 3.1. Arsenic recovery from clear (A) and HFO-doped gels (B). One gel was equilibrated in a solution of known As concentration. Gels were equilibrated for 24 hours before re-equilibration in acid, and analysis by ICP-MS.

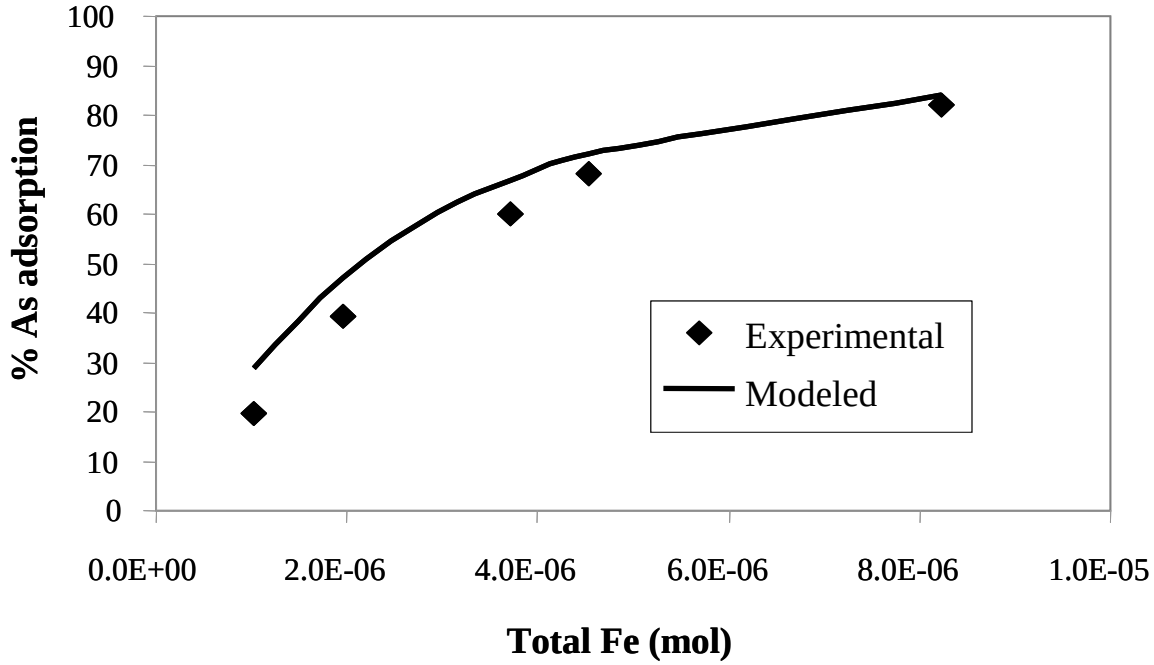

Figure 3.2. Amount of adsorbed As as a function of Fe per gel slab. MINEQL+ was used to simulate As sorption.

3.4.2 Gel equilibrium kinetics

A previous study found that clear gels reached equilibrium within 1-2 hours when directly in contact with the solution (i.e., not in a probe) but equilibration time increased to 5-7 h when placed in a probe (Kneebone 2000). This is comparable to other studies for similar types of gels (Davison et al. 1994; Docekalova et al. 2002). Sorption equilibrium with As(III) on an HFO-doped gel was reached in approximately 18 hours. The presence of phosphate did not alter the sorption kinetics, although the maximum amount of As adsorbed decreased by approximately 18% (Figure 3.3). Equilibration in both HFO and clear gels is controlled by diffusion. HFO-doped gels can take up to 10 times longer to equilibrate than clear gels, since the HFO concentrates As in the gel. The kinetics of adsorption onto HFO embedded in gel is consistent with other HFO sorption experiments without gel where equilibration can take up to 24 hours (Pierce and Moore 1982; Fuller et al. 1993).

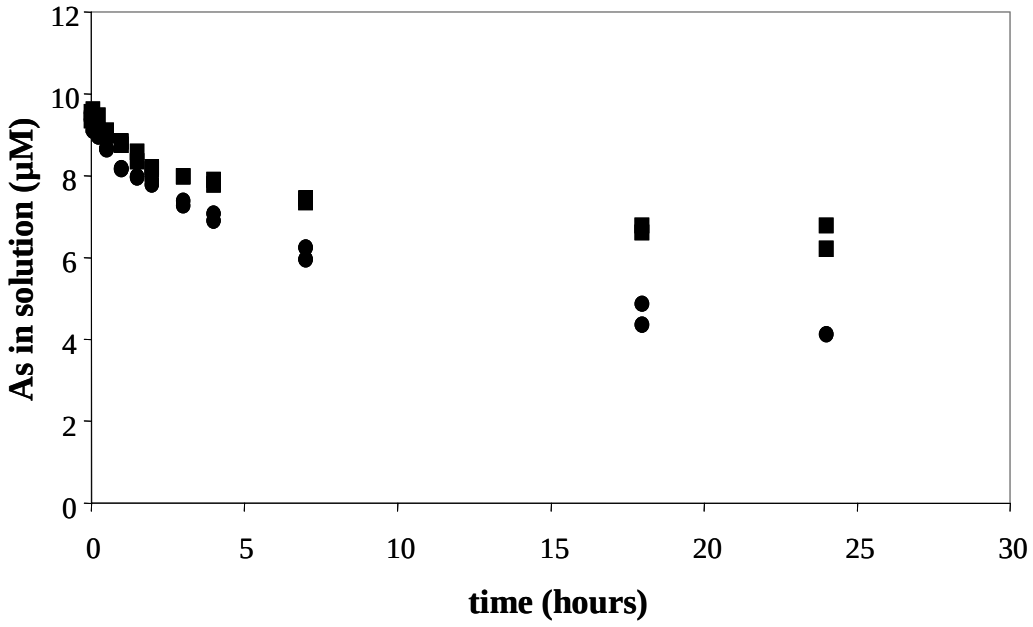

Figure 3.3. Kinetics of As(III) adsorption onto HFO-doped gels equilibrated with 10 µM As(III) in the presence of 50 µM phosphate (●) or the absence of phosphate (■).

3.4.3 XANES Calibration

Calibration standards for XANES were prepared by sorbing only As(III) or As(V) onto HFO-doped gel slabs. The XANES spectra of a set of HFO-doped gel slabs with varying proportions of adsorbed As(III) and As(V) were then collected.

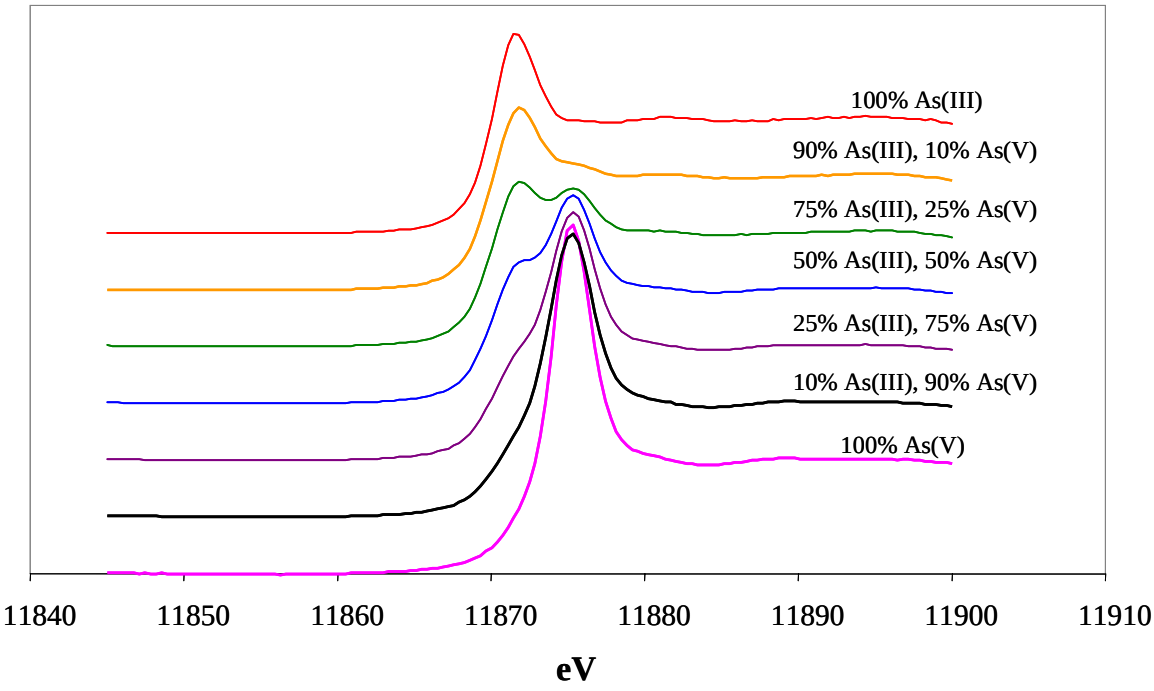

Figure 3.4. XANES calibration of As(III) and As(V) adsorbed on HFO embedded in gel. XANES edges are background normalized.

As seen in Figure 3.4, the As(V) signal is substantially stronger than the As(III) signal. As a result, peak heights are insufficient to quantitatively determine relative fractions of adsorbed As(III) and As(V) from a XANES edge. A least-squares linear combination of As(III) and As(V) end-members was chosen as an alternative. The results obtained for XANES spectra were compared with the value calculated from the residual dissolved concentrations of As(III) and As(V) measured by LC-ICP-MS after equilibration with HFO-doped gels (Table 3.1). For low As(III) fractions (<50%), the fit

has less than 1% error. However, once As(III) and As(V) are in equal abundance, a bias toward overestimating As(V) is observed. This effect is more pronounced at high As(III) fractions, where As(III) is underestimated by >10%. Nevertheless, the XANES calibration is a useful tool for determining the relative fraction of As(III) and As(V) on HFO-doped gels deployed in the field. The difference in signal response for adsorbed As(III) and As(V) may have implications for XANES edges collected on material other than HFO-doped gels, but further research is needed to compare the relative signal when the As is adsorbed on other synthetic and natural minerals.

Table 3.1. Analysis of XANES calibration by principal component analysis compared to measured values.

	LC-ICP-MS		***XANES***	
As(III):As(V)	**% As(III)**	**% As(V)**	**% As(III)**	**% As(V)**
10/90	7.9	92.1	8.0	91.7
25/75	22.4	77.6	21.4	78.5
50/50	47.4	52.6	54.6	45.6
75/25	73.9	26.1	61.2	39.1
90/10	89.5	10.5	76.7	23.5

3.4.4 As(III) and As(V) Isotherms

Adsorption site density for As(III) and As(V) on HFO embedded in gel was calculated based on sorption isotherms (Figure 3.5). The maximum sorption site capacity for As onto HFO embedded in gel is 0.12 mol_{sites}/mol_{Fe} for As(V) and 0.17 mol_{sites}/mol_{Fe} for As(III) at pH 7.1. At pH 8, the site density of As(III) drops to 0.12 mol_{sites}/mol_{Fe} (Figure 3.6).

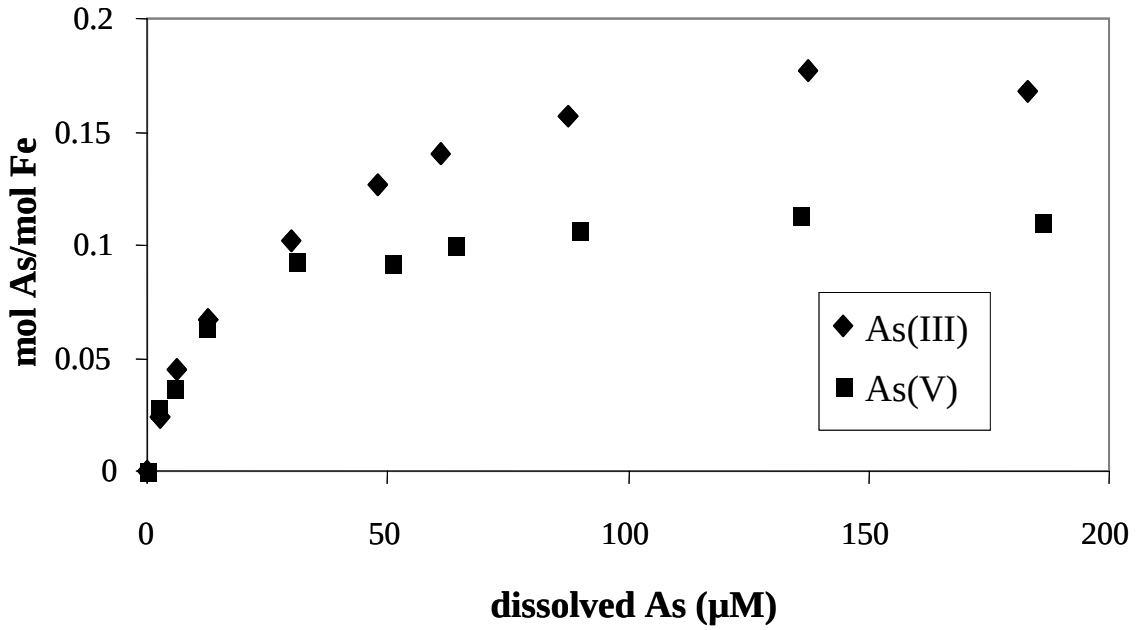

Figure 3.5. Sorption isotherms of As(III) (♦) and As(V) (■) on HFO embedded in polyacrylamide gel. One HFO-doped gel (2×10^{-6} mol Fe/gel) was equilibrated for 24 hours with 20mL of buffered arsenic solution (pH 7.1, I = 0.01 M).

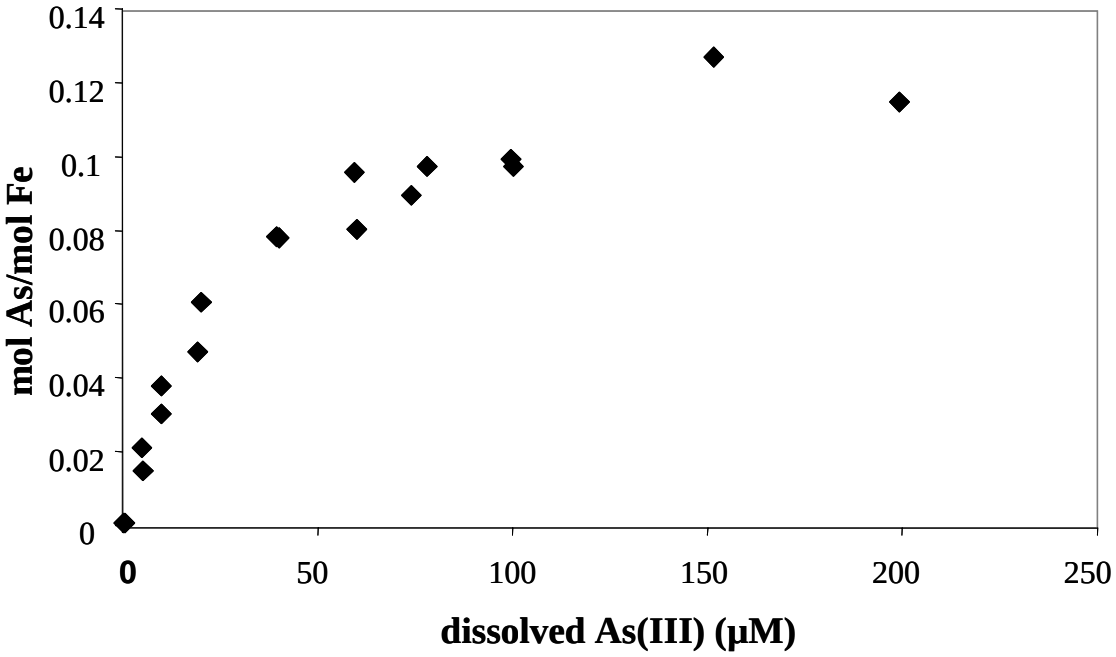

Figure 3.6. Sorption isotherm for As(III), pH 8. One HFO-doped gel (2×10^{-6} mol Fe/gel) was equilibrated for 24 hours with 20mL of buffered arsenic solution (I = 0.01 M).

The maximum sorption capacity of adsorbed As(III) onto HFO embedded in gel is less than most literature values, although the reported site density for As(III) varies considerably, from 0.043 mol As/mol Fe (Pierce and Moore 1980; Pierce and Moore 1982) to 0.31 mol As/mol Fe at pH 8 (Dixit and Hering 2003). Estimated site densities in excess of the theoretical number of surface sites have also been reported, possibly attributable to surface precipitation (Pierce and Moore 1982; Raven et al. 1998). The amount of As(III) adsorbed onto HFO depends strongly on pH (Pierce and Moore 1982; Wilkie and Hering 1996; Raven et al. 1998; Goldberg and Johnston 2001; Dixit and Hering 2003). This effect is observed in the difference in site densities at pH 7.1 and pH 8.

The site density of As(V) on HFO embedded in gel falls within the range of literature values, which vary from 0.02 mol As/mol Fe (Pierce and Moore 1982) to 0.25 mol As/mol Fe at pH 8 (Fuller et al. 1993). Co-precipitated HFO and As(V) can yield higher sorption densities (Fuller et al. 1993; Jia et al. 2006), but is not applicable to the HFO-doped gel probe, since field deployment will necessarily limit the conditions to neutral pH and post-synthesis sorption.

The maximum sorption densities of As(III) and As(V) are slightly less than reported values at comparable pH values possibly because some surface sites may be obstructed by gel. However, the site densities measured in these experiments are within the range of 0.05-0.18 mol_{sites}/mol_{Fe} reported for arsenic sorption on HFO surface sites (Dzombak and Morel 1990), and provide a valuable estimate for available surface sites in the gel probe when it is deployed in natural sediments.

3.4.5 Competitive sorption of Phosphate

It is well known that phosphate inhibits the sorption of both As(V) and As(III) on Fe (oxyhydr)oxides (Manning and Goldberg 1996; Jain and Loeppert 2000; Hongshao and Stanforth 2001; Liu et al. 2001; Holm 2002; Violante and Pigna 2002; Dixit and Hering 2003; Antelo et al. 2005). Phosphate inhibits the adsorption of both As(III) and As(V), but has a stronger effect on As(V) (Figure 3.7). At high phosphate concentrations, only 7% of total As(V) and 16% of total As(III) is adsorbed, compared to 45% adsorbed As(III) and As(V) in the absence of phosphate. The amount of As adsorbed onto the HFO in the absence of phosphate is consistent with the sorption isotherms. The maximum amount of phosphate adsorbed onto the HFO approaches 0.12 mol P/mol Fe, indicating that the maximum sorption density for phosphate is similar to As(V) at pH 7.1 (Figure 3.8). In the mixed As(III)/As(V) condition, total As sorption is slightly less than the As(III) only condition.

Previous studies have found that As(V) sorption is suppressed by phosphate to the greatest extent between pH 7 and 10, while As(III) sorption is inhibited the most at low pH (Jain and Loeppert 2000). As(V) and phosphate directly compete for surface sites, especially at neutral and alkaline pH (Manning and Goldberg 1996; Jain and Loeppert 2000). Similar maximum site densities for As(V) and phosphate in this study support this observation.

The order of sorbate addition strongly affects the extent of sorption, especially in the case of phosphate and As, which is indicative of incomplete equilibration. The sorbate added first adsorbs to a greater extent (Hongshao and Stanforth 2001; Liu et al.

2001). In this study, the sorbates (As(III), As(V), and phosphate) were added simultaneously to simulate sorption conditions in a field-deployed gel probe.

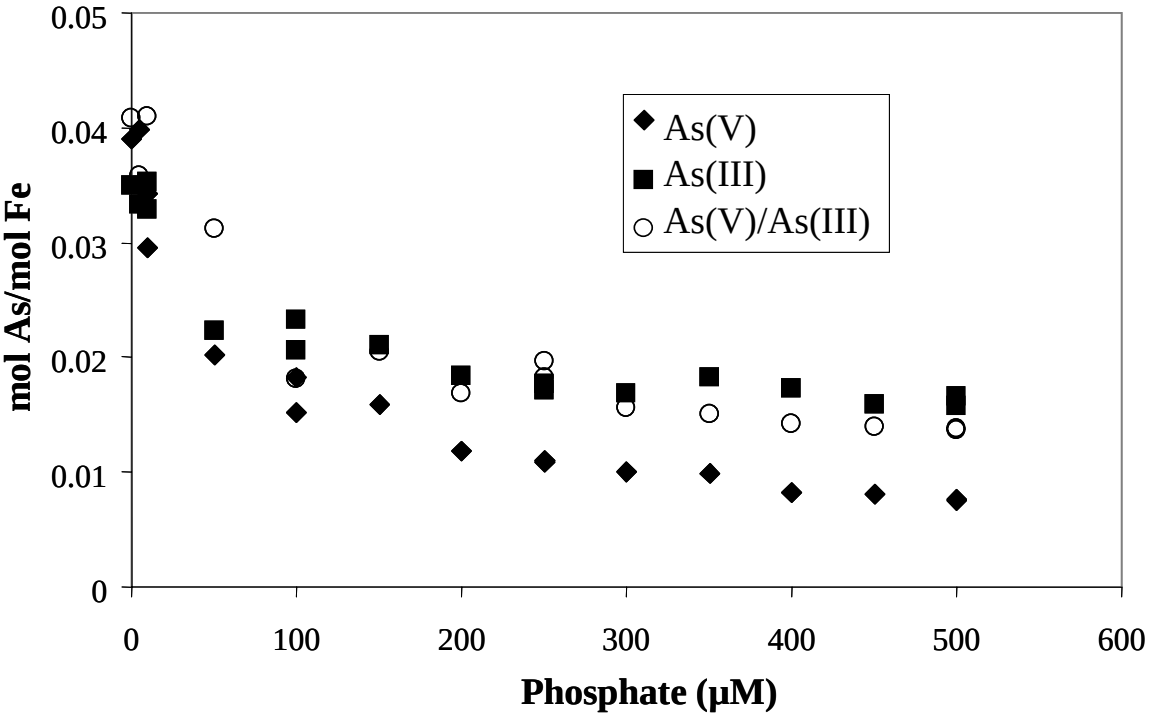

Figure 3.7. The effect of phosphate on adsorption of As(III) and As(V) on HFO-doped gels. One gel slab (2×10^{-6} mol Fe/gel) was added to a 20 mL buffered solution (pH 7.1, I = 0.01 M) of variable phosphate concentration and 10 µM As(III) (■), 10 µM As(V) (♦), or 5 µM As(III) and 5 µM As(V) (○) and equilibrated for 24 hours.

Competition between As(III) and As(V) for surface sites is minimal under the conditions of our experiments. At pH 7 and comparable concentrations (0.048 mol As/mol Fe for As(III) and As(V)), Jain and Loeppert observed that As(V) sorption is unaffected by the presence of As(III), and As(III) sorption is inhibited by As(V) by only ~1% (Jain and Loeppert 2000). Phosphate has a much stronger inhibitory effect under our experimental conditions.

At high P concentrations (P:As >10), sorption of As(V) is expected to be minimal if As(V) and phosphate directly compete for the same surface sites. Even though As(V) sorption is suppressed at large P:As ratios, a significant amount of As(V) is still adsorbed. This observation can be explained by relative surface affinity or sorption kinetics. Fe(III) minerals exhibit a slight preference for As(V) adsorption over phosphate (Hongshao and Stanforth 2001; Liu et al. 2001; Violante and Pigna 2002). However, the rate of phosphate sorption is initially faster than that of As(V) although the amount of adsorbed As(V) increases with reaction time until equilibrium is reached (Violante and Pigna 2002). The presence of adsorbed As(V), even at very high phosphate concentrations, may be due to slight preference for As(V) at equilibrium rather than sorption kinetics, although further investigation is needed to constrain this mechanism.

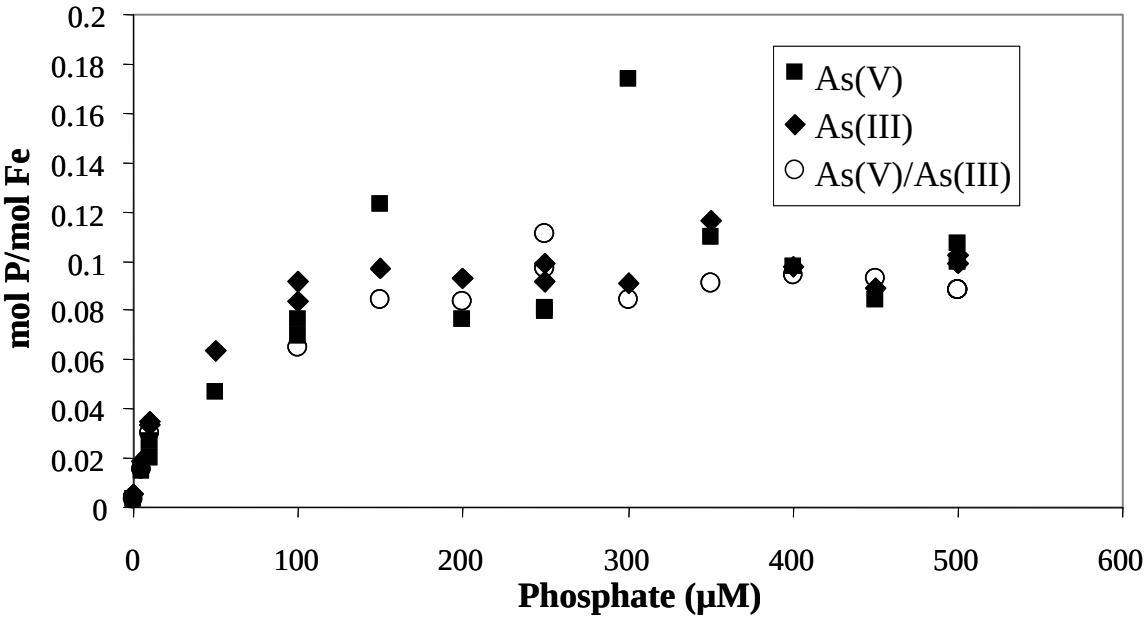

Figure 3.8. Phosphate adsorption onto HFO gels from the same experiment as Figure 3.7.

3.4.6 Competitive Sorption of Organic Matter

Soil HA and SR-NOM also inhibited adsorption of As(V) and As(III) onto HFO embedded in gel (Figure 3.9 A, B). Both types of organic matter had comparable effects and both As(V) and As(III) were similarly affected.

As(V) reduction and As(III) oxidation have both been observed in the presence of organic carbon, but this varies with the carbon source (Redman et al. 2002; Ko et al. 2004). The oxidation state may also be unaffected by organic matter. Since the nominal As oxidation states were not confirmed after exposure to organic matter in our experiments, possible interconversion of As(III) and As(V) cannot be excluded. However, similar effects were observed for As added nominally as either As(III) or As(V).

The presence of Soil HA and SR-NOM reduced the amount of As adsorbed by ~50% at high organic carbon concentrations. While phosphate had a stronger competitive effect than organic matter, both are effective at inhibiting As sorption onto HFO. The mechanism of As sorption inhibition is not known by organic carbon, but could be due to several processes. Organic carbon can sorb directly to Fe(III) mineral surfaces (Kaiser et al. 1997) and may affect As sorption through steric effects by blocking the oxide surface (Grafe et al. 2002) or electrostatic effects (Xu et al. 1991). Organic matter may also complex As in solution, most likely by inorganic bridging between Fe(III) stabilized in the dissolved phase by NOM (Redman et al. 2002; Ko et al. 2004; Warwick et al. 2005; Ritter et al. 2006). Organic carbon complexation exhibits a slight preference for As(V), but this observation is not consistent across all types of organic matter (Redman et al. 2002). Arsenic interactions with organic carbon are highly

dependent on the type of organic matter, and preferential sorption or complexation of As(III) or As(V) is sometimes, but not always, detected. Thus, it is not unreasonable to observe that organic carbon inhibits As(III) and As(V) sorption equally.

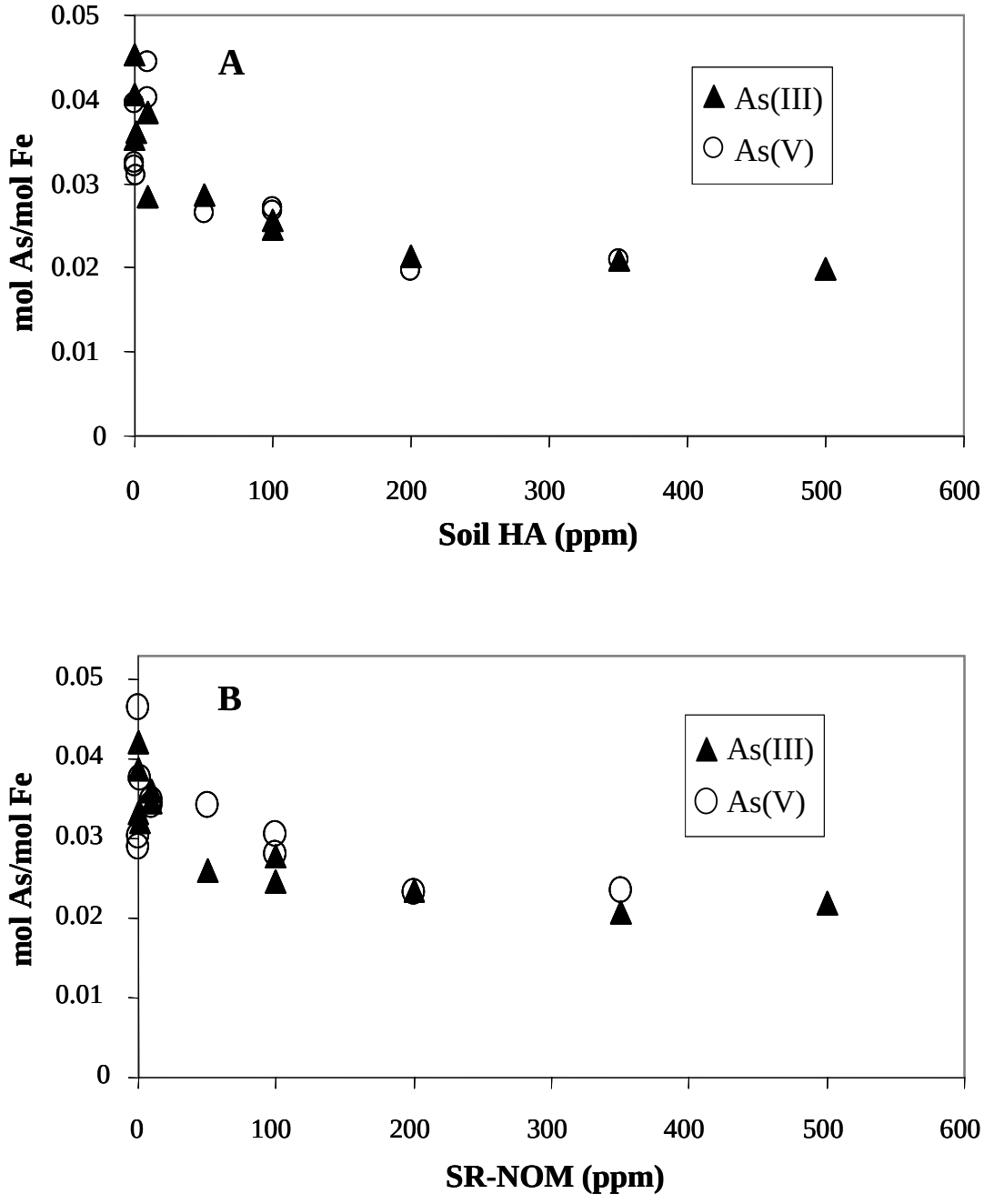

Figure 3.9. The effect of Soil HA (A) and SR-NOM (B) on As adsorption onto HFO-doped gels. One gel slab (2×10^{-6} mol Fe/gel) was added to 20 mL of buffered (pH 7.1, I = 0.01 M) solution with 10 μM arsenic and variable concentrations of organic matter. The gel was equilibrated for 24 hours, and re-equilibrated in acid.

Similar to phosphate, the extent of organic carbon inhibition on As sorption may depend on the order of sorbate addition. This was seen by Grafe and co-workers in an experiment where As adsorption onto goethite was inhibited by the presence of humic acid (HA) and fulvic acid (FA) when organic carbon and As were added simultaneously (Grafe et al. 2001). However, the opposite effect was seen on ferrihydrite-coated sand in column studies, where organic carbon was equilibrated with the solid phase first, followed by As (Grafe et al. 2002). Simultaneous addition of organic carbon and As in these experiments mimics the conditions to which an HFO-doped gel would be exposed in the field.

3.4.7 Application to field measurements

The results presented here establish a baseline of laboratory behavior for clear and HFO-doped gels. The clear gels can accurately measure the amount of As over a range of environmentally relevant concentrations. Arsenic sorption capacities for the HFO-doped gels and As behavior in simple competitive systems are essential in order to identify competitive sorption effects in a sedimentary system. By applying the XANES calibration to HFO-doped gels and LC-ICP-MS for the clear gels, both porewater and sorption speciation can be measured in field deployments. Porewater chemistry that controls As partitioning in sediments can be elucidated by comparing the sorption data presented here to the results of a field deployment of clear and HFO-doped gels.

3.4 Acknowledgements

The XANES work was done in collaboration with Rob Root and Dr. Peggy O'Day at University California, Merced. Special thanks to Nelson Rivera for help at the SSRL beamline and for assistance in fitting the XANES calibration. We thank also Dr. Megan Ferguson for her help in developing an LC-ICP-MS method for clear gels, and Dr. Suvasis Dixit and Theresa Spano for initial project development.

Chapter 4

A Gel Probe Equilibrium Sampler for Measuring Arsenic Porewater Profiles and Sorption Gradients in Sediments: Application to Haiwee Reservoir

4.1 Abstract

Arsenic (As) geochemistry and sorption behavior was measured in Haiwee Reservoir sediments by deploying undoped (clear) polyacrylamide gels and hydrous ferric oxide (HFO)-doped gels in a gel probe equilibrium sampler. The As- and iron (Fe)-rich sediments provide a unique field site to study the effects of sediment diagenesis and porewater chemistry on As partitioning between solid and aqueous phases. Gel probe measurements were accompanied by sediment core analysis. Arsenic was deposited at the sediment surface as As(V) but was reduced to As(III) in the upper layers of the sediment. Reduction of As(V) did not cause mobilization into the porewater, as a negligible about of dissolved As was observed at the sediment-water interface. Dissolved As and Fe concentrations increased at depth in the sediment column driven by the reductive dissolution of amorphous Fe(III) oxyhydroxides. As organic matter was mineralized to dissolved inorganic carbon, sorption onto the HFO-doped gels was most likely inhibited by carbonate. In this region, dissolved As concentrations were at least partially controlled by porewater composition rather than surface site availability. Deeper in the sediment column, the Fe(III) oxyhydroxides partially converted to

carbonate green rust, possibly sequestering dissolved carbonate into the solid phase. Arsenic adsorption onto the HFO-doped gels increased in this region, and the extent of adsorption was most likely controlled by the competitive effects of dissolved phosphate. The persistence of dissolved As in the porewaters may be due to the loss of sorption sites upon conversion to green rust. When sediments were recently exposed to air, the region of sorption inhibition was not observed, suggesting that oxidation affects the extent of reductive dissolution. The HFO-doped gel probe equilibrium sampler is a novel technique for measuring the effects of porewater composition on As mobilization when combined with core analysis.

4.2 Introduction

Complex biogeochemistry governs the partitioning of arsenic (As) between solid and aqueous phases in freshwater sedimentary environments. In non-sulfidogenic environments where dissolved As concentrations are not controlled by As-sulfide mineral precipitation, adsorption onto iron (Fe)- (oxyhydr)oxides can be an important sequestration mechanism (Smedley and Kinniburgh 2002). Adsorption is controlled by As redox state, solution chemistry, and sorbent properties, and is sensitive to pH. The availability of sorption sites and surface affinity will determine the extent of adsorption onto a mineral substrate. Adsorption of As can be suppressed in the presence of competitively sorbing ions such as phosphate, carbonate, silicate, organic carbon, and other compounds (Jain and Loeppert 2000; Grafe et al. 2001; Holm 2002; Dixit and Hering 2003). Changes in solid-phase properties during early sediment diagenesis can

alter As partitioning. Reductive dissolution and the resulting secondary mineral transformations can promote As mobilization under some conditions and may be important in many types of reducing sediments and aquifers (Aggett and O'Brien 1985; Peterson and Carpenter 1986; Azcue and Nriagu 1994; Nickson et al. 2000; Welch et al. 2000).

The sediment in North Haiwee Reservoir (Olancha, CA) is a unique field site for the study of various mechanisms controlling As partitioning in the subsurface environment. A natural geothermal input of As results in elevated As concentrations in the Los Angeles Aqueduct (LAA), a source of drinking water for the city of Los Angeles. Currently, the water is being treated by injecting ferric chloride into the LAA, producing an amorphous Fe oxyhydroxide floc that removes As from the dissolved phase by sorption/co-precipitation. The As- and Fe-rich floc is removed from the water via sedimentation at Haiwee Reservoir. Some initial sedimentation occurs in the inlet channel to the reservoir (Figure 4.1), which provides a location for the study of effects of early diagenesis on Fe and As distribution. Arsenic is deposited as As(V), but reduction to As(III) occurs in the surficial sediment. The change in oxidation state does not result in release of As to the porewaters (Root et al. 2006). The reduction of As(V) is most likely due to biological metabolism related to respiration (Malasarn et al. 2004; Campbell et al. 2006).

Reductive Fe(III) dissolution drives the mobilization of As in Haiwee sediments and is most likely microbially mediated. Reductive dissolution can proceed through abiotic or biotic pathways, although biological reductive dissolution is thought to be more significant in freshwater sediments (Lovley et al. 1991). Biological Fe(III) oxide

reduction can be catalyzed by a very metabolically-diverse group of organisms present in a wide variety of sediment environments (Lovley et al. 1991; Thamdrup 2000). Less crystalline Fe oxides are more bioavailable due to higher reactive surface areas and, consequently, more readily reduced by bacteria (Jones et al. 2000).

Secondary mineral transformations can be catalyzed by the Fe(II) produced during reductive dissolution (Schwertmann 1991; Zachara et al. 2002; Hansel et al. 2005; Pedersen et al. 2005). A mixed Fe(II)-Fe(III) hydroxide phase, carbonate green rust ($[Fe^{II}_4Fe^{III}_2(OH)_{12}]^{2+}\cdot[CO_3,\ nH_2O]^{2-}$), was found to be a significant mineralogical component below ~15 cm in Haiwee sediments (Root et al. 2006). Green rust is a metastable mineral resulting from bacterial Fe(III) reduction. The presence of adsorbed As, phosphate, and other anions can stabilize green rust in sediment (Bocher et al. 2004; Su and Wilkin 2005). While green rust generally has a high surface area, the effect of conversion from amorphous Fe(III) oxide to green rust on As partitioning is not well understood.

Iron reduction is not complete; Fe(III)-containing solids persist in the sediments, and are efficient sorbents for As. When sorption sites remain available on the solid, As can re-adsorb onto the solid phase even as reductive dissolution progresses (McArthur et al. 2004). Re-adsorption is affected strongly by the porewater composition, and the presence of competitively adsorbing ions can increase the amount of As in the porewater. Once the surface sites are saturated, As mobilization into the porewaters is directly related to the amount of solid reductively dissolved. Reductive dissolution in Haiwee Reservoir sediments drives the mobilization of As, but the role of porewater chemistry in controlling As partitioning is unclear. The purpose of this study is to identify the

geochemical controls on As mobilization in Haiwee Reservoir sediment. We also demonstrate the utility of a Fe(III)-doped gel probe equilibrium sampler (Chapter 3) for investigating *in situ* sorption processes.

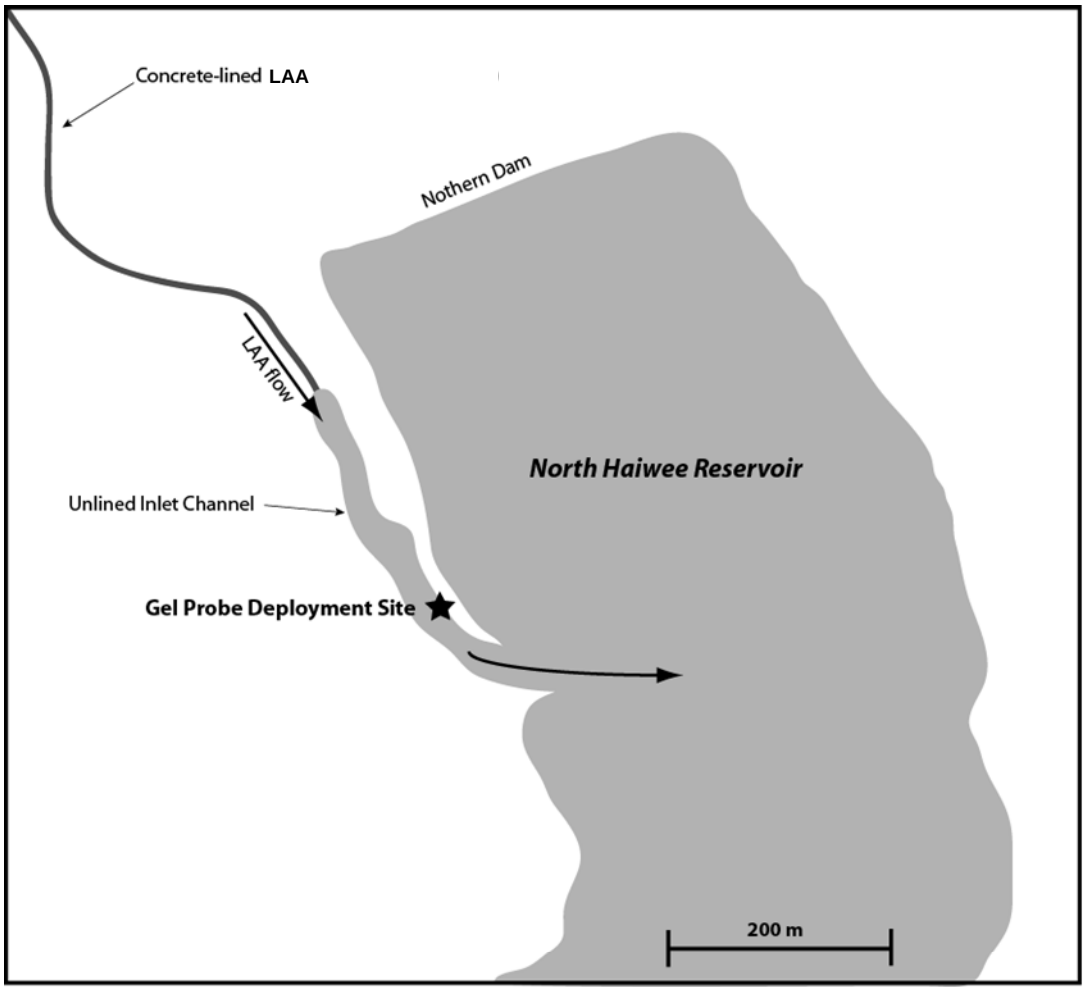

Figure 4.1. Map of North Haiwee Reservoir and the Los Angeles Aqueduct (LAA) inlet.

4.3 Materials and Methods

4.3.1 Reagents

All chemicals used were reagent grade and used without further purification unless otherwise noted. All water used was 18 MΩ-cm deionized water (Elix/Milli-Q, Millipore). Solutions were stored in plastic containers that had been acid-washed in 2-5% hydrochloric acid. Experiments were performed in trace metal-free plastic tubes. All nitric acid solutions were made with trace metal grade HNO_3 (EM Science, Omnipure, 70%).

4.3.2 Clear and HFO-doped gels

Hydrous ferric oxide (HFO) was synthesized as described in Chapter 3. Both clear and HFO-doped gels were used in this study. A detailed description of gel synthesis, casting and cutting methodology is presented in Chapter 3. All gels were cut to the final dimensions of 2 cm × 0.5 cm × 0.2 cm. The iron content of HFO-doped gels was 2×10^{-6} mol Fe/gel slab. A complete description of gel re-equilibration and analytics is provided in Chapter 3. Porewater composition (clear gels) was calculated with equation (3.1). Sorption onto HFO-doped gels is normalized to the amount of Fe in each gel slab (mol sorbate/mol Fe).

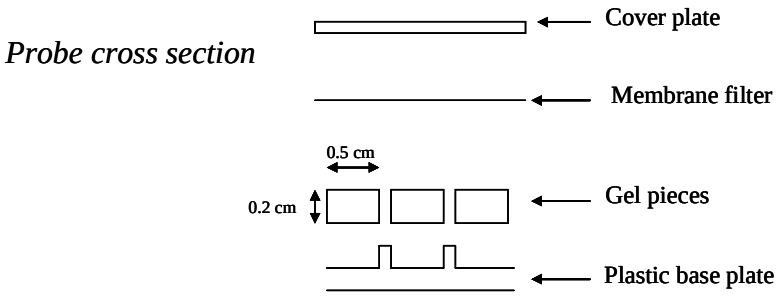

Generalized Gel Probe schematic

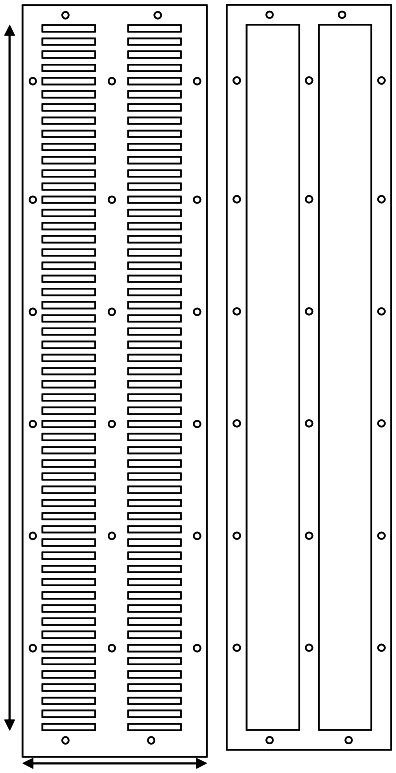

Figure 4.2A. Gel probe equilibrium sampler schematic with cross section.

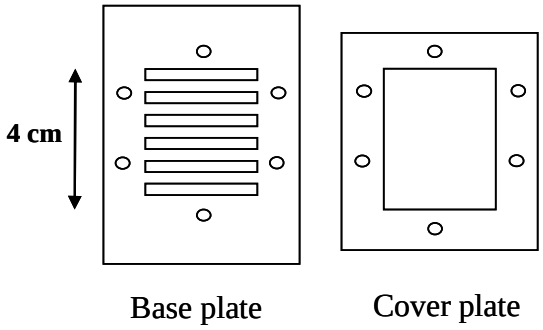

Figure 4.2B. "Mini-probe" gel probe equilibrium sampler schematic for sediment microcosms.

4.3.3 Gel Probe Design

Gel probes were designed to hold the gel slabs in individual slots etched into a plastic holder. The slots were arranged vertically in either one or two columns, holding between 54 and 80 slabs per column. The probes were between 35 and 55 cm long, measured from the top gel to the bottom gel. The probes with two parallel columns ("double probes") were designed to hold clear and HFO-doped gels at the same depth for simultaneous porewater and adsorption measurements. The gel slabs were secured with a 0.45 μm nitrocellulose membrane filter (Schleicher and Schuell) and held in place with a plastic face plate. The probes were placed in deoxygenated water and bubbled with compressed N_2 gas for at least 12 hours prior to deployment to deoxygenate the water inside the gels. The probes were transported to the field site in deoxygenated water. A double gel probe schematic is shown in Figure 4.2a.

For sediment laboratory microcosm experiments, 6 "mini-probes" were constructed. The mini-probes had a single column of 6 slots for gel slabs, and were 4 cm long. Preparation was identical to the field probe procedure. A mini-probe schematic is shown in Figure 4.2b.

4.3.4 Field Deployment

Gel probes were deployed in Haiwee Reservoir sediments at the location marked in Figure 4.1. The gel probes contained both HFO and clear gels unless otherwise noted, and were deployed in July 2003 (Appendix A), October 2003 (clear gels only), October 2004, August 2005, and May 2006. The probes were inserted vertically into the sediments parallel to the direction of overlying water flow, with several gels above the

sediment-water interface. The overlying water was ~0.5 m deep above the probes. The gel probes were deployed in an area of relatively slow flow close to the shore, and were allowed to equilibrate undisturbed for 24 hours before being gently extracted from the sediment. The outside of the probe was quickly washed with water to remove excess sediment. The membrane was then removed, and the gels were immediately extracted and placed in individual 2 mL tubes (Eppendorf). A subset of clear gels was placed in tubes pre-filled with 1.25 mL of 25 mM H_3PO_4 for As speciation measurement (August 2005 and May 2006). These gels were allowed to re-equilibrate for 6-12 hours before analysis. A subset of HFO-doped gels were preserved for X-ray absorption spectroscopy (XAS) analysis and immediately frozen on dry ice in the field until placed in a -20°C freezer (August 2005 and May 2006). The rest of the clear and HFO-doped gels were placed on ice until they were acidified in the laboratory and allowed to re-equilibrate for at least 24 hours before analysis.

4.3.5 Gel Probe Analytics

Clear gels were re-equilibrated in 1% HNO_3 for inductively-coupled plasma mass spectrometry (ICP-MS) analysis, or 25 mM H_3PO_4 for liquid chromatography coupled to ICP-MS (LC-ICP-MS) for As speciation measurements. HFO-doped gels were re-equilibrated in 5% HNO_3 for ICP-MS analysis or were frozen for As speciation measurements by X-ray absorption spectroscopy (XAS). Both clear and HFO-doped gels were analyzed for manganese (Mn), As, strontium (Sr), molybdenum (Mo), antimony (Sb), barium (Ba), tungsten (W), phosphorous (P), chromium (Cr), nickel (Ni), copper (Cu), lead (Pb), uranium (U), selenium (Se), and Fe. Fe was measured by the

phenanthroline Fe assay (Standard Methods 1995). Only As, Mn, Fe, and P were measured in July 2003, October 2003, and October 2004.

Arsenic K-edge spectra of HFO-doped gels from the May 2006 deployment were collected at the Stanford Synchrotron Radiation Laboratory (SSRL), Menlo Park, California, on wiggler beamline 11-2 at a beam energy of 80-100 mM, using a 30-element Ge detector and a Si(220) monochromator crystal. Energy was calibrated using an As foil where the energy of first inflection of the absorption was set to 11867 eV, and a sodium arsenate reference (Sigma) was analyzed to verify calibration with maximum As(V) absorption at 11875 eV. X-ray absorption near edge structure (XANES) edges were collected on HFO-doped gels that were equilibrated below 20 cm in the sediment. Scans were averaged and background subtracted using the SIXPACK software package. Background subtraction was done with a linear fit through the pre-edge region and extrapolation into the extended x-ray absorption fine structure (EXAFS) region. Spectra were normalized using the height of the edge step just above the absorption maximum. Normalized XANES spectra were fit to a binary reference set by linear combination using the program DATFIT with a least-squares linear combination. Fits were calibrated and verified to be linear by fitting endmember and known mixtures of As(III) and As(V) with DATFIT (see Chapter 3 for HFO-doped gel XANES calibration details).

4.3.6 Sediment Microcosms

Laboratory sediment microcosms were designed to determine the amount of time required for clear and HFO-doped gels in a gel probe sampler to equilibrate with sediment porewater. Surficial sediment was collected in the field, kept on ice during

transport, and homogenized in a large container prior to being frozen at -20°C. After being defrosted, the sediment was again homogenized and distributed into 6 acid-washed plastic containers in 600 mL aliquots. As the sediment settled, the overlying water at the surface of the sediment was continuously bubbled with compressed N_2 for 24 hours to allow anoxic conditions in the sediment to be established. Even after freezing, anoxia is readily established, presumably due to the ambient bacterial population. Six mini-probes were filled with alternating clear and HFO-doped gels, deoxygenated, and inserted into the sediment, one probe per container. Compressed N_2 continued to bubble in the overlying water for the entire course of the experiment. One probe was removed at each time point. The gels were immediately recovered from the mini-probes and re-equilibrated in acid for analysis.

4.3.7 Gravity Core Processing and Analysis

Several acid-washed core tubes were inserted adjacent to the gel probes at the time of deployment, and were left undisturbed until after the gel probes were removed. Once recovered, they were stored upright on ice for transport and frozen at -20°C upon return to the laboratory. An additional set of cores was taken in May 2006, four weeks prior to the gel probe deployment, and in November 2004. Cores were defrosted under N_2 in a glove box and cut into 2-4 cm sections. These sections were centrifuged to separate the bulk solid from the porewater. The porewater from each section was syringe-filtered (0.2 μm, Pallman), and acidified with 1% HNO_3 for ICP-MS and colorometric analyses.

Core sections from two August 2005 cores were dried at 60°C in a drying oven. Solid phase organic carbon was analyzed by CHN analysis (Europa Hydra 20/20 IRMS, University of California, Davis). Two samples from each section were analyzed: one sample was fumigated with HCl to remove the inorganic carbon and the other was directly analyzed for total carbon (organic and inorganic). X-ray fluorescence (XRF) on composite samples was performed to measure bulk elemental composition (SGS Minerals, Toronto).

Cores from November 2004 and August 2005 were analyzed for solid-phase As speciation by XANES at SSRL. In addition, core sections from May 2006 were extracted with 25 mM H_3PO_4, syringe-filtered (0.2 µm), and analyzed for As speciation by LC-ICP-MS.

4.4 Results

4.4.1 Sediment Microcosm

The clear gels in the sediment microcosms stabilized to a constant As concentration of ~10 µM within 10 hours (Figure 4.3a). The HFO-doped gels in the sediment microcosm required about 18 hours to reach equilibrium with the sediment porewaters (Figure 4.3b). Based on laboratory kinetics (Chapter 3), it is reasonable to expect that the HFO-doped gels require longer equilibration times than clear gels. An acceptable deployment time was determined to be 24 hours based on the sediment microcosm results.

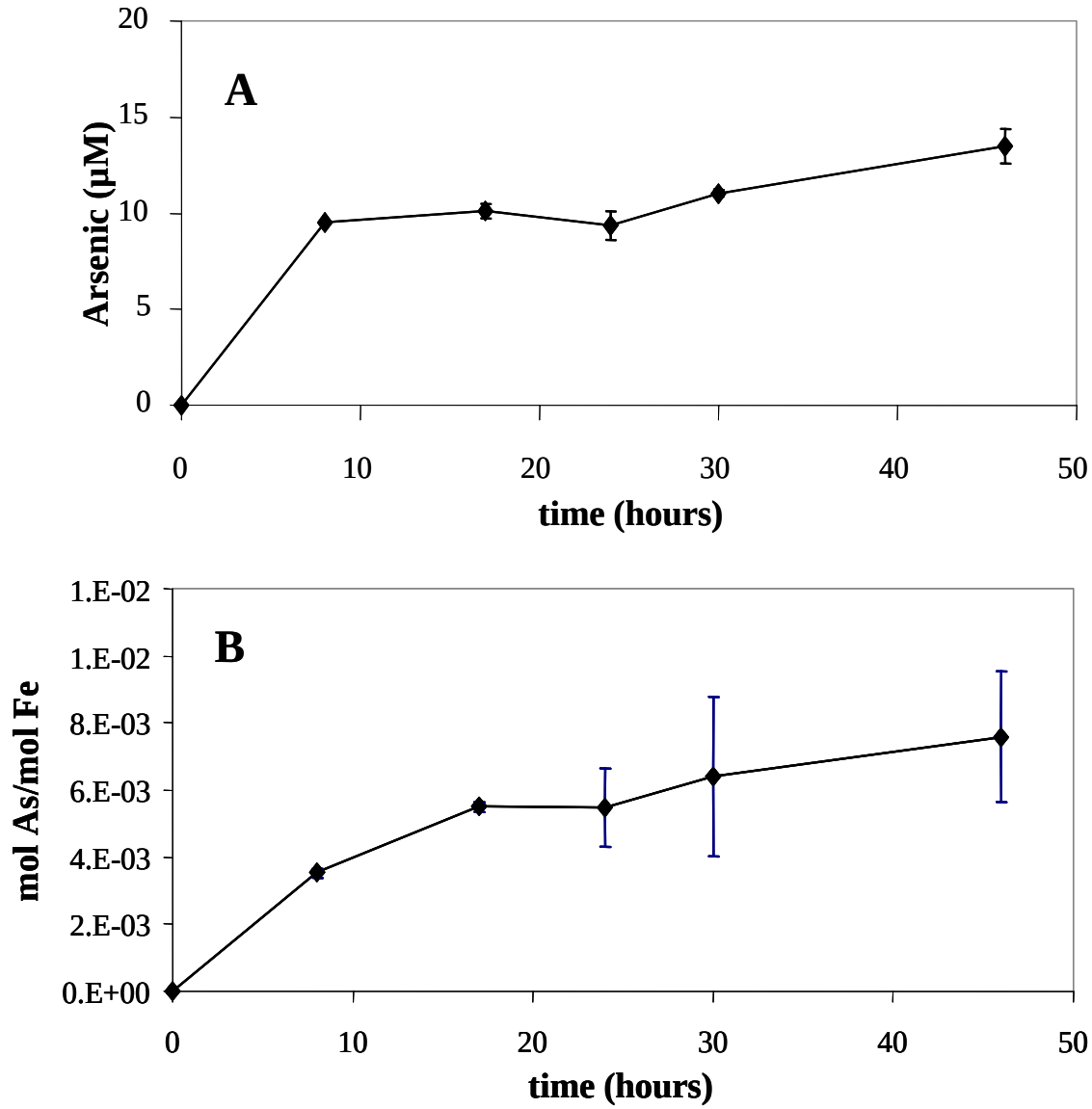

Figure 4.3. Arsenic in the porewaters (A) and adsorbed onto HFO-doped gels (B) in mini-probes equilibrated in Haiwee sediment microcosms. One probe was removed at each time point and the gels re-equilibrated in acid.

4.4.2 Comparison of clear gel concentrations and core porewater extractions

Porewater As concentrations measured by clear gels in a double gel probe are compared to porewater extractions from a core taken adjacent to the gel probe (~10 cm) in May 2006, in Table 4.1. Since the gel probe has a finer resolution than the core

sections, the gel probe porewater concentrations are reported as an average over the same depth interval as the core sections (n=4). The porewater As concentrations are consistent between the two measurement techniques. Although there is some variability, it is most likely due to natural spatial variability since there is no systematic bias between the two methods. This result also confirms the accuracy of clear gels for porewater measurements when placed in a double probe adjacent to HFO-doped gels.

Table 4.1. Comparison of porewater As concentrations from clear gels in a double gel probe and porewater extractions from a gravity core. The core was taken immediately adjacent to the gel probe in May 2006. Porewater was extracted from the core by centrifugation and the clear gels were re-equilibrated in 1% nitric acid. Gel probe values are an average over the same depth interval as the core sections (n=4).

depth (cm)	core sections (µM)	gel probe (µM)
0-3	0.38	0.43
3-6	0.74	1.01
6-9	0.70	0.99
9-12	1.73	1.36

4.4.3 Gel Probe Porewater profiles (clear gels)

Porewater concentrations as a function of depth below the sediment-water interface for October 2004 (2 double probes), August 2005, and May 2006, are presented in Figures 4.4-4.7. Porewater profiles from October 2003 are similar to October 2004; data can be found in Appendix D. In all cases, dissolved As concentrations began to increase between 2 and 5 cm depth, with very little dissolved As observed at the sediment-water interface. Arsenic concentrations peaked between 15 and 35 cm below

the sediment-water interface. There is a strong correlation between dissolved Fe and As for all sample dates, with As and Fe porewater data from October 2004 shown in Figure 4.8 as an example. Dissolved As is also correlated with dissolved P (all sample dates) and W (August 2005 and May 2006) (August 2005 shown in Figure 4.9, as an example). Since measurements were made using ICP-MS, the oxidation states of As, P, and W were not preserved. However, it is likely that P is present as phosphate and W present as tungstate, which are chemically similar to the oxyanions of As. Trace amounts of Cu, Cr, Mo, Sr, and Ba were detected in porewaters, but there was no correlation of these elements to dissolved As or Fe concentrations.

In August 2005, the fractions of dissolved As(III) and As(V) were approximately equal to 20 cm, below which about 60% of the total As was present as As(III) (Figure 4.6A). In May 2006, about 60% of the total dissolved As was present as As(III) between 5 and 25 cm depth. Below 25 cm, As(III) constituted ~80% of the total dissolved As (Figure 4.7A).

Dissolved As, Fe, Mn, P and W concentrations varied substantially both temporally and spatially. Maximum As concentrations varied from 5 to 25 µM, and maximum Fe concentrations varied between 200 and 2000 µM. In October 2004, the maximum As concentration in one gel probe was 5 µM while maximum concentration in another gel probe placed within 2 meters was ~25 µM, highlighting the substantial spatial variability at the site.

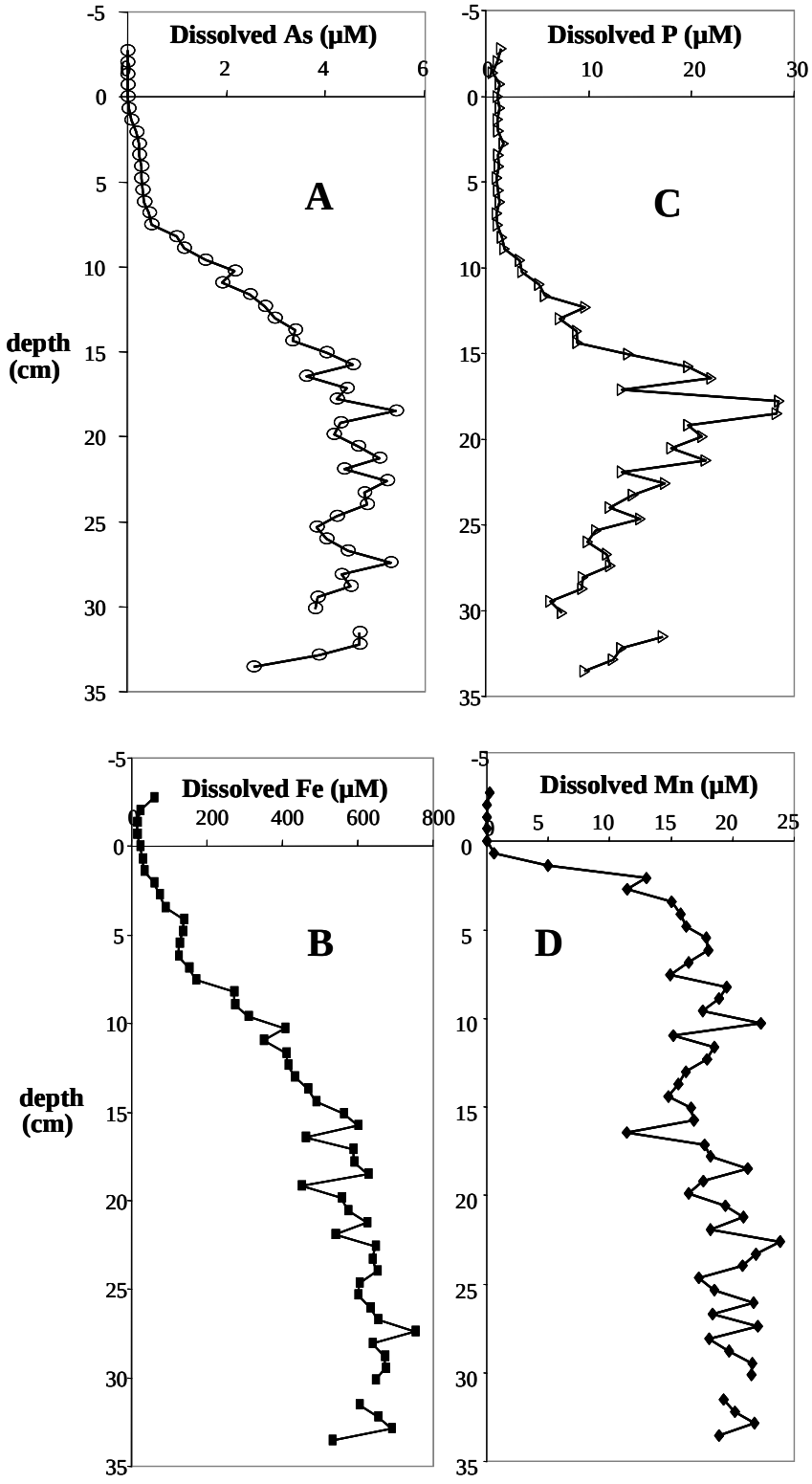

Figure 4.4. Porewater concentrations of As (A), Fe (B), P (C), and Mn (D) from double gel probe #1 deployed October 2004. The probe was equilibrated for 24 hours in the sediment. The sediment was soft and had not been recently exposed to the air.

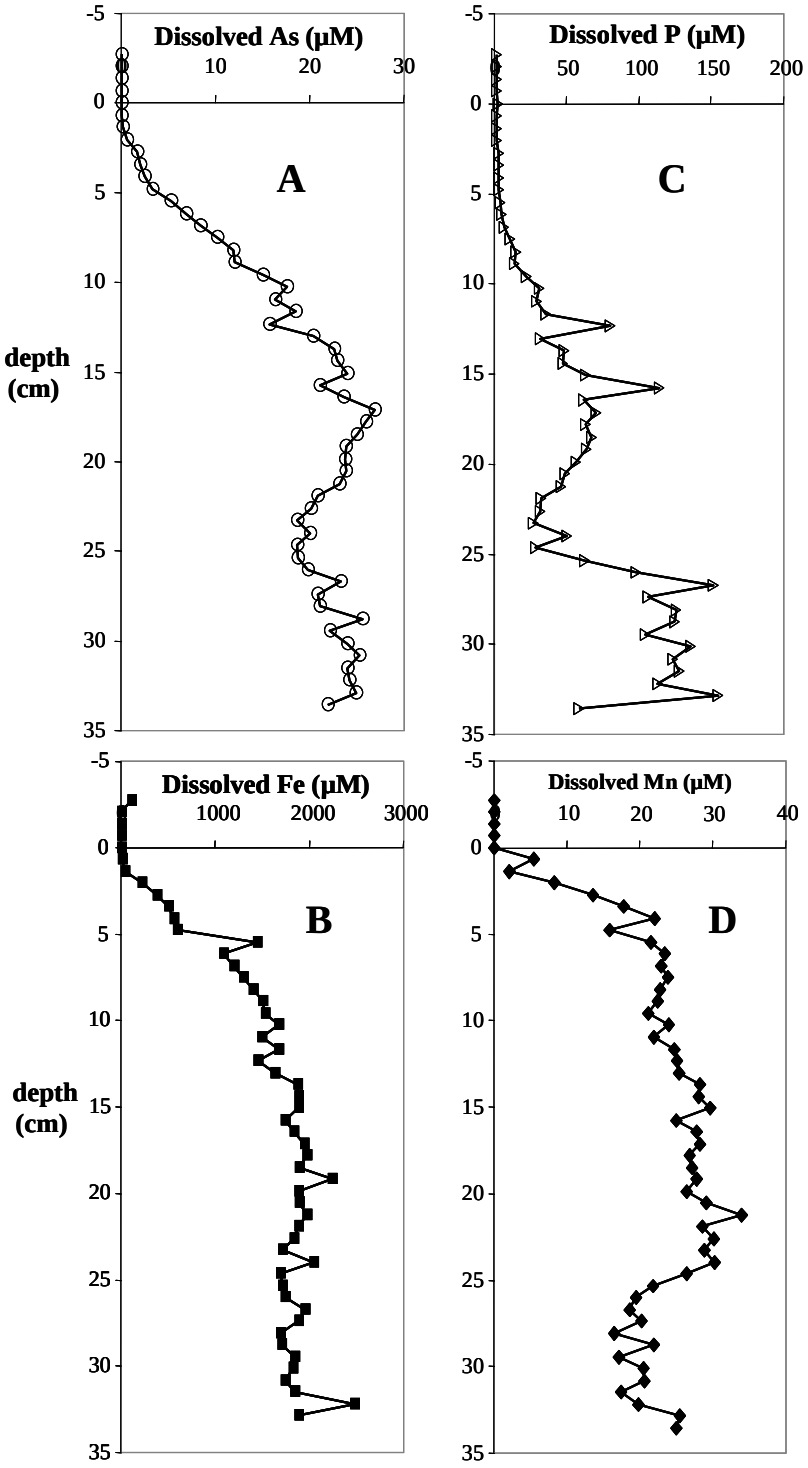

Figure 4.5. Porewater concentrations of As (A), Fe (B), P (C), and Mn (D) from double gel probe #2 deployed October 2004. The probe was deployed within 2 m of probe #1, and equilibrated for 24 hours in the sediment. The sediment was soft and had not been recently exposed to the air.

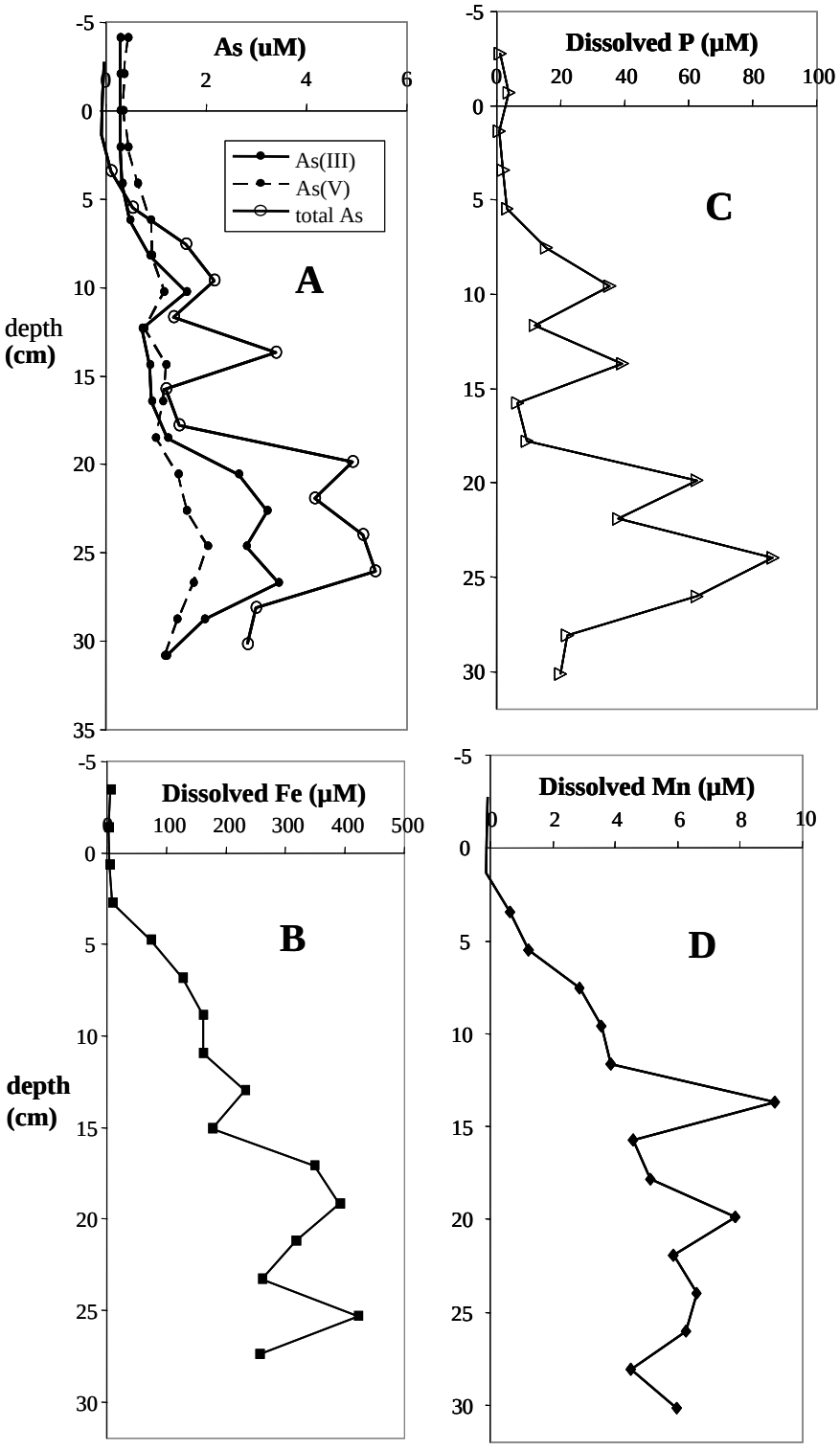

Figure 4.6. Porewater concentrations of As (A), Fe (B), P (C), and Mn (D) from a double probe deployed in August 2005. The probe was equilibrated for 24 hours. The sediment was hard and had been recently exposed to air. Arsenic speciation measurements were made by LC-ICP-MS.

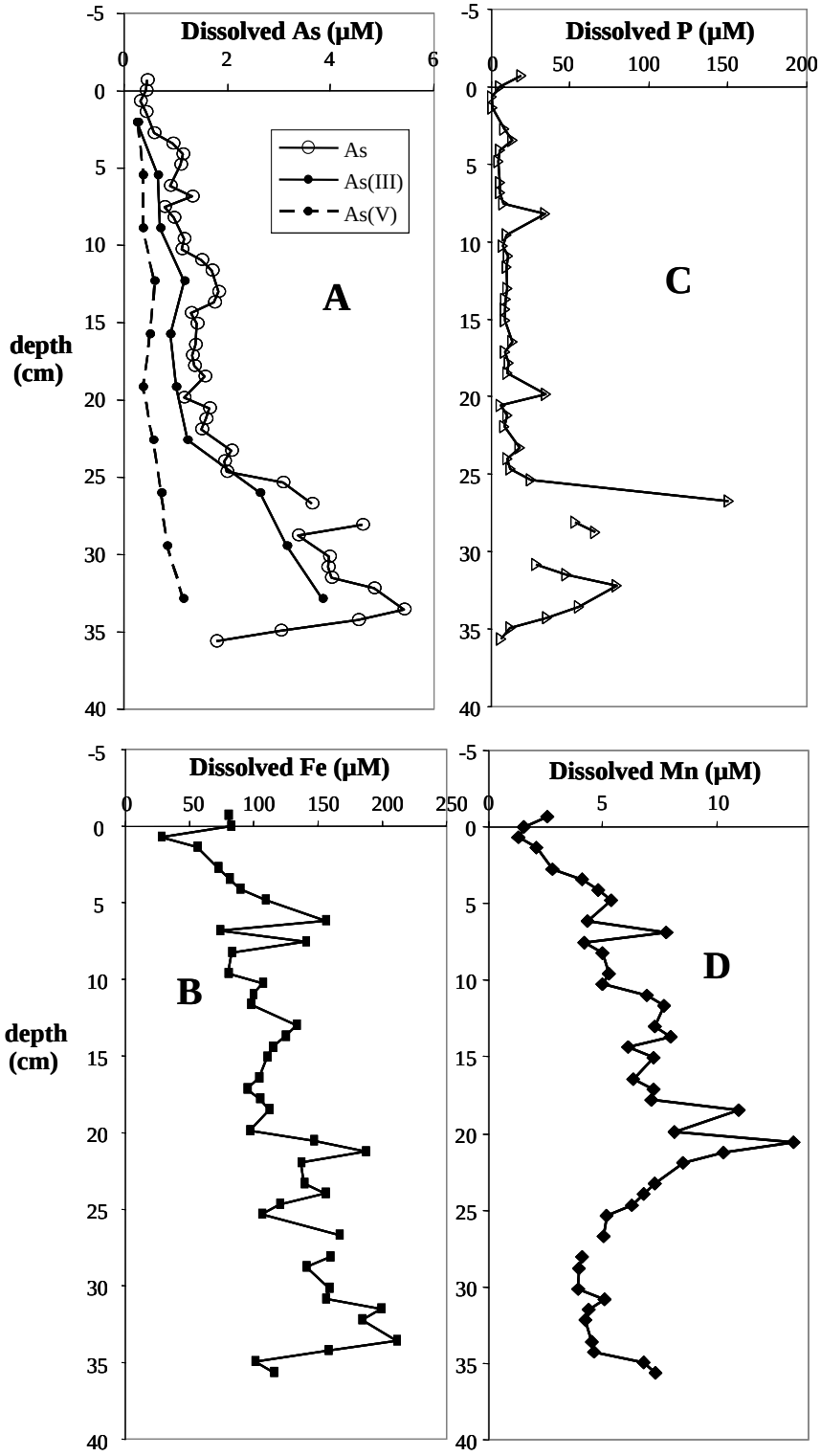

Figure 4.7. Porewater concentrations of As (A), Fe (B), P (C), and Mn (D) from a double probe deployed in May 2006. The probe was equilibrated for 24 hours. The sediment was hard and had been recently exposed to air. Arsenic speciation measurements were made by LC-ICP-MS.

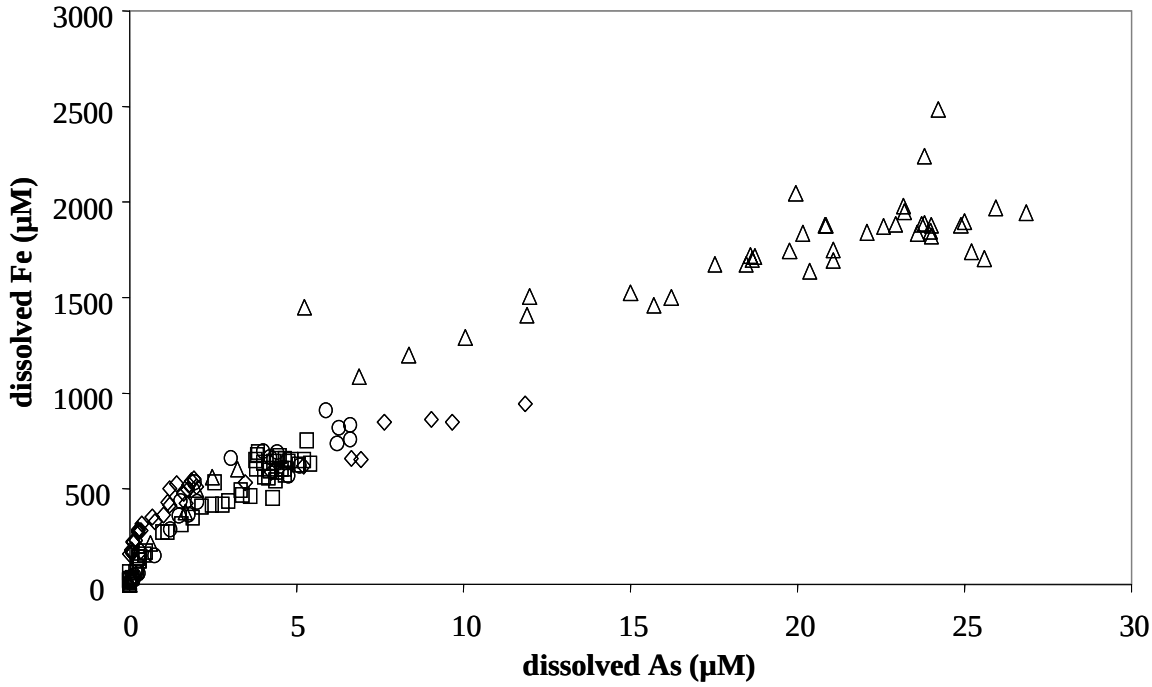

Figure 4.8. Correlation between Fe and As in porewaters from October 2004. Squares are data from gel probe #1, triangles are from gel probe #2, diamonds are from gel probe #3, and circles are from gel probe #4 (data are tabulated in Appendix D).

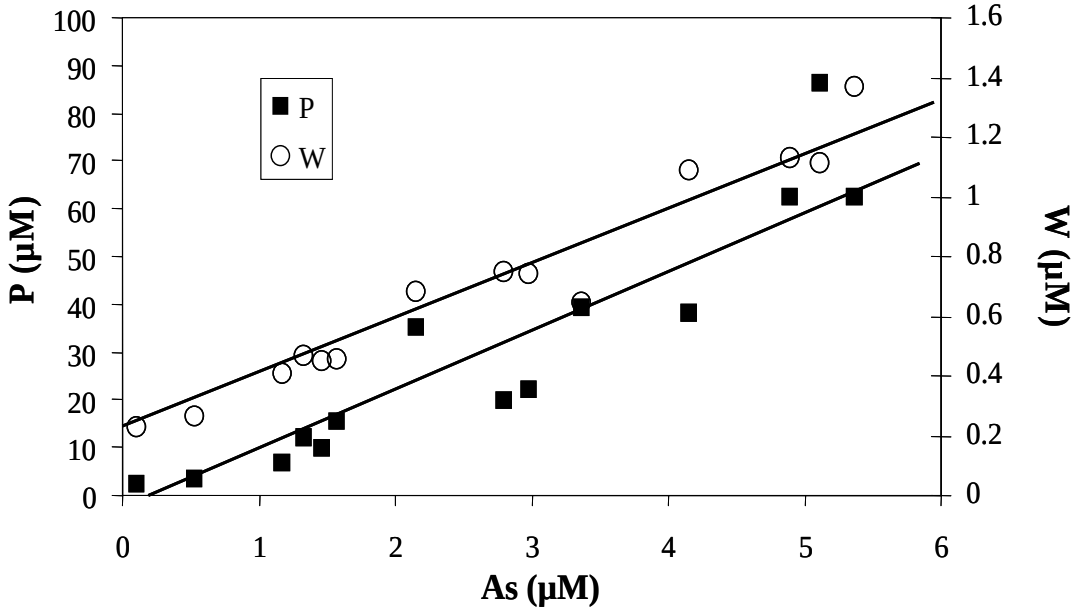

Figure 4.9. Correlation between As, P, and W in porewaters from gel probe deployed in August 2005.

4.4.4 Gel Probe Sorption profiles (HFO-doped gels)

Arsenic and P adsorption profiles from October 2004 and May 2006 are shown in Figures 4.10-4.12. The amount of As and P adsorbed onto HFO-doped gels in each field deployment is substantially less than the total available surface sites determined from sorption isotherms presented in Chapter 3. At 10 μM dissolved As(III) or As(V), about 0.05 mol As/mol Fe would adsorb if As was the only sorbate present. A maximum of only 0.01 mol As/mol Fe is observed on HFO-doped gels in the field. Similarly, adsorbed phosphate reached values between 0.05 and 0.1 mol P/mol Fe in laboratory studies as dissolved phosphate concentrations were varied between 50 – 150 μM, but a maximum of only 0.03 mol P/mol Fe was observed in the field. Although the maximum amount of As and P adsorbed onto the HFO-doped gels in the field is less than the total site content, the presence of other sorbates such as silicate and organic carbon can decrease the overall adsorption of As and P.

Adsorption of As and P onto HFO-doped gels was correlated with dissolved concentrations for some sampling events (e.g., May 2006), but not for all deployments. In October 2004, dissolved As concentrations increased between 10-20 cm without a corresponding increase in adsorption onto the HFO-doped gels. Most of the As adsorbed onto the HFO-doped gels was As(III) (>90% As(III)) in May 2006 (Table 4.2).

Table 4.2. Relative amount of As(V) and As(III) adsorbed onto HFO-doped gels deployed in May 2006. Gels were frozen in the field and analyzed by XANES at SSRL.

depth (cm)	% As(V)	% As(III)
26	89	11
29	90	9
32.5	88	10

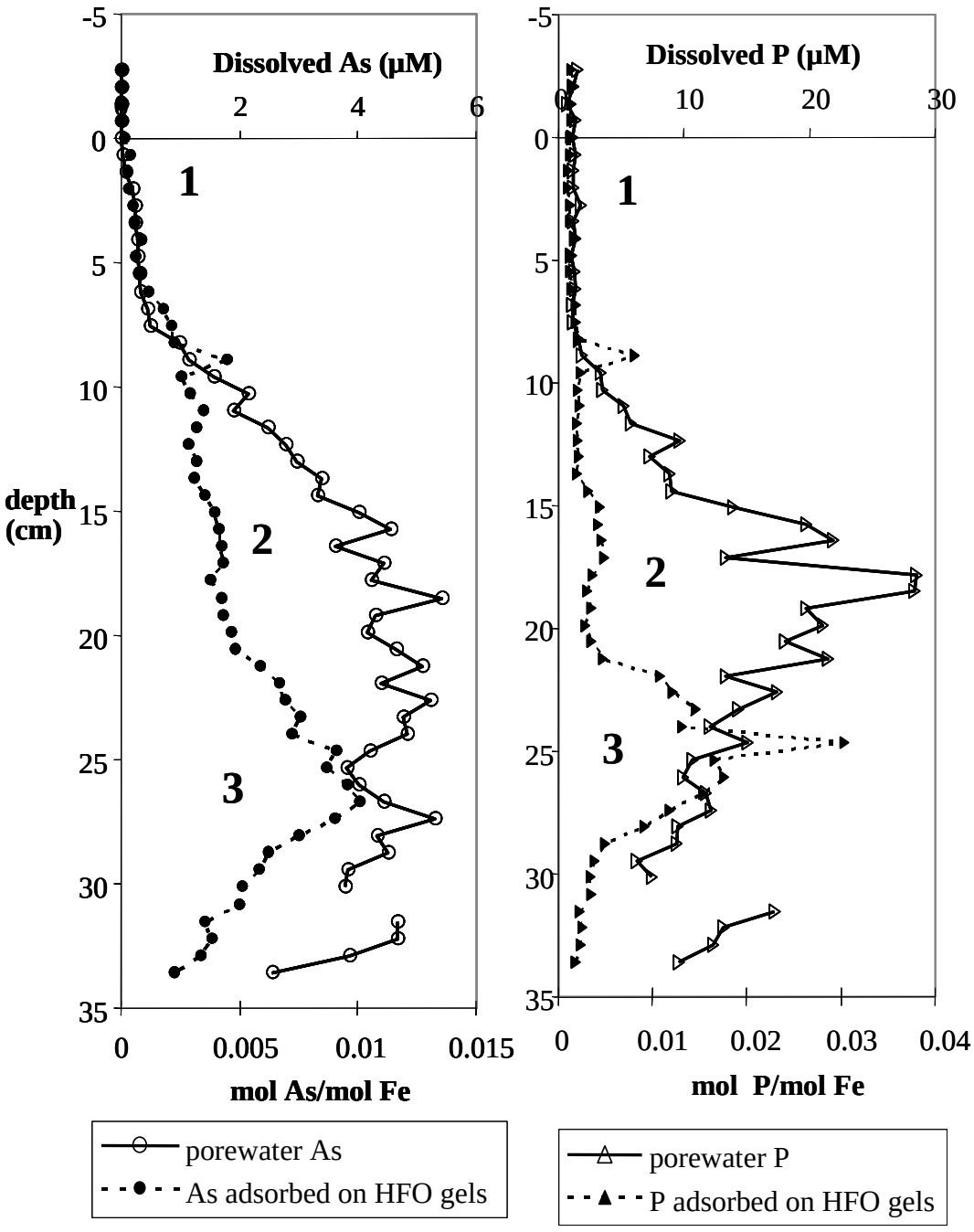

Figure 4.10. Porewater and adsorption profiles for As and P from double probe #1 deployed in October 2004. Region 1 denotes the low porewater concentrations of As and P. Region 2 denotes the region of sorption inhibition onto the HFO-doped gels. Region 3 denotes the region where As and P adsorption on HFO-doped gels increase at depth.

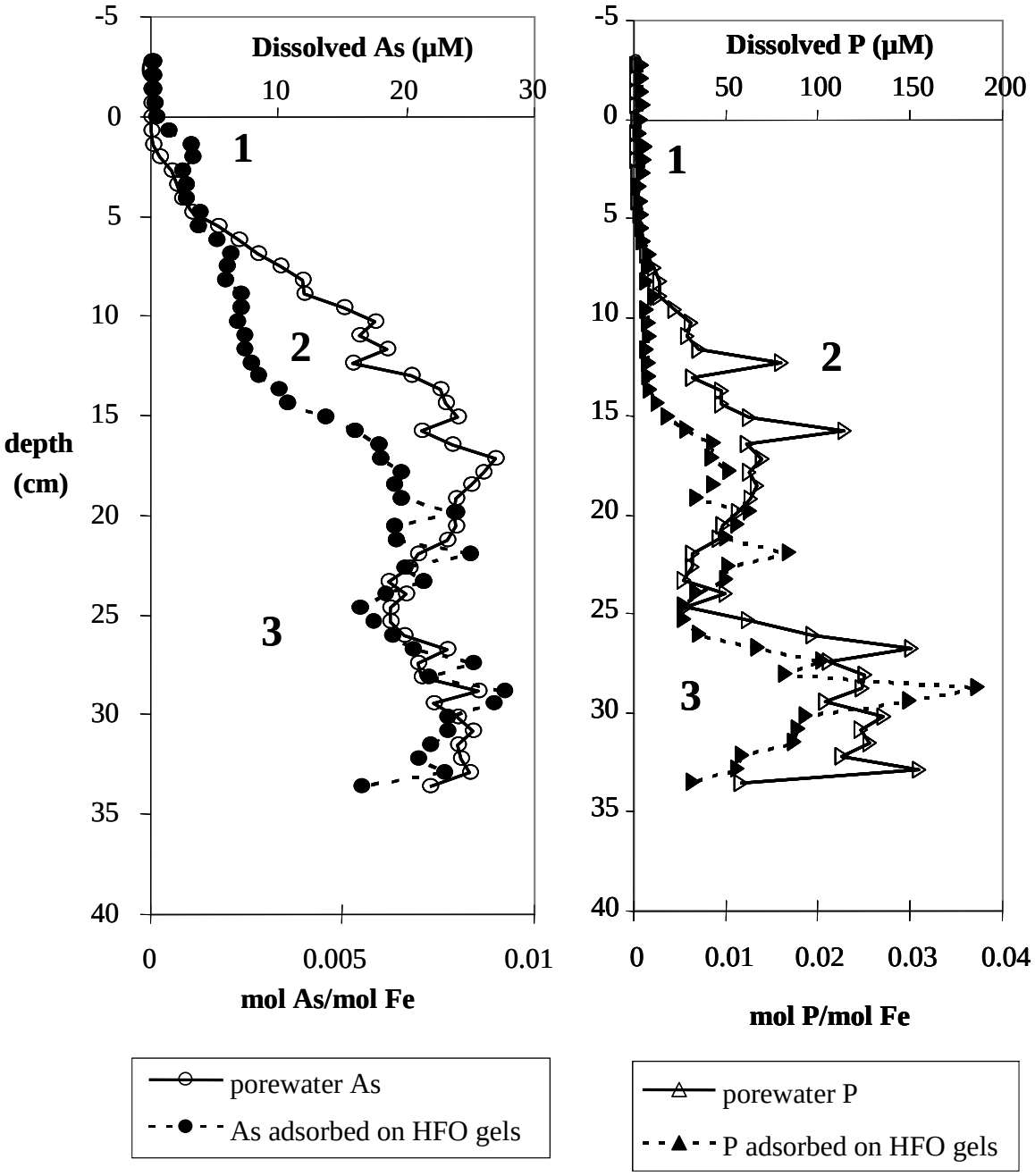

Figure 4.11. Porewater and adsorption profiles for As and P from double probe #2 deployed in October 2004. Region 1 denotes the low porewater concentrations of As and P. Region 2 denotes the region of sorption inhibition onto the HFO-doped gels. Region 3 denotes the region where As and P adsorption on HFO-doped gels increase at depth.

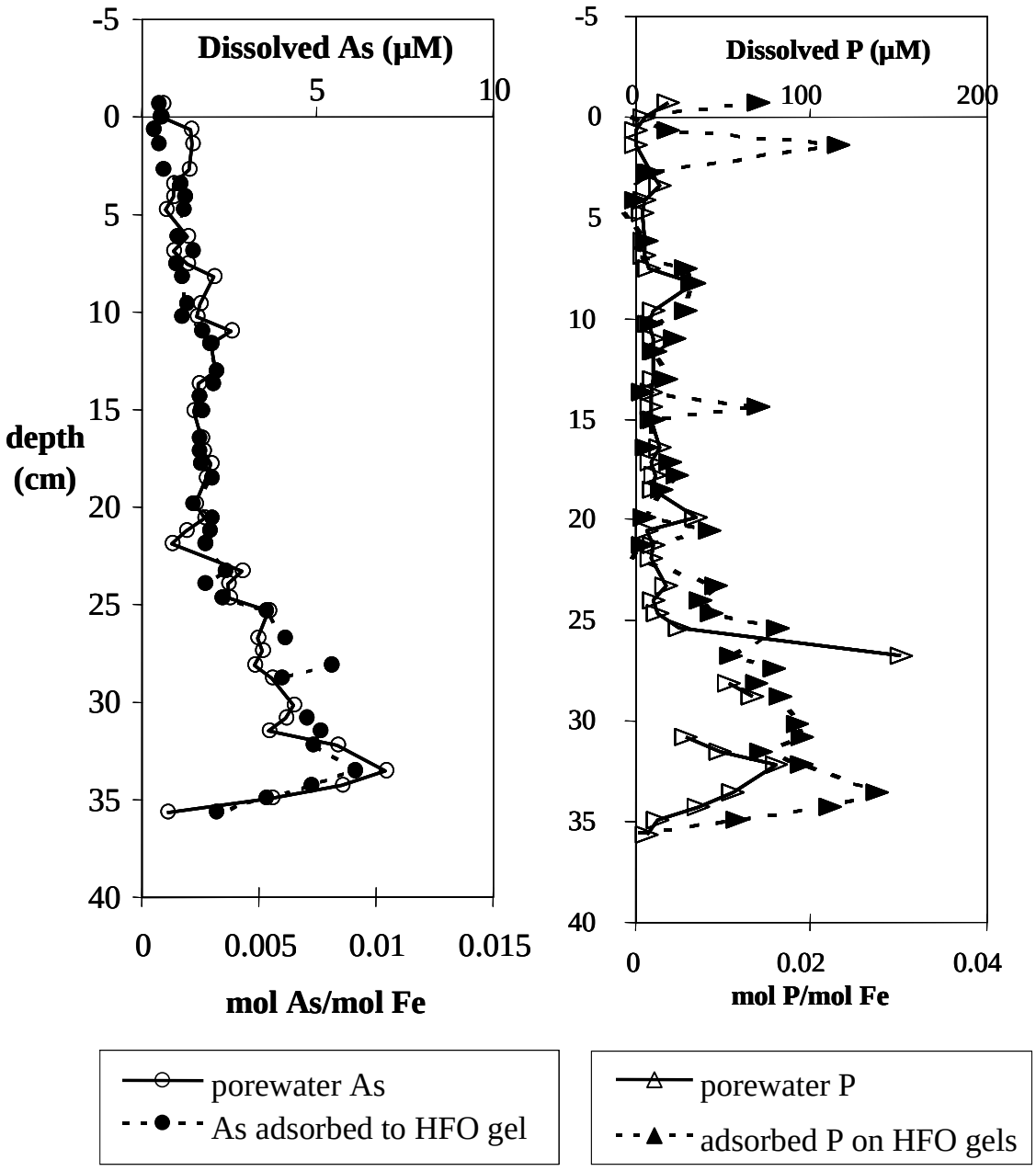

Figure 4.12. Porewater and adsorption profiles for As and P from a double probe deployed in May 2006, when the sediment was hard from recent exposure to air.

The ratio of As/P on the HFO gels is greater than the ratio in the porewaters for all sample dates (Figure 4.13, October 2004 as an example). A similar effect was observed in the competitive phosphate laboratory study, where As was adsorbed onto the HFO-doped gels even at high P concentrations (Chapter 3).

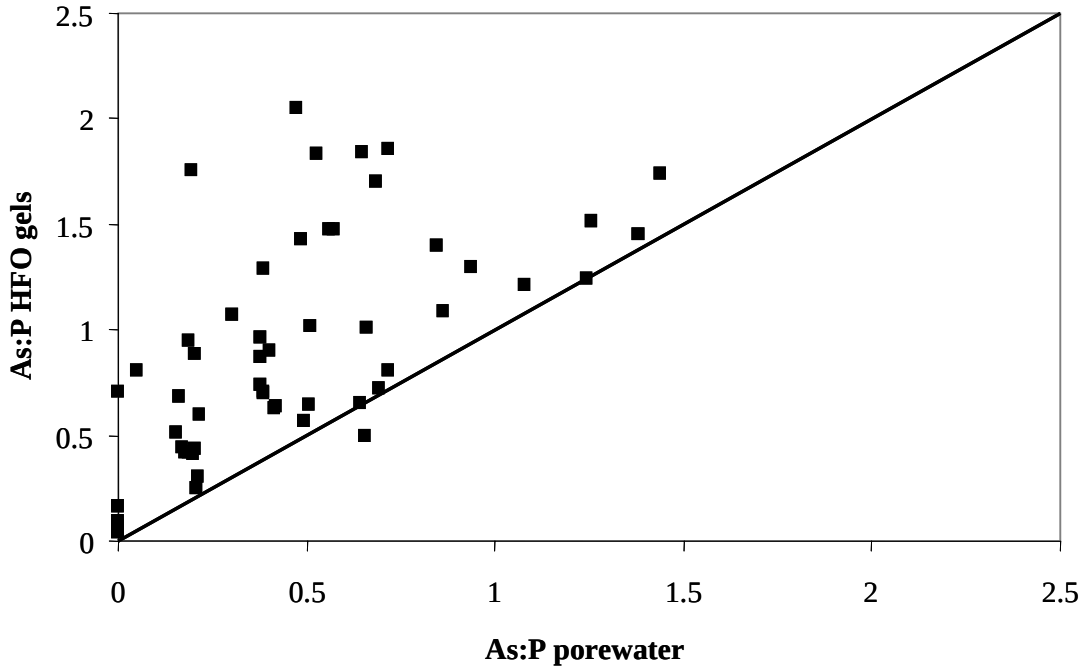

Figure 4.13. The As-to-P ratio in the HFO-doped gels versus in the porewater. The data were taken from double probe #2 from October 2004. The line indicates a perfect correlation between the As-to-P ratio in the gels and porewater.

4.4.5 Results from Sediment Cores

Bulk sediment elemental composition averaged over the sediment column is summarized in Table 4.3. The total Fe and As content is 7.89% and 210 mg/kg, respectively, consistent with previous sediment extractions (Kneebone 2000). The variation between duplicate cores was small (<0.4% for Fe and <7% for As).

Table 4.3. XRF bulk composition of cores from August 2005. Analysis was performed on a composite sample, resulting in an average over the sediment column.

	%		%	ppm		ppm		ppm
SiO2	56.5	**Al**	5.70	--	**Cs**	27.80	**Lu**	0.29
Al2O3	11.3	**Ba**	--	691.00	**La**	33.50	**Mo**	8.00
CaO	2.515	**Ca**	1.64	--	**Nd**	24.55	**Nb**	12.50
MgO	2.275	**Cr**	--	160.00	**Pb**	23.50	**Pr**	6.69
Na2O	2.07	**Cu**	--	57.00	**Be**	--	**Sm**	4.20
K2O	2.47	**Fe**	7.89	--	**Ni**	19.00	**Sn**	15.50
Fe2O3	12.15	**K**	1.93	--	**Sc**	7.50	**Ta**	1.10
MnO	0.1	**Li**	--	70.00	**Ag**	--	**Tb**	0.60
TiO2	0.52	**Mg**	1.27		**Bi**	0.60	**Th**	16.35
P2O5	0.32	**Mn**	--	675.00	**Cd**	0.25	**Tl**	0.60
Cr2O3	0.03	**P**	0.14	--	**Co**	12.00	**Tm**	0.30
LOI	8.90	**Sr**	--	206.00	**Dy**	3.15	**U**	15.80
SUM	99.15	**Ti**	0.28	--	**Er**	1.90	**Y**	18.4
		V	--	171.50	**Eu**	0.82	**Yb**	1.9
		Zn	--	96.00	**Ga**	15.00		
		Zr	--	132.00	**Gd**	4.01		
		As	--	210.00	**Ge**	8.00		
		Ce	--	57.50	**Hf**	4.50		
		Rb	--	121.00	**Ho**	0.65		
		W	--	49.00	**In**	--		

The As XANES edges of sediment core sections show a distinct transition zone between 8-10 cm in August 2005 where the dominant solid phase As species changed from As(V) to As(III) (Figure 4.14). Phosphoric acid extractions of a sediment core corroborate this result (Appendix E). The As(V) redox transition was deeper in the sediment column than observed in a previous study at Haiwee Reservoir, where the transition occurred in the upper 3 cm of sediment (Kneebone 2000).

Dissolved Fe in the porewater was mainly Fe(II), based on porewater extractions from core sections (Figure 4.15). The difference between total Fe and Fe(II) could be dissolved Fe(III) complexed by organic carbon (Ritter et al. 2006), colloidal Fe(III)

caused by bacterially induced deflocculation (Tadanier et al. 2005), or an analytical artifact due to core processing.

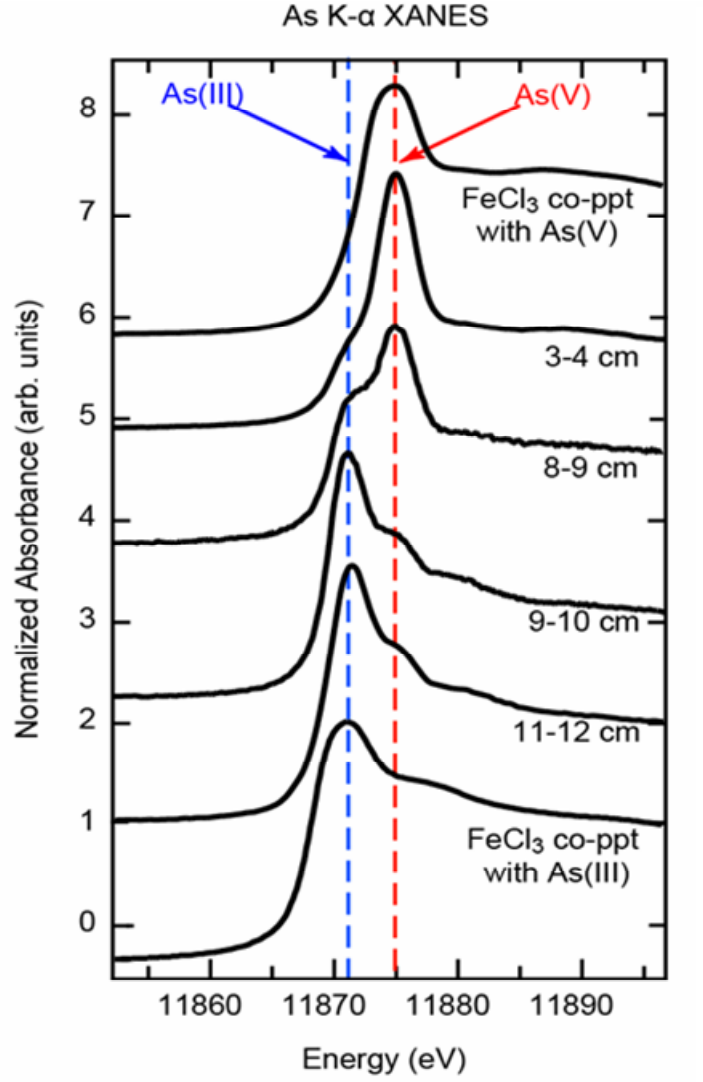

Figure 4.14. Arsenic XANES edges from core sections from August 2005. The As(III) and As(V) reference spectra are As co-precipitated with HFO. Figure courtesy of Rob Root, University of California, Merced.

Solid phase organic carbon decreased with depth (Table 4.4), and ranged from 20-34 g C/kg sediment. Between 75 and 90% of the total solid phase carbon was organic carbon.

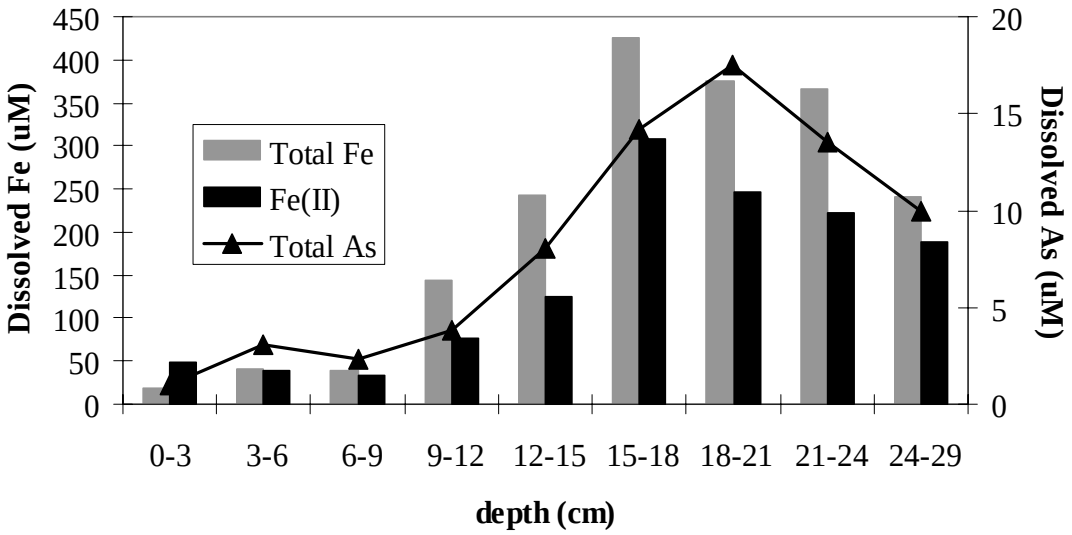

Figure 4.15. Iron and As extractions from sediment core from May 2006 prior to gel probe deployment. The sediment was soft, unlike the May 2006 gel probe deployment. Extractions were performed in an anaerobic chamber with 1% HCl.

Table 4.4. Solid phase total carbon and organic carbon measurements on dry core sections from duplicated cores sampled in August 2005. The organic carbon fraction was obtained by fumigating a dry sample with HCl before analysis.

Core 1	***Total carbon***	***organic carbon***	
depth (cm)	**g C/kg sed**	**g C/kg sed**	**% of total C as organic C**
3-6	40.7	31.6	78
6-9	42.8	32.0	75
9-12	40.3	32.3	80
12-15	25.1	20.7	82
Core 2	***Total carbon***	***organic carbon***	
depth (cm)	**g C/kg sed**	**g C/kg sed**	**% of total C as organic C**
6-9	42.8	33.9	79
9-12	37.9	30.8	81
15-18	29.8	24.3	81
21-29	22.8	20.3	89

4.4.6 Variability

Based on LAA flow data and ferric chloride dosage records, the rate and amount of Fe and As deposited in the inlet channel is not constant. The water level at the sample deployment location changes as flow varies. In addition, the aqueduct is occasionally drained to a minimal flow for repair. The floc deposited in the inlet channel may periodically be exposed to air and resubmerged as the LAA flow varies. Variation in flow also causes erosion and re-deposition of the sediment.

Because water level and floc deposition are not constant, the profiles taken at this site probably do not represent processes that result from uniform sediment aging. The depositional variability may explain the spatial and temporal variations in porewater concentrations and sorption profiles.

Gel probes deployed August 2005 and May 2006 were deployed in sediment that may have been recently exposed to air prior to sampling either due to a drop in aqueduct flow or substantial increase in base flow. The profiles for August 2005 and May 2006 were different from October 2004 with a peak of dissolved As occurring deeper (~20-25 cm, Figure 4.6-4.7) in the sediment rather than a plateau of dissolved As below ~15 cm (Figure 4.4-4.5). In addition, the solid phase As(V) transition was deeper in the sediment column than previous study results when sediment conditions were more similar to the October 2004 sampling.

4.5 Discussion

4.5.1 Equilibration of sediments and porewater

The gel probe sampler used in this study assumes that the gels inside the probe are in equilibrium with the surrounding porewater. For this to be true, one of two conditions must exist. The first condition requires that the amount of As exchanged with or concentrated into the gel is negligible compared to the amount of As in the surrounding porewater. If the first condition is not met, then the sediment must be able to resupply the amount of As lost from the porewaters to re-establish equilibrium within 24 hours. If neither of these conditions is met, then the gel probe will measure a diffusive flux (Zhang et al. 1995). The clear gels satisfy the first condition, since the volume of water inside each gel (~250 μL) is small. The HFO-doped gels do not satisfy the first condition, but the sediment is able to resupply the As to the porewaters within 24 hours, thus satisfying the second condition. The sediment microcosm showed an equilibrium state reached by both clear and HFO-doped gels within 24 hours. In addition, the porewater concentrations measured by a double probe with clear and HFO-doped gels were consistent with porewater extracted from a core (Table 4.1), confirming that the sediment was able to resupply As to the porewaters and equilibrate within 24 hours of deployment.

4.5.2 Effect of dissolved carbonate and green rust formation on As partitioning

Sediment diagenesis has significant implications for As mobilization in Haiwee sediments, since reductive dissolution not only drives As mobilization, but also mineralogical changes in the sediment. In November 2004, core sections analyzed by X-ray absorption spectroscopy (XAS) were found to have significant fractions (≤80%) of

amorphous carbonate green rust below ~15 cm (Root et al. 2006). The presence of green rust indicates that production of Fe(II) from reductive dissolution of the Fe(III) oxide and other chemical conditions was sufficient to transform the primary mineral phase. Mineralogical transitions in the sediment can be seen visually in a fresh core taken from Haiwee in October 2003 (Figure 4.16A). Cores with similar layers were observed in October 2004. The upper layers are red-orange, consistent with amorphous Fe(III) oxyhydroxide. The middle layers (~5-15 cm) are dark brown, indicative of Fe(II) re-adsorption to the Fe(III) surface. Deeper in the sediment column (~15-20cm) there is a layer of grey sediment, which may correlate to the formation of green rust. In August 2005, the sediment does not transition through a dark brown intermediate but changes directly from red-orange to grey at ~20 cm (Figure 4.16B).

Early sediment diagenesis is characterized by the mineralization of organic carbon coupled to the reduction of O_2, nitrate, Mn (III,IV) oxides, and Fe(III) oxides and is usually driven by microbial metabolism (Song and Muller 1999). As organic carbon is oxidized, the dissolved inorganic carbon in the porewaters is expected to increase with depth. Solid-phase organic carbon in Haiwee cores decreased with depth, suggesting that organic carbon was being metabolized, possibly to dissolved inorganic carbon. The presence of dissolved Mn and Fe in the porewaters confirms that diagenetic processes are occurring in the sediment, and these processes are most likely coupled to organic carbon oxidation.

Figure 4.16. Pictures of cores taken from October 2003 (A) and August 2005 (B).

The porewater and sorption profiles for October 2004 can be divided into three regions, as denoted on Figures 4.10-4.11. The surficial sediment (region 1) had negligible dissolved As, P, and Fe concentrations and minimal sorption onto the HFO-doped gels. In this region, fresh floc was being deposited and O_2 diffusing from the overlying water was consumed in the sediment. Between 10-20 cm, the correlation between dissolved As, P, and Fe indicates that reductive dissolution released As and P to the porewaters (region 2). Although the dissolved Fe and As concentrations were constant below ~15 cm, As and P adsorption onto the HFO-doped gels did not peak until

20-30 cm (region 3). The result is a region between 10-20 cm where dissolved As and P increased in the porewaters but As and P did not adsorb onto the HFO-doped gels, indicative of As and P sorption inhibition (region 2). Region 3 correlates to the depth where carbonate green rust was measured, as well as where the grey sediment layer was observed.

Inorganic carbon has been shown to inhibit As adsorption to Fe(III) oxides at concentrations of ~4 mM (Radu et al. 2005), which is possible in microbially active sediments. Elevated concentrations of dissolved carbonate from organic carbon mineralization may inhibit the re-adsorption of As and P onto the HFO-doped gels in region 2. Deeper in the sediment column, the formation of carbonate green rust may sequester enough of the dissolved carbonate to allow As and P to adsorb to the HFO-doped gels (region 3).

The sediment in August 2005 and May 2006 may have been exposed to air, and gel probes deployed on these dates exhibited slightly different porewater and sorption profiles than October 2004. In May 2006, there was a strong correlation between dissolved As and P concentrations and adsorption to HFO-doped gels even as As and P concentrations increased sharply between 25-35 cm. It is possible that due to the oxidative changes in the sediment, region 2 was absent because reductive dissolution in the upper layers (0-20 cm) had not progressed to the same extent as in October 2004. This result is corroborated by the visual transition directly from red-orange to grey sediments at ~25 cm in a core from August 2005.

4.5.3 Effect of P on As adsorption

The adsorption behavior of As onto the HFO-doped gels in region 3 (20-35 cm) in October 2004 and May 2006 is consistent with the competitive sorption effects of phosphate. An operationally-defined partition coefficient for sorption onto HFO-doped gels was calculated with equation (4.1).

$$K_D^{*} = \frac{\left(mol_{As} / mol_{Fe}\right)_{HFOgel}}{[As_{dissolved}]_{porewater}} \tag{4.1}$$

where the concentration of dissolved total As is expressed in mol/L. Although this is not a true partition coefficient, it is useful for comparing HFO-doped gel data from field deployments and laboratory experiments. K_D^{*} values are valid only when the amount of As adsorbed to the HFO is far from surface site saturation. The plots of K_D^{*} as a function of depth for the field deployments in October 2004 and May 2006 are shown in Figure 4.17 A, B. The K_D^{*} values for Figure 4.11 (October 2004, double probe #2) have not been included because the dissolved As concentrations are >20 μM. Based on sorption isotherms from Chapter 3, when As concentrations are >20 μM, As sorption is close to surface site saturation where K_D^{*} is not valid.

The large K_D^{*} values at shallow depths are due to low dissolved As concentrations. The K_D^{*} values deeper in the sediment column range from 1500-2500 when the maximum dissolved P concentrations are 150-200 μM. For comparison, K_D^{*} as a function of phosphate concentration is plotted in Figure 4.18, using data from the competitive phosphate study presented in Chapter 3. When phosphate concentrations are 150-200 μM in the laboratory study, K_D^{*} values are approximately 1500-2000 for As(V) and 2000-2800 for As(III). The agreement between the laboratory and field values for

K_D^* suggest that phosphate controls the amount of As adsorbed onto the surface of HFO-doped gels in the field in region 3 (20-35 cm).

In the competitive phosphate study from Chapter 3, phosphate inhibited As(V) sorption onto HFO-doped gels to a greater extent than As(III). In May 2006, 80% of the dissolved As in the porewater was present as As(III), but As(III) comprised >90% of the As adsorbed onto the HFO-doped gels. The enrichment of adsorbed As(III) on the HFO surface supports the hypothesis that phosphate controls As re-adsorption at depth (20-35 cm).

4.5.4 Conclusions

Reductive Fe(III) dissolution in the sediments at Haiwee Reservoir causes the release of As and P into the porewaters and drives the mineralogical change to green rust deeper in the sediment column. The mineralization of organic carbon may cause increased concentrations of dissolved inorganic carbon, which inhibits As re-adsorption onto the HFO-doped gels. This implies that As accumulation into the porewater may be at least partially controlled by porewater composition rather than available sorption sites on the sediment. Green rust formation may sequester dissolved carbonate, allowing As and P adsorption to the HFO-doped gels. The amount of As adsorbed onto the HFO-doped gels in this region is controlled by the competitive effects of P. This suggests that the elevated dissolved As concentrations at depth may be due to the lack of available surface sites as the amorphous Fe(III) oxides convert to green rust.

This study illustrates a novel way to measure the effect of porewater composition on As re-adsorption upon reductive dissolution using an HFO-doped gel probe

equilibrium sampler. Combined with core measurements, the complex mechanisms that control As partitioning between the solid and dissolved phases in sediment systems can be observed in the field.

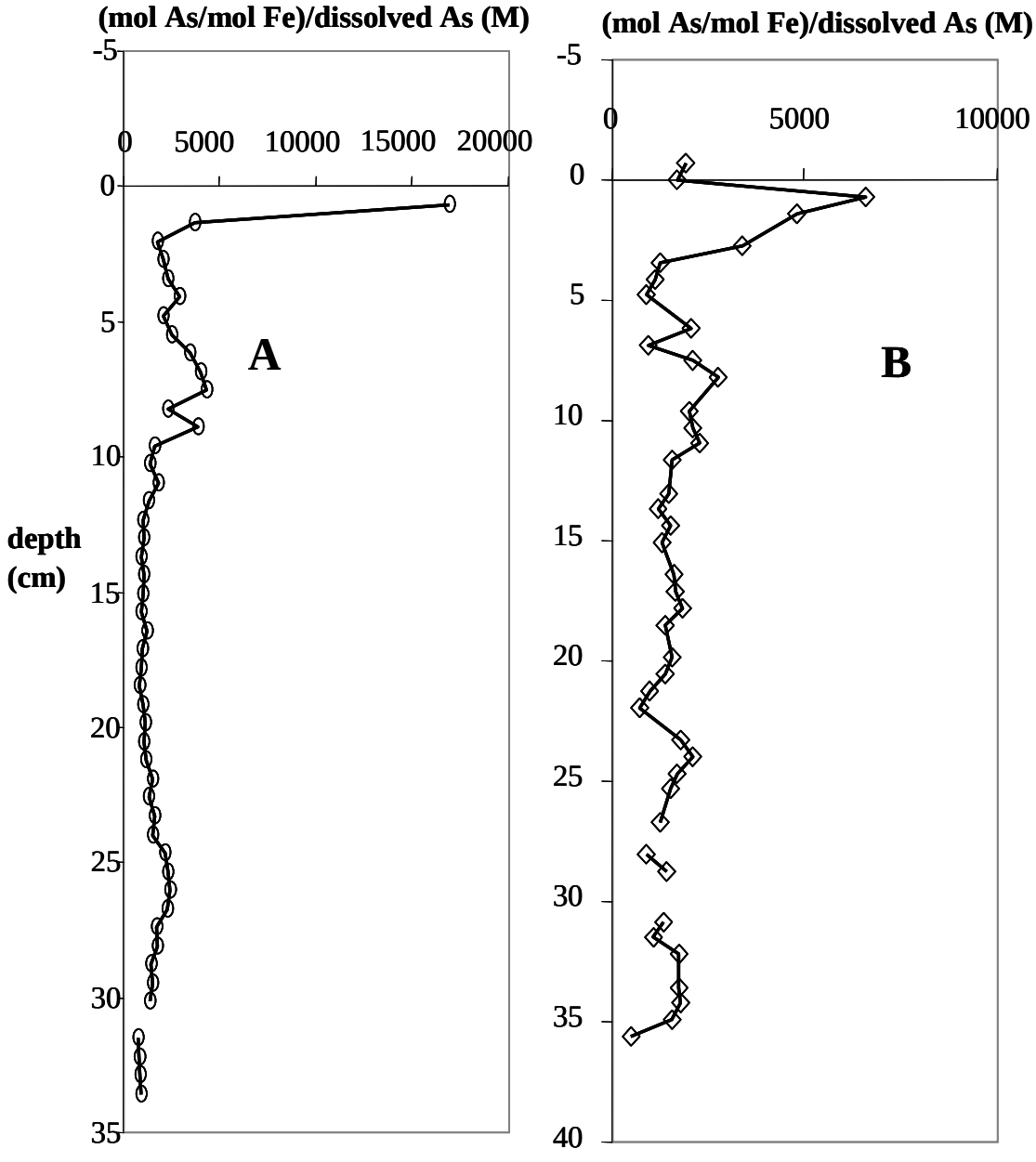

Figure 4.17. K_D^* plots for October 2004 double probe #1 (A) and May 2006 (B).

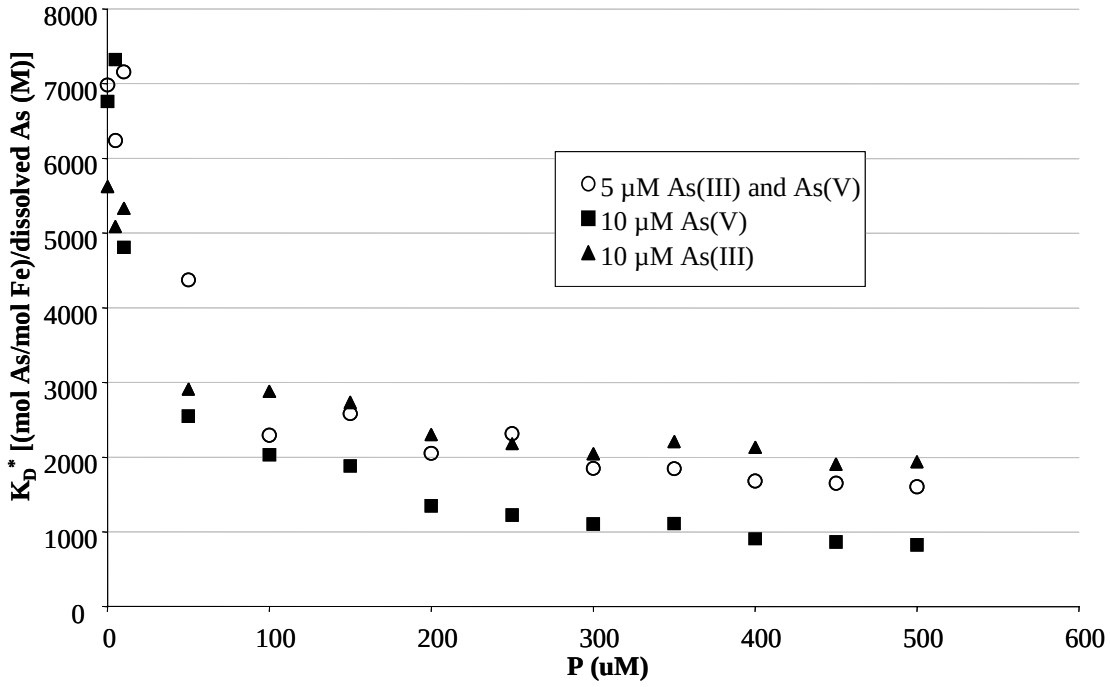

Figure 4.18. K_D^* plot for the laboratory study of the competitive effects of phosphate on As adsorption (data presented in Chapter 3). In each case, the total As concentration was 10 µM.

4.6 Acknowledgement

This work was done in collaboration with Rob Root and Dr. Peggy O'Day. The As XANES edges on core sections and the quantification of As species on HFO-doped gels were performed by Rob Root. This work was supported by funding from NSF BES-0201888 and EAR-0525387. We thank the Los Angeles Department of Water and Power (LADWP), particularly Gary Stolarik, Stanley Richardson and Fred Richardson, for access to Haiwee Reservoir. We also thank Nathan Dalleska for analytical support and Mike Vondrus for gel probe construction.

Chapter 5

Simultaneous Microbial Reduction of Iron(III) and Arsenic(V) in Suspensions of Hydrous Ferric Oxide

***** Adapted from Campbell, et al. 2006. *Environmental Science and Technology*, vol. 40, no. 19, pp 5950-5955.

5.1 Abstract

Bacterial reduction of arsenic(V) and iron(III)-oxides influences the redox cycling and partitioning of arsenic (As) between solid and aqueous phases in sediment-porewater systems. Two types of anaerobic bacterial incubations were designed to probe the relative order of As(V) and Fe(III)-oxide reduction and to measure the effect of adsorbed As species on the rate of iron reduction, using hydrous ferric oxide (HFO) as the iron substrate. In one set of experiments, HFO was pre-equilibrated with As(V) and inoculated with fresh sediment from Haiwee Reservoir (Olancha, CA), an As-impacted field site. The second set of incubations consisted of HFO (without As), As(III)- and As(V)- equilibrated HFO incubated with *Shewanella* sp. ANA-3 wild-type (WT) and ANA-3Δ*arrA*, a mutant unable to produce the respiratory As(V) reductase. Of the two pathways for microbial As(V) reduction (respiration and detoxification), the respiratory pathway was dominant under these experimental conditions. In addition, As(III) adsorbed onto the surface of HFO enhanced the rate of microbial Fe(III) reduction. In the sediment and ANA-3 incubations, As(V) was reduced simultaneously or prior to Fe(III),

consistent with thermodynamic calculations based on the chemical conditions of the ANA-3 WT incubations.

5.2 Introduction

Arsenic (As) causes severe health effects when ingested, and evidence for this type of poisoning is apparent in countries such as Bangladesh, where millions of people are affected by drinking As-contaminated groundwater (NRC 1999; NRC 2001; Nordstrom 2002; Smedley and Kinniburgh 2002). In Bangladesh and many other As-impacted areas, As commonly co-occurs with iron (Fe) minerals in sediments as an adsorbed species, and the fate of Fe and As are often closely linked (McGeehan and Naylor 1994; Dixit and Hering 2003; Akai et al. 2004). As mobility can be affected by redox chemistry (i.e., the cycling between the +III and +V oxidation states), and also by sediment transformations, particularly the reductive dissolution of Fe(III) (hydr)oxides.

Microorganisms can mediate redox cycling of both As and Fe (Newman et al. 1998; Nickson et al. 2000; Oremland and Stolz 2003). Microbially-driven As redox transformations have been observed in laboratory and field studies (Ahmann et al. 1997; Zobrist et al. 2000; Oremland and Stolz 2003; Islam et al. 2004). There are two known microbial pathways for reduction of As(V) to As(III). The respiratory pathway (*arrA* pathway) couples the oxidation of an organic substrate to As(V) reduction, resulting in cell growth (Cervantes et al. 1994; Laverman et al. 1995; Dowdle et al. 1996; Newman et al. 1998; Malasarn et al. 2004). The detoxification pathway (*arsC* pathway) is used by the cell to convert As(V) to As(III), which is actively transported out of the cell; this process requires ATP (Cervantes et al. 1994).

Dissimilatory Fe reducing bacteria (DIRB) are wide-spread and considered to be the primary agent in the reductive dissolution of Fe minerals in sedimentary environments (Lovley et al. 1991; Smedley and Kinniburgh 2002; Akai et al. 2004). Less crystalline Fe phases with higher surface areas are more susceptible to biological reduction (Roden and Zachara 1996; Jones et al. 2000; Roden 2003; Hansel et al. 2004; Roden 2004). Furthermore, rates of reductive dissolution are affected by Fe mineralogy and accumulation of Fe(II) reaction products. As the parent mineral is reduced, reaction products, including sorbed or precipitated Fe(II), accumulate on the mineral surface, slowing the reduction rate (Urrutia and Roden 1998; Urrutia et al. 1999; Hansel et al. 2004; Roden 2004; Royer et al. 2004). The observed rates and products of these microbial reactions depend on experimental conditions such as bacterial strain, initial Fe mineral, and flow-through or batch incubation.

The amount of As released into solution due to the bacterial reductive dissolution of Fe (hydr)oxides has been shown to depend on As oxidation state and Fe mineralogy (Ahmann et al. 1997; Langner and Inskeep 2000; Zobrist et al. 2000; Islam et al. 2004; van Geen et al. 2004; Herbel and Fendorf 2005). The oxidation state of As at the onset of Fe reduction is crucial to As mobility, since As(V) and As(III) sorption and complexation can be significantly different at environmentally relevant pH values when competing sorbates, such as phosphate, are present (Dzombak and Morel 1990; Dixit and Hering 2003). As a result, whether As(V) is reduced prior to Fe(III) may partially determine the amount of As mobilized into sediment porewaters. In addition, while the rates of Fe(III) and As(V) reduction are affected by Fe mineralogy, the effect of adsorbed As species on rates of Fe reduction has not been investigated.

This study addresses the relative order of microbial As(V) and Fe(III) reduction, as well as the effect of sorbed As species on rates of Fe reduction. Two microcosm studies were performed with a synthetic iron oxyhydroxide slurry and incubated with bacteria from two types of microbial inocula. One inoculum was fresh sediment containing the ambient microbial community from Haiwee Reservoir (Olancha, CA), where Fe- and As-rich sediment have been deposited as a result of *in situ*, full-scale water treatment (Kneebone 2000; Kneebone et al. 2002). Arsenic in Haiwee sediment is primarily adsorbed to a poorly crystalline Fe(III) oxyhydroxide phase. Iron and As in the sediment porewaters are strongly correlated, consistent with reductive dissolution. In the solid phase, As(V) was detectible only in the surficial sediment with As present as As(III) throughout the sediment column (Kneebone et al. 2002; Malasarn et al. 2004). The other type of inoculum was a well-studied laboratory strain, *Shewanella* sp. strain ANA-3 wild-type (WT), and a mutant strain with a deletion of the *arrA* gene. ANA-3 WT is capable of both Fe and arsenate reduction. ANA-3 is a reasonable model organism since an isolate of native arsenate-reducing bacteria from Haiwee Reservoir sediments was found to be a strain of *Shewanella* bacteria, also capable of Fe and As reduction (unpublished data).

Inocula of Haiwee sediment or ANA-3 were incubated with hydrous ferric oxide (HFO), an amorphous Fe(III) oxyhydroxide similar to the Fe phase in Haiwee Reservoir sediments (Kneebone et al. 2002; Cooper et al. 2005). For experiments with Haiwee sediment inoculum, HFO was equilibrated with As(V) prior to inoculation and experiments were conducted with varying organic substrates (lactate, acetate, or no added organic carbon). For experiments with ANA-3, HFO was equilibrated with either As(V)

or As(III) before inoculation or used without exposure to As. The order of microbial As(V) and Fe(III) reduction, the effects of organic substrates on As(V) and Fe(III) reduction, and the effect of adsorbed As(V) and As(III) on microbial Fe(III) reduction were examined.

5.3 Materials and Methods

5.3.1 Reagents

All chemicals used were reagent grade and used without further purification. Solutions were prepared with 18 MΩ-cm deionized water (Barnstead, Nanopure infinity) and stored in plastic containers that had been washed in 10% oxalic acid. For bacterial incubations, all solutions were autoclaved before use with the exception of the bicarbonate buffer, which was filter-sterilized (0.2 µm pore size) and added to the autoclaved medium. The bacterial minimal growth medium (Appendix C) was buffered with 50 mM bicarbonate and had a total phosphate concentration of 50 µM and an ionic strength of 0.06 M.

5.3.2 Preparation of HFO and As-equilibrated HFO

HFO was prepared by the drop-wise addition of 0.5 M NaOH to 0.05 M $Fe(NO_3)_3$ until the solution stabilized at pH 8 (Schwertmann and Cornell 1991). The suspension was equilibrated for >3 h under constant stirring, adjusting any pH drift as necessary with 0.5 M NaOH. The HFO was then washed three times with sterile water and centrifuged

at 7000×g for 10 minutes. The HFO was not autoclaved after synthesis to avoid changes in mineralogy.

After the final wash, the HFO was resuspended in an As solution and equilibrated overnight with constant stirring. For the sediment incubations, 15 g of HFO was resuspended in 1 L of 0.05 M Na_2HAsO_4 (Sigma) at pH 7.2. For the ANA-3 incubations, 5 g of HFO was suspended in 0.5 L of 0.02 M Na_2HAsO_4 and 3 g of HFO was suspended in 0.5L of 0.02 M $NaAsO_2$ (Sigma) at pH 8.0. These conditions ensured that all available surface sites for As sorption were saturated with As at the given pH. In all cases, the HFO was washed twice with sterile water to remove excess As that was not sorbed and resuspended in bacterial minimal medium to a final slurry composition summarized in Table 5.1. The pH was adjusted to 7.2 for the sediment incubations, and pH 8 for the ANA-3 incubations with 0.5 M NaOH prior to inoculation. In the case of HFO without any adsorbed As, the solid was resuspended directly in bacterial medium after the initial washing and adjusted to pH 8. Uninoculated controls were maintained over the course of the experiment to ensure that no contamination was introduced in the synthesis, washing, distribution, and sampling of the HFO slurries.

5.3.3 Incubation Experiments

The HFO suspension was transferred under sterile conditions to acid-washed and autoclaved plastic bottles with a screw-cap lid; 200 mL of HFO slurry was added to each bottle. The bottles were transferred to an anaerobic chamber (80% N_2, 15% CO_2, 5% H_2) and equilibrated for 24 h with the lid loosely covering the bottle mouth to allow for passive gas exchange before inoculation. The bottles were inoculated in the anaerobic

chamber and then incubated in the dark at 30°C in the anaerobic chamber for the remainder of the experiment. The bottles were not stirred during incubation, but were shaken vigorously prior to each sampling. All experiments were repeated in triplicate. In each experiment, an additional bottle was left uninoculated as a control, and sampled in an identical manner.

Table 5.1. Summary of Experimental Conditions

Inoculum	Solid	mol_{As} per g_{HFO}	Solid-to-Solution ratio (g/L)	pH	Carbon Source	Carbon (mM)
Haiwee Sediment	HFO/As(V)	0.002	2.0	7.2	Lactate	19
	HFO/As(V)	0.002	2.0	7.2	Acetate	17
	HFO/As(V)	0.002	2.0	7.2	No carbon added	0
Shewanella sp. strain ANA-3 WT	HFO/As(V)	0.001	2.8	8.0	Lactate	14
	HFO/As(III)	0.003	2.7	8.0	Lactate	14
	HFO/no As	—	1.9	8.0	Lactate	14
Shewanella sp. strain ANA-3 *ΔarrA*	HFO/As(V)	0.001	2.8	8.0	Lactate	14

5.3.3.1 Incubations with Haiwee Sediment

Bacterial minimal medium was amended with lactate, acetate, or left unamended (no added carbon source). The slurry consisted of HFO pre-equilibrated with As(V). The bottles were inoculated with fresh sediment from Haiwee Reservoir (2 g wet sediment/200 mL slurry), extracted from a core (5-10 cm depth) and homogenized in the

anaerobic chamber. Control bottles consisted of inoculation with pasteurized sediment or autoclaved sediment, but both controls showed both As and Fe reduction. Formaldehyde prevented further reduction in autoclaved sediment control bottles (data not shown), suggesting that the reduction was microbially catalyzed. Uninoculated bottles did not show evidence of growth. Aliquots were taken from the bottles approximately every 12 h for 112 h, and analyzed as described below.

5.3.3.2 Incubations with ANA-3

Incubations were also performed using a laboratory isolate, *Shewanella* sp. strain ANA-3 WT, and mutant ANA-3Δ*arrA*, which has a deletion of the respiratory *arrA* gene (Saltikov and Newman 2003). Slurries were prepared with HFO with adsorbed As(V), HFO with adsorbed As(III), or HFO only (no As). ANA-3 WT was inoculated into bottles with HFO/As(V), HFO/As(III) and HFO. The ANA-3 Δ*arrA* mutant was inoculated into bottles containing HFO/As(V), as a control for respiratory arsenate reduction. Lactate was included in all bottles as the electron donor. Bottles were inoculated with 10^5 total cells initially, corresponding to 500 cells/mL. Samples were taken approximately every 12 h for 131 h. The pH was monitored with pH indicator strips (EM, ColorpHast) at the time of each sampling.

5.3.4 Analytics

At each time point, samples were removed from the bottles and processed as follows. For determination of dissolved concentrations, 1 mL of sample was filtered through a microcentrifuge filter with a 0.2 µm pore size (Costar, nylon Spin-x) in the glove box; filtered samples were analyzed for lactate, acetate, As(III), As(V), Fe(II), and

total dissolved Fe. For determination of total concentrations, 20 µL of concentrated phosphoric acid was added to 1 mL of sample to dissolve the HFO. Ten µL of sample was added to 90 µL of 1 M HCl in a 96-well plate for total Fe(II) analysis and the remainder of the sample was analyzed for lactate, acetate, As(III), and As(V). At the first and last time point, an additional 0.375 mL of slurry was removed and acidified for total Fe analysis. Total and dissolved Fe(II) and total Fe (Fe(II) + Fe(III)) were measured by the ferrozine method (Stookey 1970) on a 96-well plate prepared in the anaerobic chamber, and analyzed immediately. The limit of detection for all iron analysis was 10µM. All other samples were frozen at -80°C until analysis by high performance liquid chromatography (HPLC, Waters 2487 detector, 715plus autosampler, 515 HPLC pump). HLPC analysis was conducted using a Hamilton PRP-X300 column in series with a BioRad Aminex HPX-87H column, heated to 50°C, with a 30 mM phosphate mobile phase at 0.6 mL/min flow rate. As(V), As(III), lactate and acetate were detected by absorbance at 210 nm. The detection limit for As(III) and As(V) was 100 µM.

A sediment core was sectioned anoxically and dried at 70°C for 2 days. The dry sediment was fumigated with HCl in a desiccator for 8 hours to remove inorganic carbon. The residue was then analyzed for organic carbon by CHN analysis (University of California Davis Stable Isotope Facility).

5.3.5 Thermodynamic calculations

The thermodynamic driving force (ΔG) for both arsenate reduction and Fe reduction coupled to lactate oxidation was calculated based on experimental conditions observed in the ANA-3 WT/HFO/As(V) time course. The coupled reactions of arsenate

or iron reduction to lactate oxidation were obtained from the appropriate redox half reactions with dominant dissolved species at pH 8 (Table 5.2).

Table 5.2. Reactions and constants used for thermodynamic calculations. Constants were taken from reference (Latimer 1952).

Redox Half Reactions	**log K**	**ΔG^0 (kJ/mol)**
$CH_3CHOHCOO^- + 2H_2O = 5H^+ + CH_3COO^- + HCO_3^- + 4e^-$	-5.81	
$am\text{-}Fe(OH)_{3(s)} + e^- + 3H^+ = Fe^{2+} + 3H_2O$	16.2	
$HAsO_4^{2-} + 4H^+ + 2e^- = H_3AsO_3 + H_2O$	28.21	
Coupled Reactions		
$CH_3CHOHCOO^- + 2\ HAsO_4^{2-} + 3H^+ = CH_3COO^- + HCO_3^- + 2H_3AsO_3 + 2\ H_2O$	50.41	-287.2
$4\ am\text{-}Fe(OH)_{3(s)} + CH_3CHOHOO^- + 7H^+ = 4\ Fe^{2+} + CH_3COO^- + HCO_3^- + 10H_2O$	58.99	-336.24

Values of ΔG at 25°C were calculated from the expression:

$$\Delta G = \Delta G^0 + RT(\ln 10) \log Q = \Delta G^0 + 5.7081 \log Q \quad (5.1)$$

where

$$Q_1 = \frac{[CH_3COO^-][HCO_3^-][H_3AsO_3]^2}{[CH_3CHOCHOO^-][HAsO_4^{2-}]^2\{H^+\}^3} \quad (5.2)$$

for the As(V) reduction reaction, and

$$Q_2 = \frac{[CH_3COO^-][HCO_3^-][Fe^{2+}]^4}{[CH_3CHOCHOO^-]\{H^+\}^7} \quad (5.3)$$

for the HFO reduction reaction, where the activity of HFO is assumed to be 1, and $\{H^+\}$ corresponds to the measured pH. Total concentrations (dissolved plus adsorbed) of As(V), As(III), lactate, acetate, and Fe(II) were measured at each time point. Total lactate and acetate concentrations were directly substituted into the equations, since their

total and dissolved concentrations were approximately equal. The pH remained between 7.9-8.1 for the entire incubation, and therefore $\{H^+\}$ was assumed to be 10^{-8} for all time points. The bicarbonate concentration was assumed to be constant and in equilibrium with the $CO_{2(g)}$ present in the glove box gas mixture at pH 8. The ionic strength was 0.06 M.

Since dissolved concentrations of H_3AsO_3, $HAsO_4^{2-}$, and Fe^{2+} were below the detection limits of the analytical methods, MINEQL+ (Schecher and McAvoy 1998) was used to calculate these concentrations based on experimental measurements.

Fe_T was determined at t=0. Fe(III) at each time point was determined by:

$$Fe(III) = Fe_T - Fe(II) \quad (5.4)$$

From Dzombak and Morel (Dzombak and Morel 1990), $[\equiv Fe^{wk}OH] = 0.2\ Fe_T$ and $[\equiv Fe^{st}OH] = 0.005\ Fe_T$ and the specific surface area for HFO is assumed to be 600 m^2/g. The value of $0.2 mol_{sites}/mol_{Fe}$ is a general average, with values for arsenic sorption between 0.05-0.18 mol_{sites}/mol_{Fe}. Based on isotherm studies (Chapter 3) with HFO synthesized identically to this study, $0.12 mol_{sites}/mol_{Fe}$ more accurately describes the sorption site capacity for arsenic in this system. Assuming that the ratio of strong-to-weak sites is the same as the general value from Dzombak and Morel (i.e., $[\equiv Fe^{st}OH] / [\equiv Fe^{wk}OH] = 0.025$), the site density is:

$$[\equiv Fe^{wk}OH] = 0.117\ Fe_T \quad (5.5)$$

$$[\equiv Fe^{st}OH] = 0.0029\ Fe_T \quad (5.6)$$

Only ferrihydrite was allowed to precipitate in the model. The ionic strength was calculated from the bacterial medium salts concentration, and was found to be 0.06M.

The double-layer FeOH sorption model was used to calculate the amount of sorbed and dissolved As(V), As(III), and Fe(II) species at each time point. The intrinsic surface complexation constants used in the model are given in Table 5.3. Activity coefficients were calculated in MINEQL+, using the Davies equation correction for ionic strength. The contribution of lactate and acetate complexation are neglected in these calculations, since complexation with As(III), As(V), and Fe(II) species is weak (Urrutia and Roden 1998).

Table 5.3. Intrinsic surface complexation constants used in the MINEQL+ model

Surface Reaction	**log K** (I = 0 M, 25°C)	**Reference**
As(V) reactions		
$\equiv FeOH + AsO_4^{3-} + 3H^+ = \equiv FeH_2AsO_4 + H_2O$	29.31	(Dzombak and Morel 1990)
$\equiv FeOH + AsO_4^{3-} + 2H^+ = \equiv FeHAsO_2^- + H_2O$	23.51	(Dzombak and Morel 1990)
$\equiv FeOH + AsO_4^{3-} = \equiv FeOHAsO_4^{3-}$	10.58	(Dzombak and Morel 1990)
As(III) reactions		
$\equiv FeOH + AsO_3^{3-} + 3H^+ = \equiv FeH_2AsO_3 + H_2O$	38.76	(Dzombak and Morel 1990)
Fe(II) reactions		
$\equiv Fe^{wk}OH + Fe^{2+} = \equiv Fe^{wk}OFe^+ + H^+$	-2.98	(Appelo, Van der Weiden et al. 2002)
$\equiv Fe^{st}OH + Fe^{2+} = \equiv Fe^{st}OFe^+ + H^+$	-0.95	(Appelo, Van der Weiden et al. 2002)
$\equiv Fe^{wk}OH + Fe^{2+} = \equiv Fe^{wk}OFeOH + 2H^+$	-11.55	(Appelo, Van der Weiden et al. 2002)

Table 5.4. Concentrations of species used in thermodynamic calculations (pH=8.0)

Time	As(V)		As(III)		Fe(II)		Lactate	Acetate	HCO_3^-	H^+
	As^V_{total} measured (M)	$H_2AsO_4^-{}_{(aq)}$ calculated (M)	As^{III}_{total} measured (M)	$H_3AsO_{3(aq)}$ calculated (M)	Fe^{II}_{total} measured (M)	$Fe^{2+}_{(aq)}$ calculated (M)	measured (M)	measured (M)	calculated (M)	measured (M)
19	2.1×10^{-3}	5.0×10^{-4}	2.3×10^{-4}	6.5×10^{-7}	2×10^{-4}	1.4×10^{-7}	1.4×10^{-2}	2.2×10^{-4}	1.0×10^{-1}	1×10^{-8}
35	5.0×10^{-4}	1.1×10^{-6}	1.8×10^{-3}	3.2×10^{-6}	1.3×10^{-3}	8.2×10^{-6}	1.2×10^{-2}	1.8×10^{-3}	1.0×10^{-1}	1×10^{-8}
59	4.1×10^{-4}	1.7×10^{-8}	1.9×10^{-3}	4.4×10^{-6}	1.9×10^{-3}	2.7×10^{-5}	1.2×10^{-2}	2.3×10^{-3}	1.0×10^{-1}	1×10^{-8}

5.4 Results

The two experimental time courses in this study were designed to investigate the effects of organic substrates on As(V) and Fe(III) reduction and adsorbed As species on the rate of Fe(III) reduction. Dissolved concentrations of Fe and As were undetectable throughout the course of both microcosm experiments. Thus, Fe(II), As(V), and As(III) were predominantly associated with the solid phase.

5.4.1 Incubations with Haiwee Sediment

Both As(V) and Fe(III) were reduced in all of the incubations inoculated with Haiwee sediment (Figure 5.1). Reduction of As(V) began before Fe(III) reduction and ceased after 40-60 h in the lactate- and acetate-amended bottles. Even though the rate and extent of reduction varied with carbon amendment, the onset of As(V) reduction preceded Fe(III) reduction in all cases. For part of the time course, reduction of As(V) and Fe(III) proceeded simultaneously, after which As(V) reduction ceased and Fe(III) reduction continued until the termination of the experiment.

The rate and extent of As(V) and Fe(III) reduction depended on the type of organic substrate, with the greatest amount of reduction occurring in the lactate-amended bottles. Arsenate reduction was achieved within 50 h with lactate, 70 h with acetate, and proceeded from 20 h until the termination of the experiment in the unamended bottles. Although As(V) was not completely reduced, the termination of As(V) reduction in the lactate-amended bottles occurred concurrently with the complete consumption of lactate (~45 h). Fe(III) reduction continued even after the lactate was exhausted, but as the experiments with the unamended bottles show, some As(V) and Fe(III) reduction can

occur without organic carbon amendment. About 13-14% of the Fe(III) was reduced in the lactate- and acetate-amended bottles, while 8% of the Fe(III) was reduced in the unamended bottles.

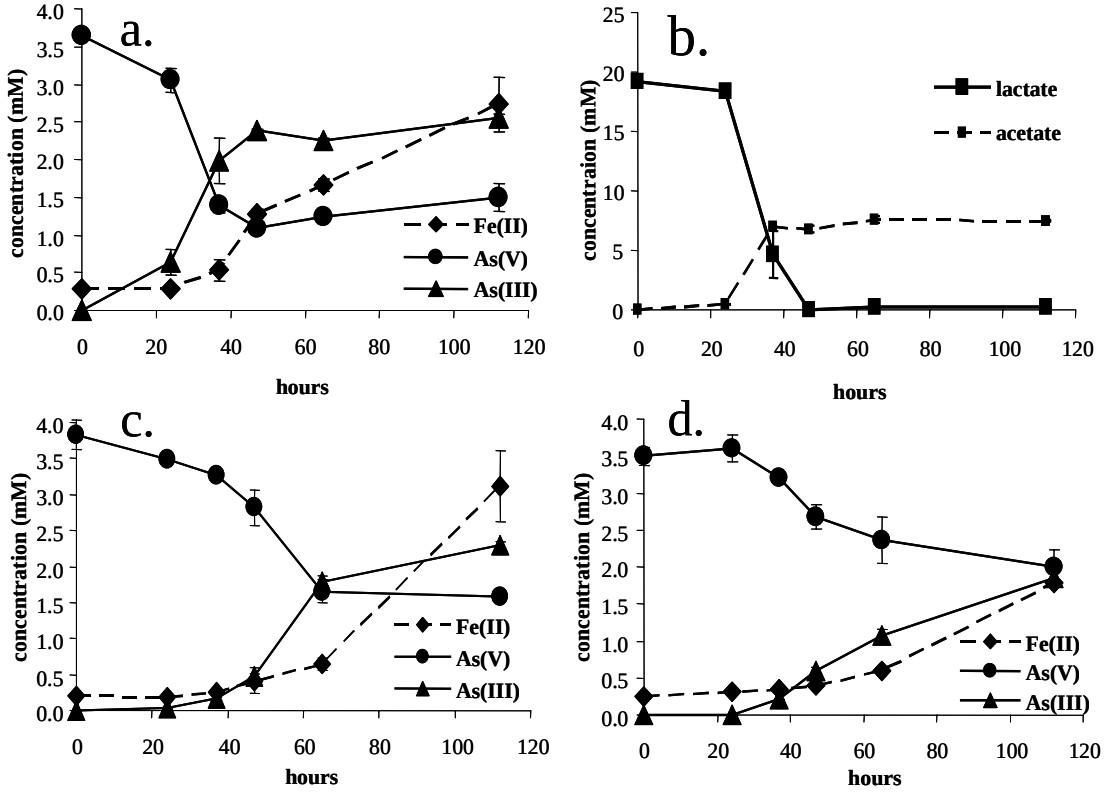

Figure 5.1. Measured total concentrations of As(III), As(V), Fe(II) and organic carbon for sediment incubations a) and b) amended with lactate, c) amended with acetate, and d) without a carbon amendment. The HFO was pre-equilibrated with As(V), and inoculated with fresh sediment from Haiwee Reservoir, introducing a natural bacterial community to the slurry. The error bars represent one standard deviation of measured concentrations of triplicate samples, and if not visible, are smaller than the symbol. For experimental conditions, see Table 5.1.

In the lactate-amended bottles, the changes in lactate and acetate concentration exceeded the values expected based on the stoichiometry of Fe(II) and As(III)

production. Since the sediment inoculum introduced a mixed microbial community, it is possible that some consumption of lactate proceeded through alternative pathways not involving Fe(III) or As(V) reduction, such as nitrate or manganese reduction.

Reduction of As(V) and Fe(III) was observed in the unamended microcosm inoculated with Haiwee Reservoir sediment, indicating that the bacteria were able to utilize the ambient carbon from the small amount of sediment introduced with the inoculum. The carbon content of the sediment is 2.8% on a dry weight basis.

5.4.2 Incubations with ANA-3

As(V) and Fe(III) were simultaneously reduced in the incubations with ANA-3 WT with HFO/As(V) (Figure 5.2a). As(V) reduction was achieved within 40 h of incubation, although it was not completely converted to As(III). HFO reduction continued throughout the course of the experiment. No As(V) reduction was observed in the ANA-3 Δ*arrA* mutant incubation on HFO/As(V), and acetate production (Figure 5.2c) was coupled to Fe(III) reduction (Figure 5.3). As(III) concentrations remained constant over time in experiments where ANA-3 WT was incubated with HFO/As(III). In all incubations with ANA-3, conversion of lactate to acetate was observed consistent with previous observations (Saltikov et al. 2003). Although acetate concentrations were less than expected, lactate was consumed stoichiometrically based on As(III) and Fe(II) production (Table 5.5). Fe(III) reduction was observed in all incubations with ANA-3 but the rates of Fe(III) reduction varied in the different incubations (Figure 3). The mutant ANA-3 Δ*arrA* showed the lowest rate of Fe(III) reduction. With ANA-3 WT,

more Fe(III) reduction was observed with HFO was pre-equilibrated with either As(V) or As(III) than with HFO alone.

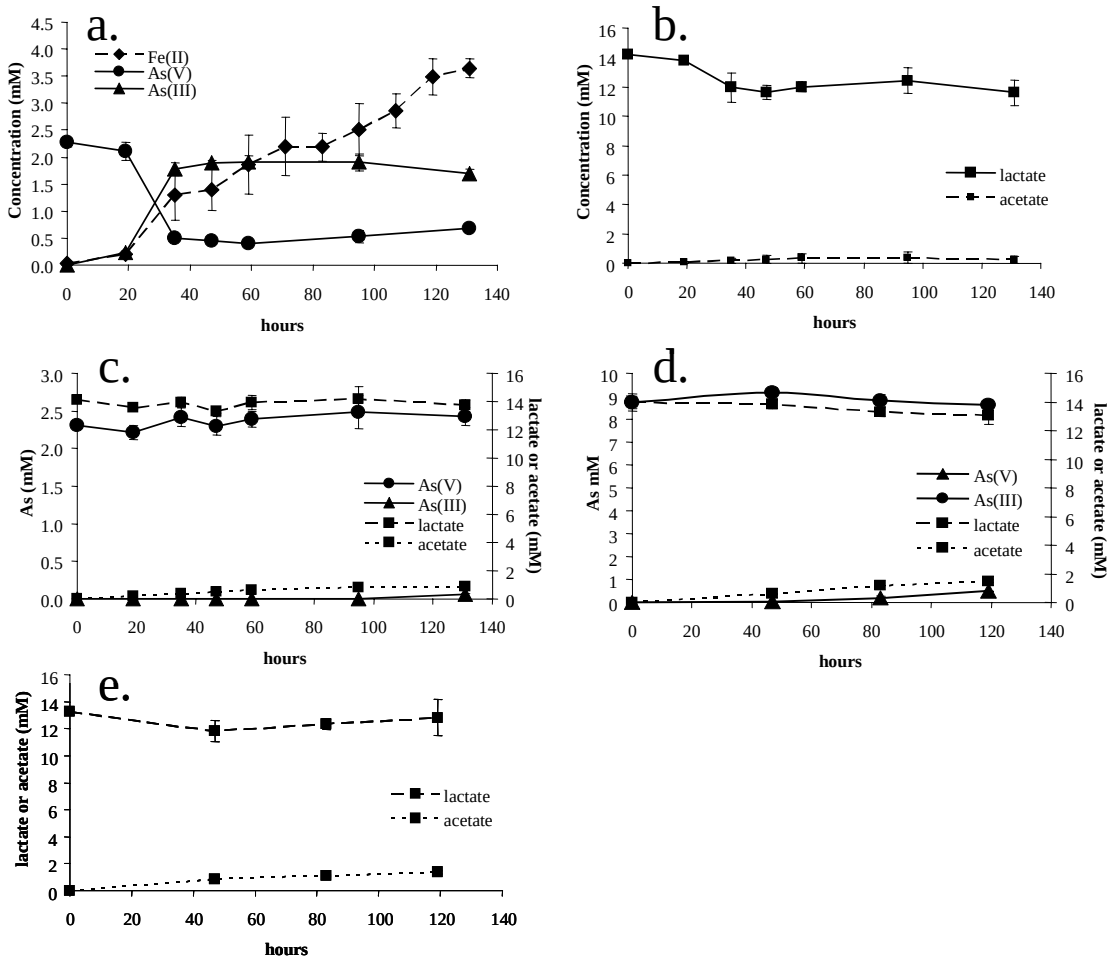

Figure 5.2. Measured total concentrations of As(V), As(III), Fe(II), lactate and acetate in incubations with (a,b) ANA-3 WT incubated with As(V)-equilibrated HFO, (c) ANA-3 Δ*arrA* mutant incubated with As(V)-equilibrated HFO, (d) ANA-3 WT incubated with As(III)-equilibrated HFO, (e) ANA-3 WT incubated with HFO (no As). ANA-3 WT or Δ*arrA* mutant was inoculated into the appropriate HFO slurry at a final cell density of 500 cells/mL slurry. For experimental conditions, see Table 5.1.

Table 5.5. Comparison of initial and final concentrations in ANA-3 microcosm experiments. Changes in concentration are expressed in equivalents to normalize for stoichiometry in equations (1) and (2) in the text (1 Fe equiv./mol; 2 As equiv./mol; 4 lactate or acetate equiv./mol).

	HFO/As(V)			HFO/As(III)			HFO only		
	initial mol	**final mol**	**Δequiv.**	**initial mol**	**final mol**	**Δequiv.**	**initial mol**	**final mol**	**Δequiv.**
lactate	2.8×10^{-3}	2.2×10^{-3}	-2.4×10^{-3}	2.8×10^{-3}	2.6×10^{-3}	-8.0×10^{-4}	2.8×10^{-3}	2.6×10^{-3}	-8.0×10^{-4}
acetate	0	6.0×10^{-5}	2.4×10^{-4}	0.0	3.0×10^{-4}	1.2×10^{-3}	0.0	2.8×10^{-4}	1.1×10^{-3}
HFO (as Fe(III)	6.4×10^{-3}	--	--	6.1×10^{-3}	--	--	4.2×10^{-3}	--	--
Fe(II)	0.0	7.2×10^{-4}	7.2×10^{-4}	0.0	5.2×10^{-4}	5.2×10^{-4}	0.0	1.8×10^{-4}	1.8×10^{-4}
As(V)	4.6×10^{-4}	1.4×10^{-4}	-6.4×10^{-4}	0.0	8.0×10^{-5}	1.6×10^{-4}	0.0	0.0	0.0
As(III)	0.0	3.4×10^{-4}	6.8×10^{-4}	1.74×10^{-3}	1.72×10^{-3}	-4.0×10^{-5}	0.0	0.0	0.0

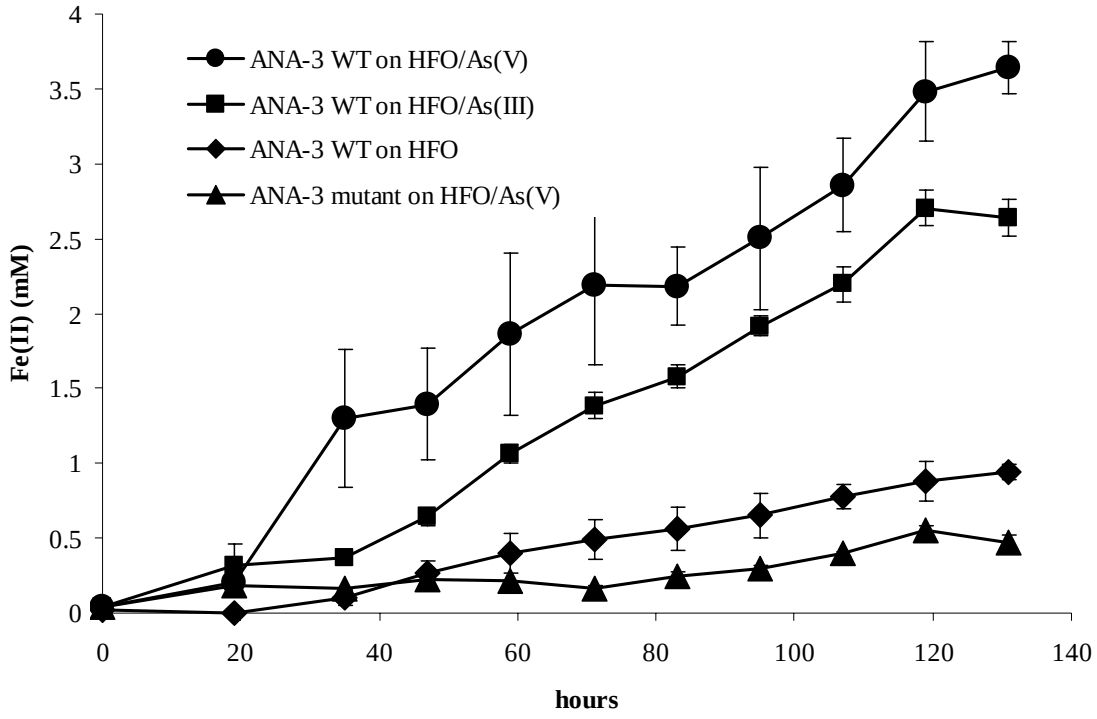

Figure 5.3. Measured total concentrations of Fe(II) for ANA-3 WT grown on HFO pre-equilibrated with As(V), As(III), or HFO only (no As), and ANA-3 Δ*arrA* mutant on HFO pre-equilibrated with As(V). The rates of Fe(II) production after 40 h of incubation are 0.024 mM Fe/h for ANA-3 WT on HFO/As(V), 0.028 mM Fe/h for ANA-3 WT on HFO/As(III), 0.009 mM Fe/h for ANA-3 WT on HFO only, and 0.003 mM Fe/h for ANA-3 Δ*arrA* mutant. The presence of As(III) adsorbed onto HFO enhances the rate of Fe(III) reduction.

5.5 Discussion

5.5.1 Utilization of terminal electron acceptors (TEA)

In both sediment and ANA-3 microcosm experiments, As(V) reduction occurs concurrently or even prior to Fe(III) reduction. In the ANA-3 WT microcosms, the utilization of As(V) as a terminal electron acceptor prior to or concurrently with Fe(III) is consistent with calculations of the thermodynamic driving force for As(V) and Fe(III) reduction coupled with lactate oxidation. For conditions where the reactant As(V) and

the products As(III) and Fe(II) are predominantly sorbed to HFO, As(V) reduction is more favorable than Fe(III) reduction throughout the course of the experiment (Table 5.6), even as ΔG becomes less favorable for both reactions as they progress. Decreased driving force (less negative ΔG) has been calculated in other Fe systems, where Fe(II) accumulation decreases the driving force for bacterial reduction of hematite over time (Royer et al. 2004). In the ANA-3 microcosms, As(V) was not reduced completely to As(III), indicating that the residual As(V) may have been limited by kinetic factors such as inaccessibility of residual As(V), rather than thermodynamic considerations.

Table 5.6. Thermodynamic driving force calculation results for ANA-3 WT microcosm.

Time (hours)	$\Delta G_{As(V)}$ (kJ/mol)	ΔG_{HFO} (kJ/mol)
19	-200	-189
35	-144	-143
59	-133	-130

Thermodynamics alone do not always predict the utilization of TEAs in these types of reactions, since other factors such as enzyme kinetics may influence the rates and extent of TEA consumption. However, the thermodynamic calculations presented here show that the effects of chemical reactions such as adsorption can greatly affect the energetics of the system.

Our study illustrates the importance of considering the speciation of As and Fe associated with the solid phase both in assessing the full extent of As(V) and Fe(III) reduction and in comparing the energetics of As(V) and Fe(III) reduction. In other

studies where As and Fe were measured only in the dissolved phase, Fe(II) either accumulated in solution prior to the increase in dissolved As(III), or As and Fe(II) were released simultaneously into solution (McGeehan and Naylor 1994; Ahmann et al. 1997; Zobrist et al. 2000; Islam et al. 2004). However, the amount of Fe and As in solution is dependent not only on the extent of reduction of each element but also the extent to which they are sorbed onto the solid phase. Therefore, measurement of both dissolved and solid phase redox speciation is necessary to follow the energetics of the reactions.

Although the bicarbonate, As, and Fe concentrations used in the microcosms are higher than would be generally found in natural systems, the HFO used in this study is a reasonable laboratory model for the Fe floc deposited in Haiwee sediments. Thus, the observed order of terminal electron acceptor utilization may be expected for Haiwee sediment. Our laboratory results are consistent with field observations at Haiwee Reservoir, where As(V) was converted to As(III) in the surficial sediments and Fe(III) reduction occurred deeper in the sediment column (Kneebone et al. 2002). In addition, the *arrA* gene was identified in Haiwee sediments (Malasarn et al. 2004) indicating that the respiratory pathway of As(V) reduction may be important. This suggests that the redox transitions observed in Haiwee sediments are due to microbial As(V) and Fe(III) reduction.

5.5.2 Respiratory and Detoxification Pathways

The ANA-3 ΔarrA mutant in an HFO/As(V) slurry did not reduce any As(V) (Figure 5.2 C), although both ANA-3 WT and ANA-3ΔarrA mutant are capable of As(V) reduction for the purpose of detoxification using the ArsC reductase. Therefore, the

detoxification pathway did not play a significant role in this incubation. The threshold for expressing the *ars* detoxification genes is >100 µM As(V), while the *arr* respiratory genes are expressed at As(V) concentrations of 100 nM (39). Dissolved concentrations of As(V) were below the detection limit of 100 µM and, therefore, also below the threshold for *ars* expression. Thus, detoxification should not be a significant pathway for As(V) reduction, consistent with the experimental observations.

In the sediment microcosms, the reduction of arsenate ceased after approximately 40 h of incubation in lactate-amended bottles, which corresponds to the complete consumption of lactate. The correlation between As(V) reduction and lactate consumption is indicative of the respiratory pathway and suggests it may be dominant in the sediment microcosms as well. This is consistent with previous studies suggesting that rates of As(V) reduction via the detoxification pathway may be slower than the respiratory pathway in other bacterial strains (Jones et al. 2000).

It is evident that bacteria can reduce As(V) for respiration or detoxification even under conditions where As(V) is predominantly adsorbed to or associated with an Fe mineral matrix (Ahmann et al. 1997; Jones et al. 2000; Langner and Inskeep 2000; Zobrist et al. 2000; Herbel and Fendorf 2005). The arsenate reductase ArrA is thought to be located in the periplasm of the bacterial cell on the basis of genetic similarities to other known proteins (Krafft and Macy 1998; Saltikov and Newman 2003) and to require a phosphate transporter to translocate dissolved As (i.e., after desorption from the solid) into the periplasm. This would imply that the dissolved As(V) in our experiments, although below the detection limit, was sufficient to support the observed microbial

reduction. However, the question remains as to whether a bacterial cell can directly utilize adsorbed As(V) or requires desorption of As(V) from the solid phase.

5.5.3 Effect of sorbed As on Fe(III) reduction

The presence of adsorbed As(III) increased the rate of Fe reduction in the ANA-3 WT microcosm experiments. In the incubations with HFO/As(V), sorbed As(V) was reduced to As(III) within approximately 40 h. Once most of the As(V) was reduced (>40 h) and As(III) was the dominant species adsorbed onto the HFO, the rate of Fe reduction was comparable to the HFO/As(III) case (0.024 mM Fe/h for HFO/As(V) microcosm and 0.028 mM Fe/h for the HFO/As(III) microcosm) from 40 h to 130 h. The HFO-only and HFO/As(V)/mutant incubations show substantially less Fe reduction (0.009 and 0.003 mM Fe/h, respectively) than observed in the HFO/As(V) and HFO/As(III) microcosms, which indicates that sorbed As(III) enhances the bacterial reduction of HFO.

The rate of microbial reduction of Fe(III) oxyhydroxides depends on the surface area and crystallinity of the oxide mineral (Jones et al. 2000; Zobrist et al. 2000; Hansel et al. 2004). Changes in these properties could be related to the observed differences in rates of Fe reduction. The time scale of this experiment (~4 days) is considerably less than the timescale of ~15 days over which substantial re-crystallization of HFO, with or without adsorbed As, was observed in abiotic batch experiments (Ford 2002). In flow-through experiments, however, a transition from HFO to lepidocrocite has been observed within 2 days of incubation with bacteria (Benner et al. 2002; Hansel et al. 2003). The absence of dissolved As in our study suggests that surface area did not decrease substantially over the course of the experiment.

The enhancement of microbial Fe reduction observed when As(III) was adsorbed on the HFO substrate was unexpected and may have significant environmental implications. Bacterial reduction of As(V) to As(III) may increase the rate of reductive dissolution of poorly crystalline Fe hydroxides, possibly leading to an increase in As mobility into groundwater in sediment systems.

5.6 Acknowledgements

This work was done in collaboration with Davin Malasarn, Dr. Chad Saltikov, and Dr. Dianne Newman. Davin grew the two ANA-3 strains in the laboratory, helped collect cores in the field, and assisted in time course samples and analysis. Chad created the ANA-3 *ΔarrA* mutant, helped collect the cores in the field, and developed the HPLC As method.

Chapter 6

Effects of adsorbed arsenic on HFO aggregation and bacterial adhesion to surfaces

6.1 Introduction

Trace elements can be released to sediment porewaters upon reductive dissolution of iron (Fe) oxides. The rate and extent of Fe(III) oxide reductive dissolution is dependent on crystallinity, mineral solubility, surface area, and the presence of adsorbed ions (Bondietti et al. 1993; Roden and Zachara 1996; Larsen and Postma 2001; Bonneville et al. 2004; Pedersen et al. 2006). Adsorbed anions such as arsenate (As(V)) and arsenite (As(III)) can retard reductive dissolution by chemical reductants, but the effect of adsorbed As on microbial Fe(III) reduction has not been studied in detail.

In incubations with *Shewanella* species strain ANA-3, microbial Fe(III) reduction was enhanced by the presence of As(III) adsorbed onto the surface of hydrous ferric oxide (HFO), an amorphous Fe oxyhydroxide (see Chapter 5). *Shewanella* sp. strain ANA-3 wild-type (WT) was incubated with hydrous ferric oxide (HFO) pre-equilibrated with As(III) (HFO/As(III)) or As(V) (HFO/As(V)) or without As (HFO only). ANA-3 *ΔarrA*, a mutant unable to respire As(V), was incubated with HFO/As(V) as a control for As(V) reduction. Interestingly, the rates of Fe(III) reduction for the *ΔarrA* mutant on HFO/As(V) and ANA-3 WT on HFO were similar, while the rates of ANA-3 WT grown on HFO/As(III) and HFO/As(V) were significantly higher. ANA-3 WT reduced the

majority of adsorbed As(V) to As(III) within 40 hours of incubation. Once As(III) was the dominant species on the surface, the rates of Fe(III) reduction was comparable to the rates of ANA-3 WT incubated with HFO/As(III). The presence of adsorbed As(III) on HFO increased the rate of Fe(III) reduction. An explanation for this result was not immediately obvious, and could be due to HFO surface properties, aggregation, bacterial adhesion and/or genetic factors. The purpose of this study is to investigate the properties of HFO with adsorbed As(III) compared to HFO with adsorbed As(V) and HFO without adsorbed As in an attempt to explain increased rates of microbial Fe(III) reduction in the presence of adsorbed As(III). Surface properties were investigated by light microscopy and environmental scanning electron microscopy (ESEM). The rates of bacterial and chemical reduction was measured and the extent of bacterial adhesion onto the surface in the presence and absence of As was compared.

6.2 Materials and Methods

All chemicals used were reagent grade and used without further purification. Solutions were prepared with 18 MΩ-cm deionized water (Milli-Q, Millipore) and stored in plastic containers that had been washed in 2-5% nitric acid. For bacterial incubations, all solutions were autoclaved before use with the exception of the bicarbonate buffer, which was filter-sterilized (0.2 μm pore size) and added to the autoclaved medium. The bacterial minimal growth medium (Appendix C) was buffered with 50 mM bicarbonate and had a total phosphate concentration of 50 μM and an ionic strength of 0.06 M.

6.2.1 Arsenic-equilibrated HFO preparation

HFO was prepared by the drop-wise addition of 0.5 M NaOH to 0.067 M $Fe(NO_3)_3$ until the solution stabilized at pH 8 (Schwertmann and Cornell 1991). The suspension was equilibrated for >4 h under constant stirring, adjusting any pH drift as necessary with 0.5 M NaOH. The HFO was then washed three times with sterile water and centrifuged. The HFO was not autoclaved after synthesis to avoid changes in mineralogy.

After the final wash, the HFO was resuspended in an As solution, and equilibrated overnight with constant stirring. For the ESEM experiments, 1 g of HFO was equilibrated in 200 mL of 0.01 M of Na_2HAsO_4 (Sigma) or $NaAsO_2$ (Sigma) at pH 8.0. For all other experiments, 0.25 g of HFO was equilibrated in 40 mL of 0.015 M As(III) or As(V) solution. These conditions ensured that all available surface sites for As adsorption were saturated with As at pH 8. The HFO was washed once with sterile water to remove excess As and resuspended in bacterial minimal medium (pH 8) to a final slurry concentration of 3 g_{HFO}/L. In the case of HFO without any adsorbed As, the solid was resuspended directly in bacterial medium after the initial washing and adjusted to pH 8. A subset of HFO, HFO/As(III) and HFO/As(V) solids were resuspended in water rather than bacterial medium as a control for the ESEM experiments.

6.2.2 Incubations with ANA-3

40mL of each type of HFO slurry were transferred into a sterile tube with a screw-cap lid and placed in an anaerobic chamber (80% N_2, 15% CO_2, 5% H_2).

Shewanella sp. strain ANA-3 and *Shewanella* sp. strain ANA-3Δ*arrA*, a mutant with a deletion in *arrA*, were used as inocula. See Chapter 5 for more information on the bacterial strains. A summary of the experimental conditions is presented in Table 6.1. Each tube was inoculated with 2×10^4 cells of ANA-3 WT or the *ΔarrA* mutant, or left uninoculated. Each condition was measured in duplicate. All tubes were incubated at 30°C in the dark in the anaerobic chamber.

At each time point, dissolved Fe(II) and total Fe(II) concentrations were determined by the ferrozine method (Stookey 1970). A 500 µL aliquot was filtered through a microcentrifuge filter with a 0.2 µm pore size (Costar, nylon Spin-x) in the anaerobic chamber for dissolved Fe(II) analysis. Ten µL of slurry was added directly to 90 µL of 1 M HCl in a 96-well plate for total Fe(II) determination. Time points were collected after 55 hours and 91 hours of incubation.

Table 6.1. Experimental conditions. Samples incubated in the time course are denoted "TC" and s samples run on ESEM are denoted "ESEM". Each condition was performed in duplicate.

	ANA-3 WT, minimal medium	***ΔarrA* mutant, minimal medium**	**no bacteria, minimal medium**	**no bacteria, water only**
HFO	TC, ESEM	TC, ESEM	TC	TC, ESEM
As(III)	TC, ESEM	TC, ESEM	TC	TC, ESEM
As(V)	TC, ESEM	TC, ESEM	TC	TC, ESEM

6.2.3 Environmental Scanning Electron Microscopy (ESEM)

ESEM is a technique particularly suited for imaging surface structures of hydrated solids because the beam can be operated at relatively high pressures. The structure is preserved when the solid is frozen and the water slowly evaporated from the surface.

After 91 hours of incubation, all tubes were centrifuged and washed once with sterile deoxygenated water to remove the bacterial minimal medium. The solids were then resuspended in 20 mL of water, and transferred into a sterile Balch tubes. The tubes were capped before removal from the anaerobic chamber.

ESEM images were taken at the Jet Propulsion Laboratory (JPL) on a Phillips XD30 scanning electron microscope, operating in environmental mode. The samples were extracted from the Balch tubes with a syringe and placed on a sample holder. Excess water was quickly wicked away from the sample before placing the sample holder on a Peltier stage cooled to 3.2-3.3°C. Conditions inside the chamber were maintained at 4.5 torr (~75% relative humidity), and the vacuum was applied such that the water was slowly removed from the sample surface (~15 min). The beam was operated at 20 kV and 332 μA.

6.2.4 Chemical Rates of Reduction

The chemical rates of reduction of HFO, HFO/As(V), and HFO/As(III) were compared by measuring the Fe(II) produced by reaction with l(+)-ascorbic acid (EM Science) at pH 8. All solutions were deoxygenated and the experiment was carried out in an anaerobic chamber. 18 mL of 100 mM of ascorbic acid in HEPES buffer (pH 8) was added to a concentrated stock solution of HFO, HFO/As(V) or HFO/As(III) to a final

slurry concentration of 0.3 g/L. Each condition was performed in duplicate. At each time point, 10 µL of sample was added to 90 µL of 1 M HCl in a 96-well plate for ferrozine analysis of total Fe(II).

6.2.5 Bacterial adhesion assay

A *Shewanella* sp. strain ANA-3Δ*arrA* derivative expressing unstable green fluorescent protein (GFP) was created by transferring pTK4 (Teal et al. 2006) into ANA-3Δ*arrA* through conjugation and selection on 15 µg/mL tetracycline. pTK4 expresses a variant of GFP, GFP(AAV), containing a C-terminal oligopeptide extension that makes it susceptible to fast degradation by native intracellular proteases. The *gfp*(AAV) gene is driven by the *Escherichia coli rrnB* P1 promoter, which is growth regulated such that cells fluoresce when they are actively growing.

Cultures of ANA-3Δ*arrA* carrying pTK4 were grown to midexponential phase on LB supplemented with tetracycline at 15 µg/mL. These cells were washed twice in LB with no antibiotic and resuspended in anaerobic minimal medium to remove tetracycline, which can form complexes with HFO and increase solubility (Gu and Karthikeyan 2005). Under anaerobic conditions, 100 µL of washed cells at ~5 x 10^8 cells/mL were mixed with 100µL of HFO, HFO/As(III), or HFO/As(V) slurry and stored at room temperature anaerobically in a glove box for 1 hr. Samples were resuspended by gentle pipetting and 5µL were placed on a slide with no cover slip and brought out of the glove box for microscopy. Images were obtained using a Zeiss Axioplan microscope with a 20x NEOFLUAR plan objective lens using light (exposure time 0.05 seconds) and fluorescent excitation (exposure time 10 seconds).

6.3 Results and Discussion

6.3.1 Biological and chemical rates of reduction

The rate and extent of Fe(II) production for ANA-3 WT (HFO, HFO/As(III), HFO/As(V)) and ANA-3 *ΔarrA* mutant (HFO/As(V)) is consistent with the more detailed time course in Chapter 5. The highest concentrations of Fe(II) are found in incubations with ANA-3 WT with HFO/As(V) and HFO/As(III). ANA-3 WT incubated with HFO only produces significantly less Fe(II) than ANA-3 WT incubated with HFO/As(III) and HFO/As(V). Iron(II) production in ANA-3 *ΔarrA* mutant incubations with HFO only and HFO/As(III) are similar. However, increased Fe(II) production is evident in the ANA-3 *ΔarrA* mutant HFO/As(III) incubations. Both ANA-3 WT and ANA-3 *ΔarrA* mutant incubations confirm the that the presence of adsorbed As(III) increases the rate of Fe(II) production (Table 6.2). Only a background amount of Fe(II) was measured in the control tubes over the course of the experiment, indicating that bacterial contamination was negligible.

Table 6.2. Total Fe(II) concentrations (mM) from the incubations used in the ESEM experiment after 55 and 91 hours of incubation. Tubes were incubated at 30°C in an anaerobic chamber. The slurry concentration in all tubes is 3 g/L and was buffered at pH 8. The data reported is an average of duplicate tubes.

	Bacterial incubations			
	ANA-3 WT		**ANA-3 *ΔarrA* mutant**	
Incubation time	55 h	91 h	55 h	91 h
HFO	0.23	0.65	0.20	0.38
As(III)/HFO	0.65	1.04	0.67	1.01
As(V)/HFO	3.00	4.24	0.25	0.47
	Control tubes (no bacteria)			
	Bacterial medium		**Water**	
Incubation time	55 h	91 h	55 h	91 h
HFO	0.15	0.15	0.14	0.15
As(III)/HFO	0.14	0.14	0.13	0.14
As(V)/HFO	0.12	0.16	0.11	0.16

The amount and rate of Fe(II) production by ascorbic acid is similar for HFO, HFO/As(V), and HFO/As(III) (Figure 6.1). Therefore, the chemical rates of reduction are independent of adsorbed As.

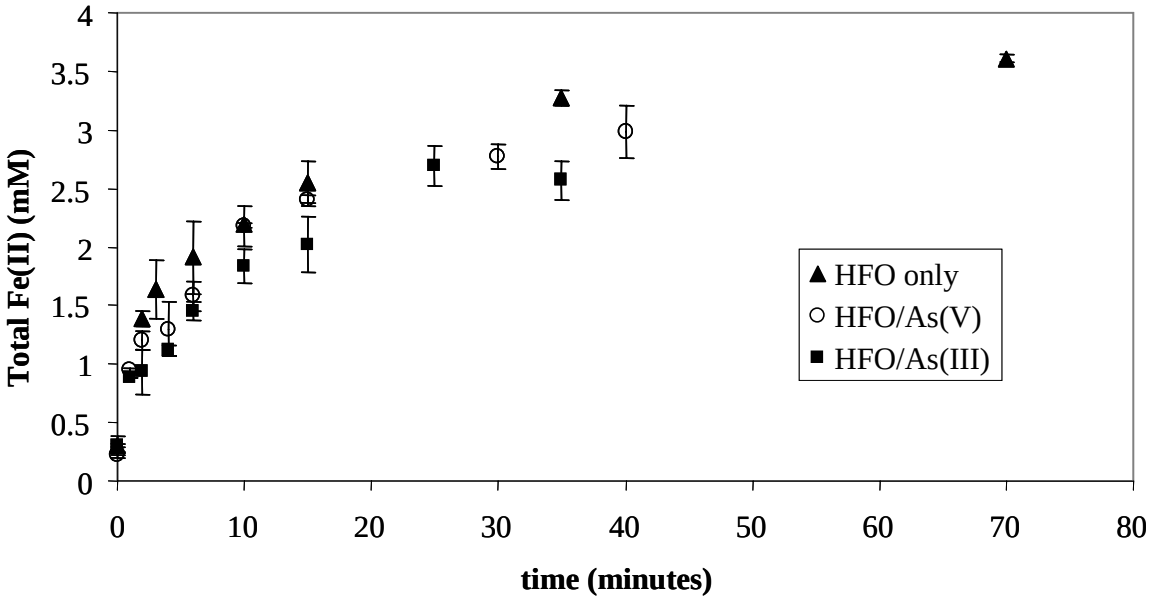

Figure 6.1. Total Fe(II) production during the chemical reduction of HFO, As(V)/HFO and As(III)/HFO by 100 mM ascorbic acid at pH 8. The error bars indicate the standard deviation of duplicate samples.

6.3.2 Effect of adsorbed As on HFO aggregation

Adsorbed As(III) made HFO more bioavailable for reduction, presumably by effecting HFO aggregation or surface properties. Slower settling was observed from HFO with adsorbed As(III) (Figure 6.2), suggesting smaller particle size or less efficient aggregation. When imaged by light microscopy after vigorously shaking the tubes, the particle sizes in all three cases appear to be the same size (~50 μm) (Figure 6.5). However, imaging the supernatant after allowing the solid to settle for >24 hours, only the HFO/As(III) tube had traces of particles that would not settle (Figure 6.3). Although they may comprise only a small fraction of the total mass of HFO/As(III) in the tube, the presence of the small particles may explain the increased rates of Fe(III) reduction.

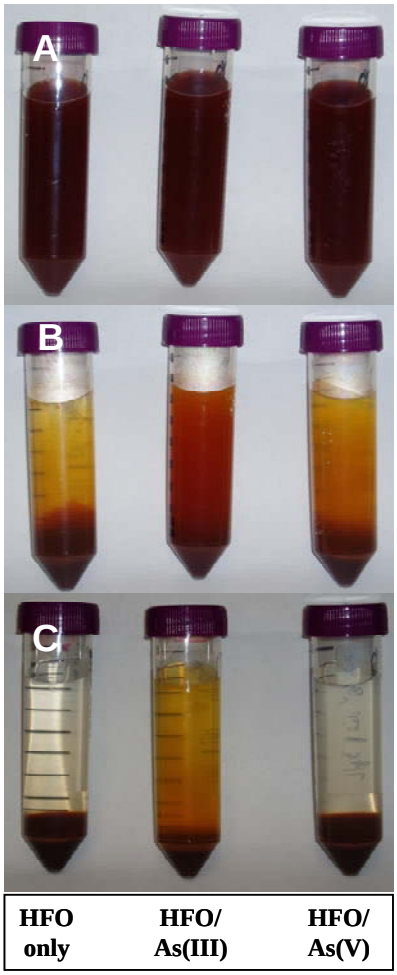

Figure 6.2. Tubes of HFO only (left tube), HFO/As(III) (middle tube), and HFO/As(V) (right tube) immediately after shaking (A), after 2 hours (B), and after >24 hours of settling (C). The HFO in all tubes is suspended in bacterial medium (no inoculation, pH 8, ionic strength = 0.01 M).

ESEM was used to observe the surface morphology of HFO in the presence and absence of adsorbed As(III) and As(V). All three solids had similar morphologies, but there were some subtle differences. HFO and HFO/As(V) had clusters of ball-shaped mounds (Figure 6.4A,B). These mounds were actually collections of smaller, nanoparticles of HFO, consistent with previous studies of HFO aggregates (Cornell and

Schwertmann 1996). HFO/As(III) had a slightly different surface structure, exhibiting smoother surfaces and fewer ball-shaped mounds (Figure 6.4C).

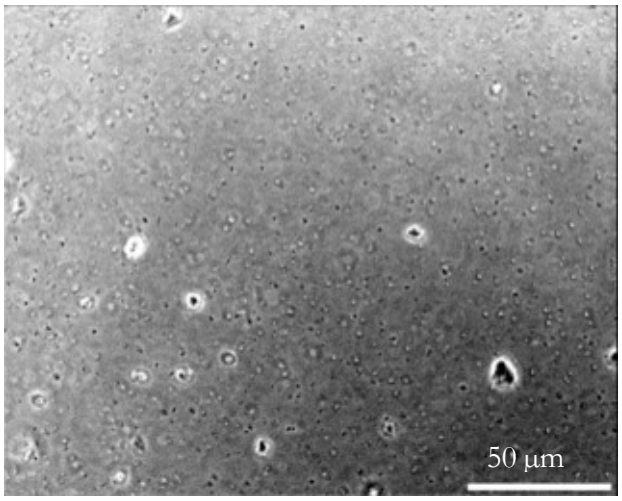

Figure 6.3. Light microscope image of the particles in the supernatant of HFO/As(III) that had been left undisturbed for >24 hours.

ESEM images were also taken after 91 hours of incubation with ANA-3 WT and *ΔarrA* mutant. The morphology of all three solids (HFO, HFO/As(III), HFO/As(V)) after incubation with either ANA-3 WT or ANA-3 mutant was similar to the starting material (Figure 6.5 A,B,C). In the case of HFO/As(V) incubated with ANA-3 WT, most of the As(V) had been reduced to As(III) after 91 hours of incubation. Even though the majority of the As on the surface was As(III), the morphology was more similar to HFO/As(V). Therefore, the change in oxidation state from As(V) to As(III) did not significantly affect the morphology of the surface.

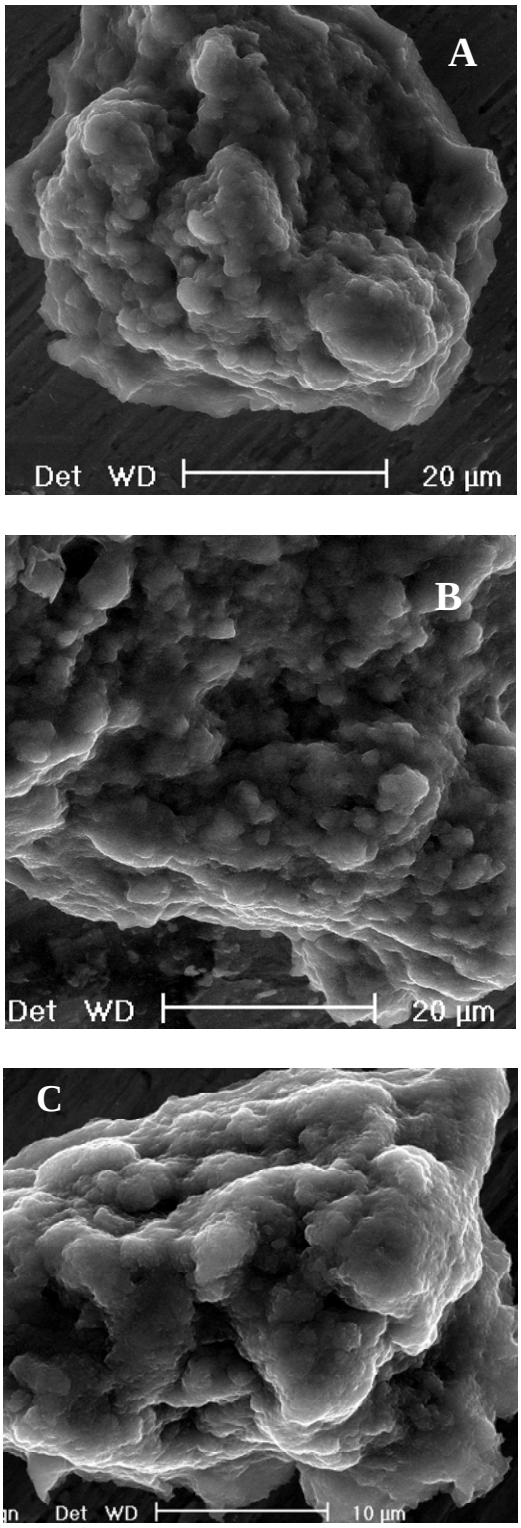

Figure 6.4. ESEM images of HFO only (A), HFO with As(V) (B) and HFO with As(III) (C) without bacteria. The solids were suspended in water. Samples for imaging were taken immediately after shaking the tubes.

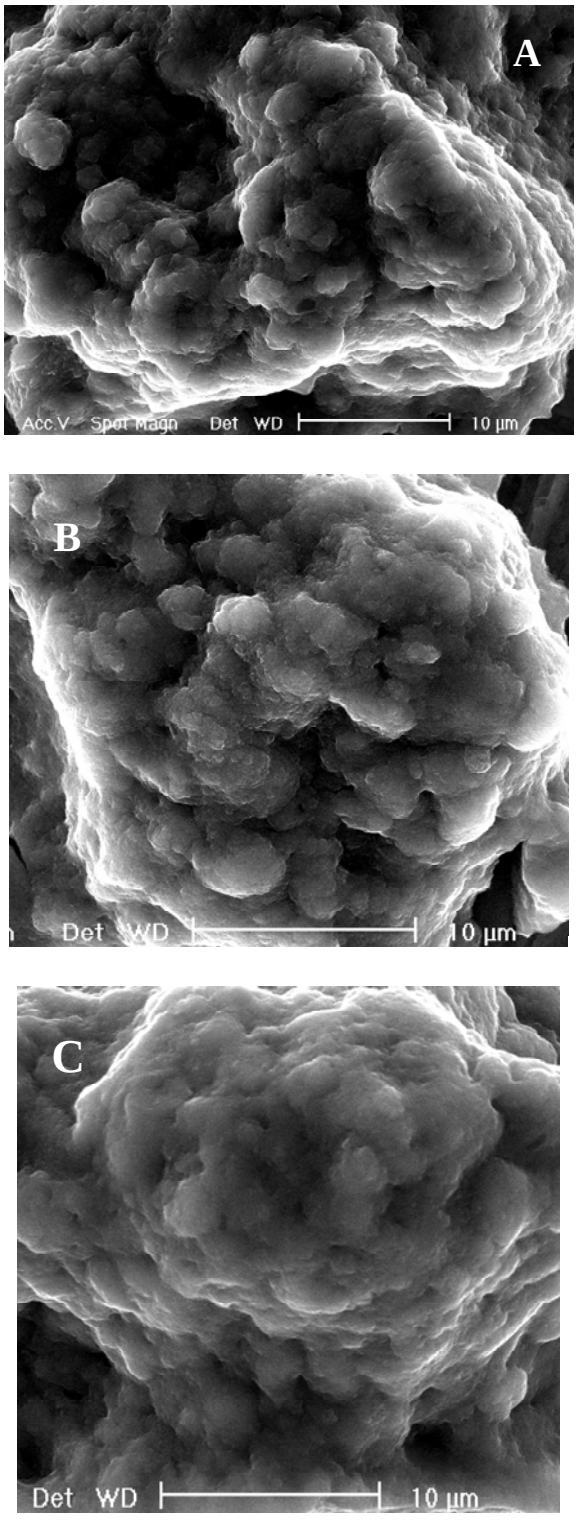

Figure 6.5. ESEM images of HFO only (A), HFO with As(V) (B), and HFO with As(III) (C) after 91 hours of incubation with *Shewanella* sp. strain ANA-3 WT. Samples for imaging were taken immediately after shaking the tubes.

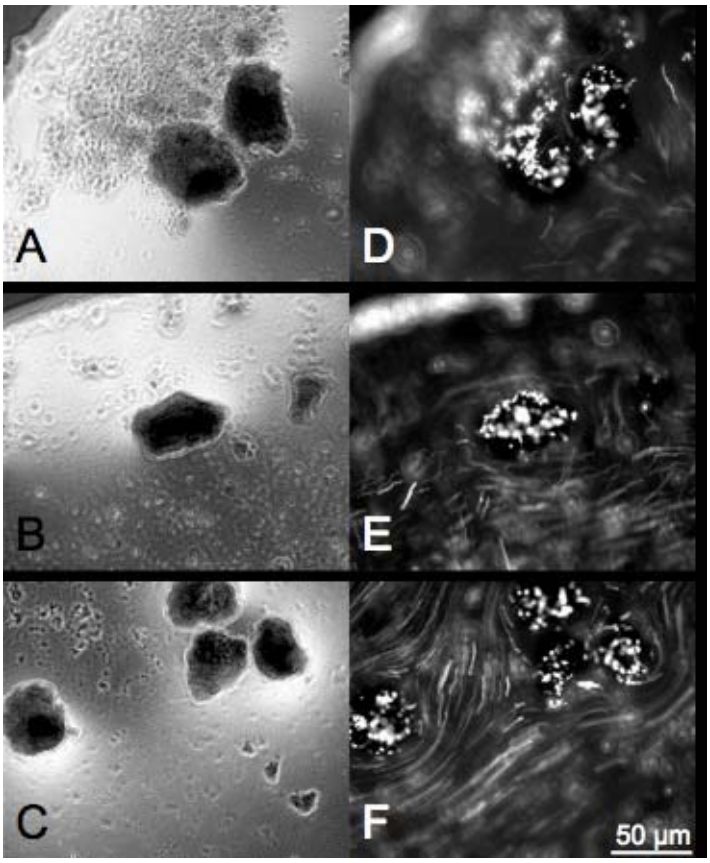

Figure 6.6. Adhesion of active *Shewanella* sp. strain ANA-3Δ*arrA* onto HFO. Light microscope images of solid HFO (A), As(III)-sorbed HFO (B), and As(V)-sorbed HFO (C). Fluorescent images of GFP(AAV)-expressing ANA-3Δ*arrA* in the same field of view corresponding to light images in the adjacent panel (D to F).

6.3.3 Bacterial adhesion

To understand the contribution of cell adhesion to the differences in iron reduction rates, adhesion assays were carried out using ANA-3 Δ*arrA* expressing a growth-regulated unstable GFP variant. Performance of this assay used a high cell number for a short amount of time to allow visualization to be completed in the absence of growth, which would have resulted in differences in total cell number. Use of the growth-regulated, unstable GFP allowed direct observation of cells that were metabolically active.

After incubating the cells with the HFO samples for 1 hour, actively growing fluorescent cells were found attached to particles under all three conditions (Figure 6.6). This suggests that the differences in surface properties due to adsorbed As(III) did not significantly affect cell adhesion.

6.3.4 Conclusion

The presence of adsorbed As(III) on the surface of HFO significantly increased the rate of Fe(III) reduction by ANA-3 WT and ANA-3 *ΔarrA* mutant, but did not affect the rates of chemical reduction by ascorbic acid. The reduction of As(V) to As(III) by ANA-3 WT did not change the surface morphology, and there was no evidence for preferential bacterial adhesion to HFO/As(III). While most of the particles in all three cases are approximately the same size, the presence of colloidal HFO/As(III) particles may explain the increased rates of Fe(III) reduction. The colloidal particles may be about the same size or smaller than the bacterial cells, which may make the Fe(III) particles more bioavailable for reduction.

Colloidal stabilization of Fe(III) oxides by As(III) adsorption has not been reported in the literature and it would be valuable to investigate this property further (e.g., effects of pH on colloidal stability and the effect of varying As(III) concentration) to determine whether this observation may be relevant to natural sediments. Although the As concentrations used in this study are higher than observed in most natural environments, the presence of As(III)-stabilized Fe oxide colloids may have environmental implications, even at lower concentrations. In Haiwee Reservoir, As(III)

is the dominant species in the Fe reduction zone. Even if only a small fraction of the solid phase is affected by As(III)-stabilized colloids, it may impact the overall rate of Fe reduction. The fraction of Fe and As in the sediments that would have to be mobilized in order to support the observed porewater concentrations is <2.5% (Hering and Kneebone 2001). Thus, even as a small fraction of the total solid phase, the presence of As(III)-stabilized colloids may affect the bioavailability of the Fe phase, and ultimately the mobilization of As.

6.4 Acknowledgements

This work was done in collaboration with Davin Malasarn and Dr. Dianne Newman. Davin created the GPF strains of ANA-3, performed the bacterial adhesion assay, obtained the light microscope images, and helped collect the time course samples. We especially thank Randall Mielke at JPL for the ESEM images.

Chapter 7

Concluding Remarks

7.1 Summary

The biogeochemical mechanisms controlling arsenic (As) mobilization in Haiwee Reservoir sediments were investigated. A hydrous ferric oxide (HFO)-doped gel probe equilibrium sampler was developed to simultaneously measure porewater composition and As adsorption behavior. Gel probe deployment was combined with laboratory studies, bacterial incubations, and solid phase measurements. The purpose of this chapter is to summarize the findings of this study and answer the questions posed in section 1.3.

7.1.1. What circumstances cause mobilization of As, Fe, and other elements into Haiwee sediment porewater?

Early diagenetic changes in the sediment cause redox transformations of both As and iron (Fe). In the surficial sediment, oxygen is rapidly consumed, and the sediment becomes reducing. Arsenic adsorbed onto the floc in the LAA is in the oxidized form (As(V)), as expected in the flowing, oxygenated water of the aqueduct. Upon deposition, As(V) is reduced to As(III) in the upper layer of the sediment. Arsenate reduction may be microbially mediated, as laboratory microcosms showed that the ambient microbial population was capable of reducing As(V). In addition, laboratory microcosms with a pure culture of bacteria, *Shewanella* sp. strain ANA-3, incubated with As(V) adsorbed onto HFO, provide evidence that dissimilatory As(V) reduction is more favorable than

Fe(III) reduction when coupled to lactate oxidation. This observation supports the As(V) reduction observed in the upper layers of Haiwee Reservoir sediments. In both the laboratory microcosms and in the field, As(V) reduction occurs even when most of the As is adsorbed to the Fe(III) oxide phase. Since As oxidation state affects the extent of sorption onto Fe oxides, the reduction of As(V) to As(III) may affect the partitioning between solid and aqueous phases.

Reductive dissolution of Fe(III) oxides in the sediment, which is most likely microbially mediated, drives the mobilization of As and other elements into the porewaters. The strong correlation between dissolved Fe, As, P, and W indicates that reductive dissolution is the primary process responsible for mobilization to the porewater. However, the accumulation of dissolved As is partly due to the effects of porewater chemistry.

7.1.2. What are the mechanisms controlling the partitioning of As and Fe between the sediments and porewaters?

A wide variety of compounds can inhibit As adsorption on Fe(III) oxides, including phosphate, carbonate, silicate, and organic carbon. Using an HFO-doped gel probe, the role of competing ions in inhibiting As sorption was measured *in situ*. The HFO-doped gels introduced fresh adsorption sites into the subsurface to measure the extent of As sorption as a function of depth and porewater composition. The HFO-doped gel probes were used to observe whether the presence of dissolved As in the porewater was due to lack of available surface adsorption sites on the sediment or to sorption inhibition by competitive ions.

At intermediate depths (10-20 cm), dissolved carbonate from the mineralization of organic matter may inhibit adsorption onto the HFO-doped gels. In this region, the presence of dissolved As is at least partially controlled by the porewater composition rather than sorption site availability.

Deeper in the sediment column (15-30cm), carbonate green rust formed. In this region, As adsorbed to a greater extent on the HFO-doped gels, and As adsorption behavior was consistent with the presence of dissolved phosphate. The persistence of dissolved As in the porewater suggests that As partitioning is controlled primarily by lack of available sorption sites as the amorphous Fe(III) oxide converts to green rust.

The sediment diagenetic processes affecting carbon, Fe, and As cycling in Haiwee Reservoir sediments is summarized in Figure 7.1.

7.1.3. What processes determine the fraction of total As and Fe in the solid phase that is mobilized into the porewater?

The amount of Fe(III) available for bacterial reduction is often less than the total pool of Fe(III). In addition, the conversion of amorphous Fe(III) oxyhydroxide to green rust may also decrease the susceptibility of the solid phase to microbial Fe reduction. As a result, the extent of Fe(III) reduction is probably the main reason why only a few percent of the total As and Fe in the solid phase accumulates in the porewater.

Figure 7.1. Schematic diagram of sediment diagenetic processes in Haiwee Reservoir sediment.

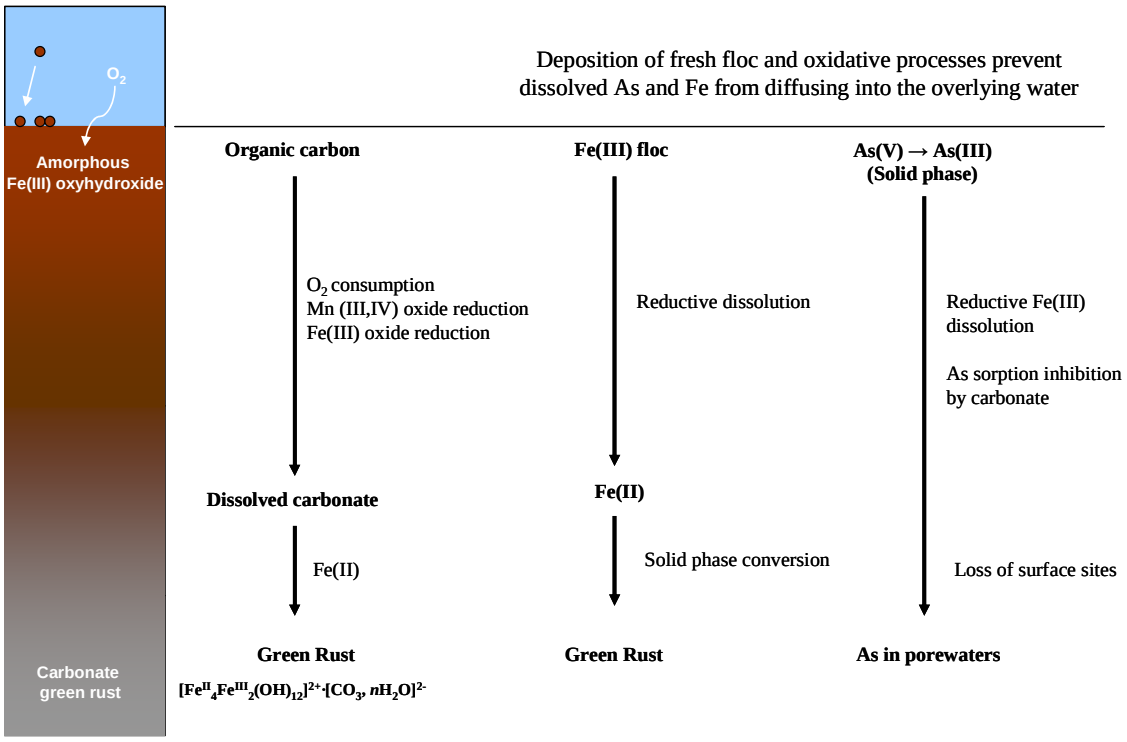

7.2. Wider Implications

The detailed mechanisms presented in this study may be somewhat unique to Haiwee Reservoir, since the sediments contain an artificially high amount of As and Fe from the water treatment process. However, the effects of porewater chemistry on As adsorption were directly measured using a gel probe equilibrium sampler. The ability to observe whether sorption site availability and/or porewater composition controls As partitioning using a gel probe is a valuable addition to the wide array of field-based techniques.

The gel probe equilibrium sampler is applicable to other sedimentary environments where Fe(III) oxides are prevalent. Amorphous Fe(III) oxyhydroxide was chosen for this study because it is mineralogically similar to the floc precipitated in the LAA, but the gels could be doped with any other Fe(III) oxide depending on the field application. In addition, the gel probe could be modified to measure *in situ* rates of Fe(III) reduction by extending the deployment time. The rates of Fe(III) reduction is a very important parameter for modeling the fate of contaminants such as As.

This study also highlights the importance of microbially-driven processes, especially Fe and As reduction. The observation that As(V) reduction may be more favorable than Fe(III) reduction under certain circumstances challenges the commonly held notion that Fe(III) reduction occurs before As(V) reduction. Adsorption chemistry can affect the thermodynamic driving force of these reactions.

An interesting outcome of the field observations at Haiwee Reservoir is that there appears to be very little diffusion of As from the sediment porewaters into the overlying water, either due to oxidation processes occurring at the surface of the sediment, or the deposition of fresh floc. This observation is important for the efficacy of the water treatment operation, but also raises some questions about the stability of the sediments. If the ferric chloride injection at Cottonwood ceased for any significant length of time, the effect it would have on the "capping" of the sediments with respect to As diffusion into the surface water is uncertain. It is important to study in more detail the precise mechanism that prevents As from diffusing from the porewaters into the surface water, determine under what circumstances these processes would be insufficient to prevent As contamination in the surface water, and assess whether dilution into the main body of the

reservoir would be adequate to maintain As concentrations below the drinking water standard.

Appendix A

July 2003 Gel Probe Deployment

The gel probes were taken into the field on two occasions, July 2003 and October 2003. In July, a combination of clear and HFO gels were inserted into the probe in order to compare the sorption behavior in HFO gels to a porewater profile in close proximity. Gel probes were equilibrated for 7 hours. In October, only clear gels were deployed in several locations to estimate spatial variability.

There is evidence of As mobilization at depth from the field deployment. However, the concentrations of As in the porewater (clear gels) are substantially less when placed with HFO gels than in previous studies and in the October sampling. As the porewater comes into equilibrium with the clear gels, minimal perturbation is expected due to the small volume of each gel. However, the HFO gels may perturb the system significantly by concentrating As and other constituents onto the HFO through sorption, thus depleting the surrounding porewater. This is possibly reflected in the low concentrations in the clear gel profile when placed next to HFO gels. The extent of perturbation is determined by diffusion of constituents from surrounding porewaters, ability of the sediment to resupply As to the porewater, and kinetic controls on As sorption to HFO.

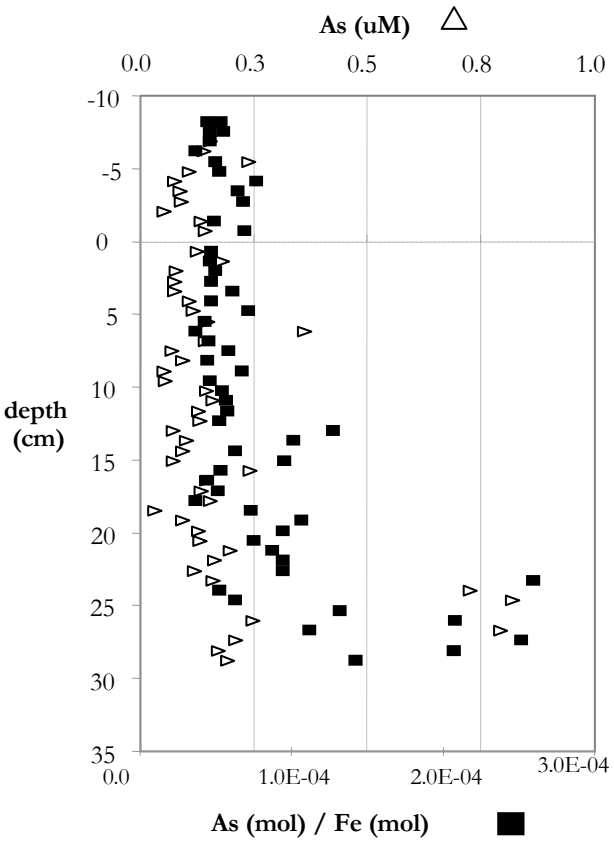

Figure A.1. Profile from July 2003 deployment of gel probe sampler. The sediment/water interface is at depth = 0. Open triangles are porewater concentrations (clear gels) and closed boxes are amount of As sorbed in HFO gels normalized to the amount of Fe per gel. The deployment time for this probe was 7.5 hours. The clear gels and the HFO gels were deployed simultaneously, and were placed within 3 cm of each other.

Appendix B

Additional ESEM images

B1. Methodology

The methods for Environmental Scanning Electron Microscopy (ESEM) and bacterial incubations are described in Chapter 6. The results presented here are observations from the HFO only, and HFO with adsorbed As(III) or As(V). The solids were either imaged without bacteria or after incubation with bacteria (*Shewanella* sp. strain ANA-3 wild-type (WT) or *ΔarrA* mutant).

B2. HFO morphology

The surface structure of HFO without adsorbed As or bacteria is shown in Figure B.1. The images are of one large aggregate of HFO, with increasing magnification. In Figure B.1d, structures of ~100 nm are visible.

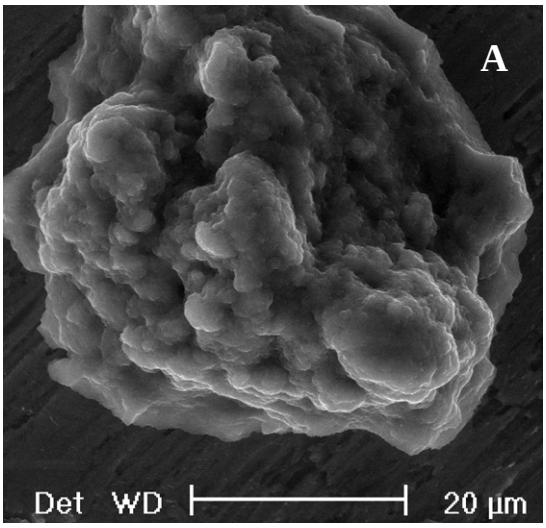

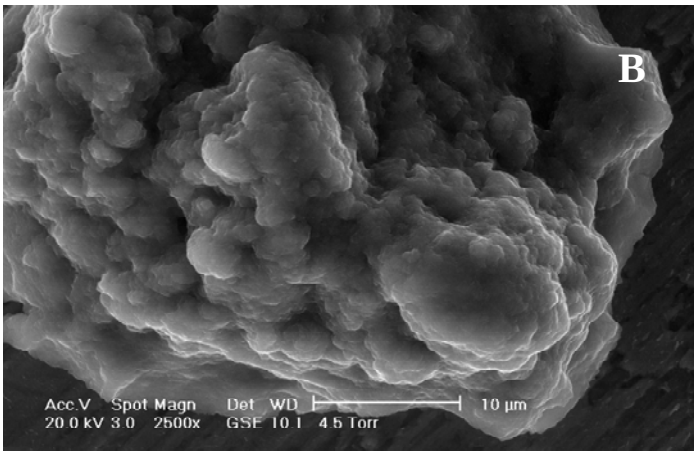

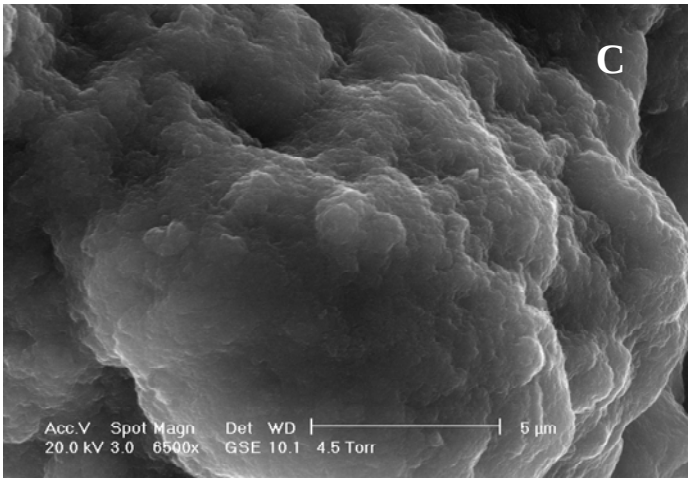

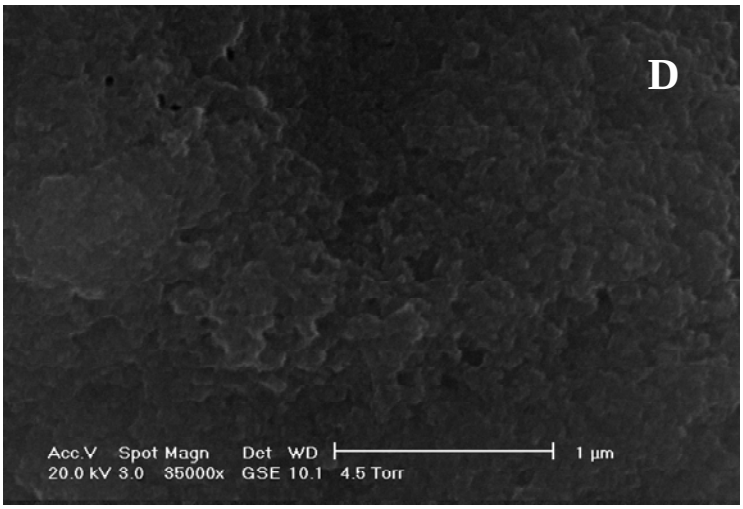

Figure B.1 a-d. Surface structure of HFO only (no adsorbed As). The solid was not incubated with any bacteria before the images were taken.

B.3 Fine structures after incubation with ANA-3 WT or mutant strain

After incubation with either the WT or mutant strain of ANA-3, several types of structures were visible in between or on the surface of the large aggregates of HFO with adsorbed As(V). The first type of structure is a thin rosette-like formation, characterized by a round configuration, occasionally with a radial pattern, and 1-10 μm in diameter (Figure B.2A,B). Figure B.2A shows the rosettes directly on the stage, which is visible as diagonal streaks from upper right to lower left. The rosettes were fragile and destroyed by the electron beam when imaged at a higher magnification, indicating that they are very thin. Figure B.2B shows a similar rosette structure on the surface of a larger aggregate. While the composition of the rosettes is unknown, it is possible that they are a secondary precipitate formed because of microbial Fe(III) reduction. It is not known whether the rosettes are formed with As(III) or HFO only.

The second kind of structure is a thin pitted structure shown in Figure B.2C. Although this was only observed in HFO incubated with ANA-3 WT, it was only a small fraction of the total sample, and may have been easily missed. Like the rosettes, its fragility prevented measurement of its composition, but it could also be a secondary mineral precipitate.

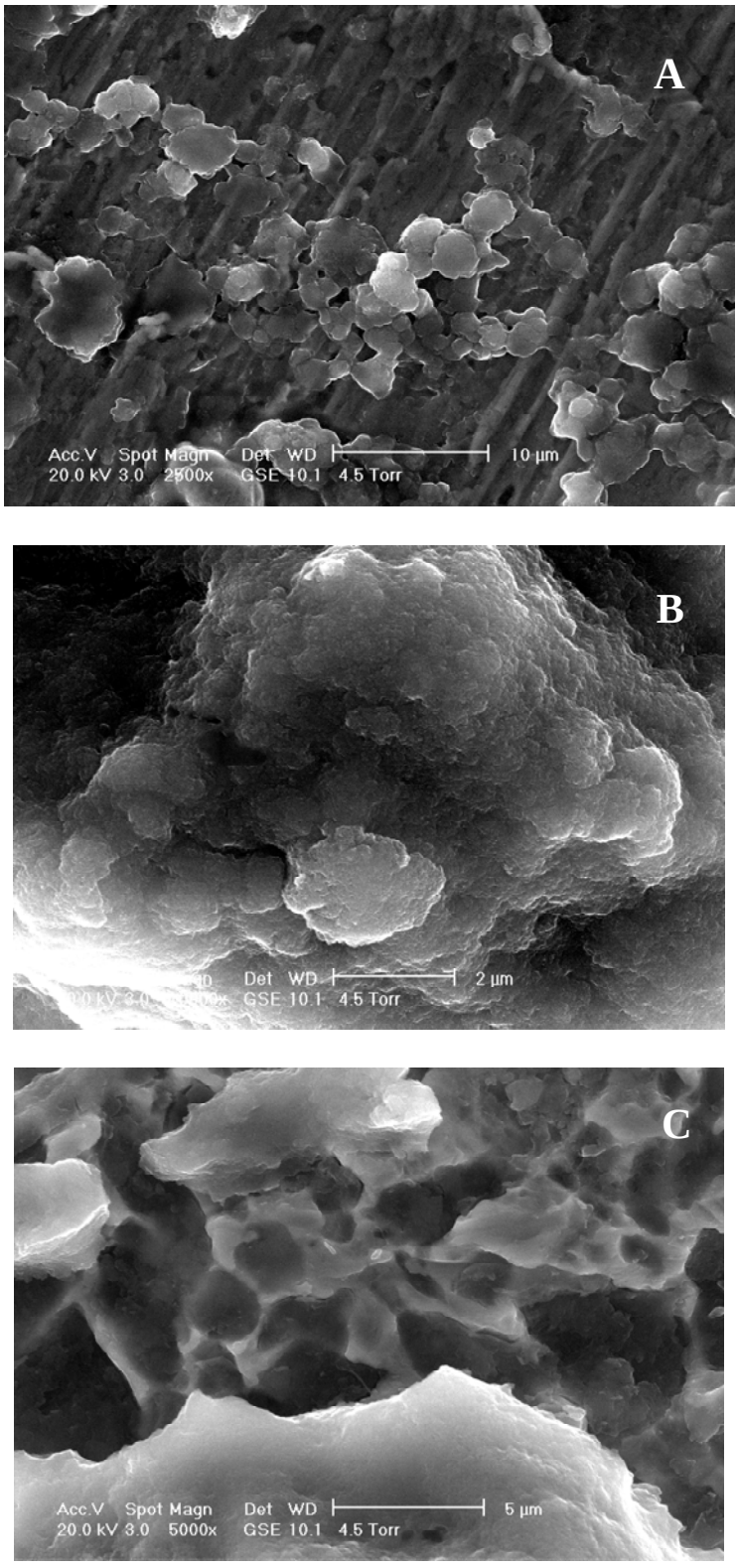

Figure B.2. Rosette structures in HFO pre-equilibrated with As(V) and incubated with ANA-3 WT (a) and mutant (b). Pitted structure of HFO incubated with ANA-3 WT (c).

B4. Bacterial interactions with the mineral surface

Bacteria can be seen on the HFO surfaces, with and without adsorbed As. They appear as darker ovals ~1 μm in length, indicated with arrows in Figure B.3a,b,c. The bacteria appear to be encapsulating themselves in a secondary precipitate or borrowing into the HFO surface (Figure B.3c, Figure B.4a,b,c).

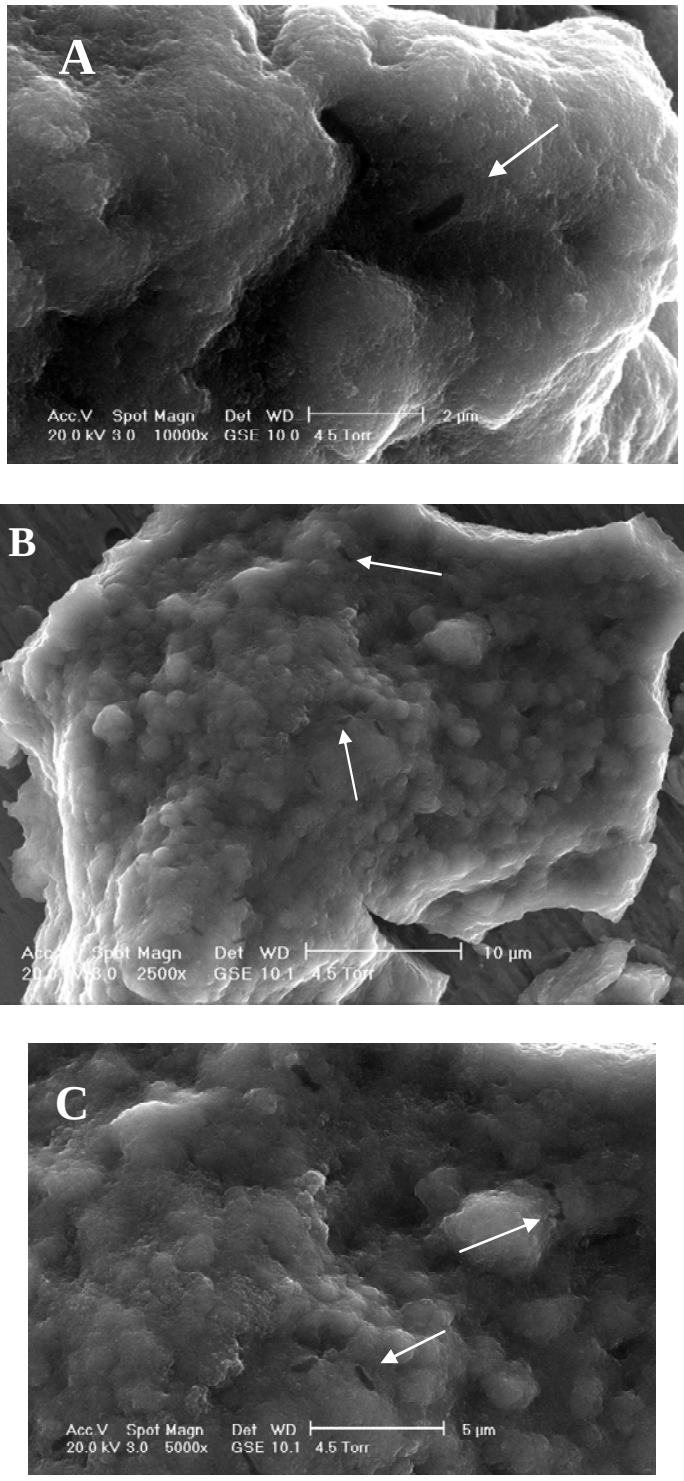

Figure B.3. ANA-3 WT (a) and ANA-3 mutant (b,c) on HFO pre-equilibrated with As(III). Arrows indicate bacterial cells on the HFO surface.

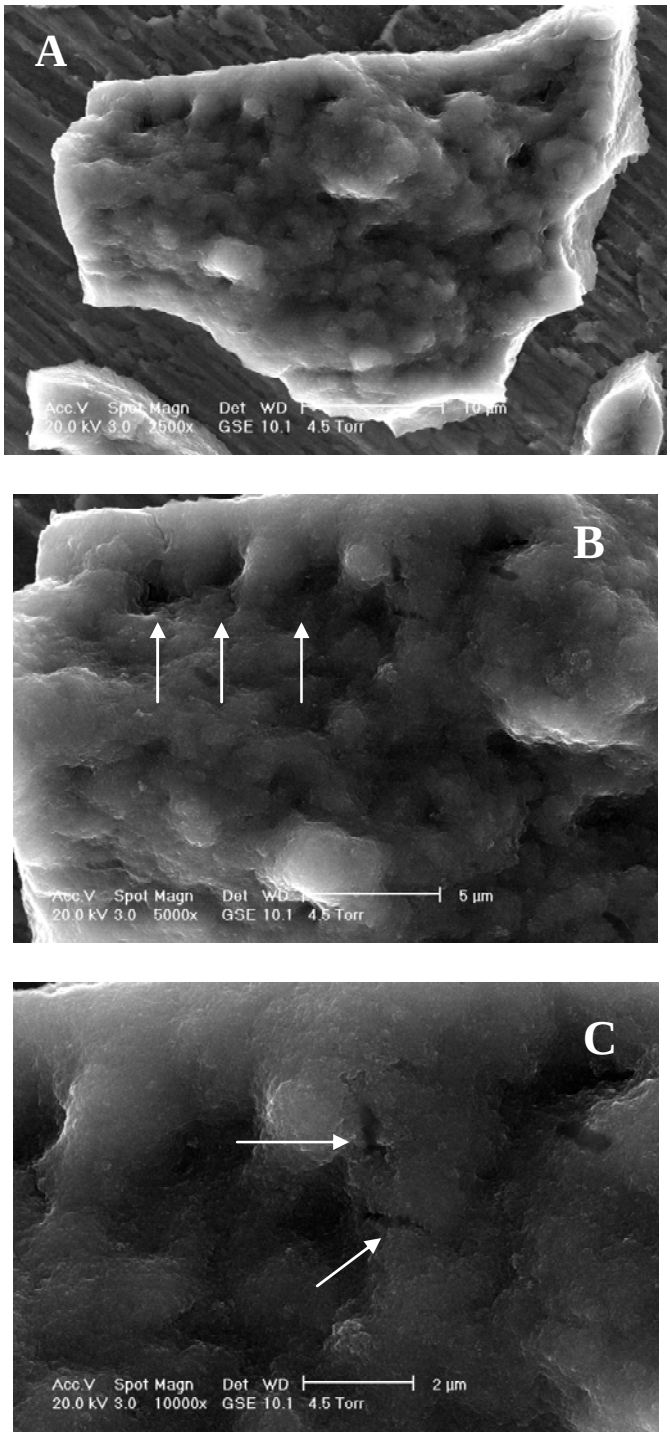

Figure B.4a-c. ANA-3 mutant on HFO pre-equilibrated with As(III). Images are taken from the same particle with increasing magnification. Arrows indicate pits possibly due to bacteria (b) or probable bacterial cells partially encrusted with secondary precipitates (c).

Appendix C

Bacterial Minimal Medium

Table C.1. Chemical constituents of the bacterial minimal medium

Chemical Formula	**Concentration**	**Brand and Purity**
K_2HPO_4	0.05 g/L	Mallinckrodt, AR-ACS, 100.0%
KH_2PO_4	0.035 g/L	Mallinckrodt, AR-ACS, 99.8%
NaCl	0.46 g/L	Mallinckrodt, AR-ACS, 100.1%
$(NH_4)_2SO_4$	0.225 g/L	Mallinckrodt, AR-ACS
$MgSO_4 \cdot 7H_2O$	0.117 g/L	Allied Chemical, 99.5%
$NaHCO_3$	8.4%	Mallinckrodt, AR-ACS, 100.2%
NaOH	1M	Mallinckrodt, AR-ACS, 99%
HCl	1M	Mallinckrodt, ACS reagent grade
$NaC_3H_5O_3$	60% syrup	Sigma
$NaC_2H_3O_2 \cdot 3H_2O$		J.T. Baker, 99.9%
Vitamin Mix	5mL	See Table 5.2
Mineral Mix	5 mL	See Table 52

Table C.2. Vitamin and minerals used in bacterial minimal medium

Vitamin Mix	
Biotin	2 mg/L
Folic acid	2 mg/L
Pyridoxine HCl	10 mg/L
Riboflavin	5 mg/L
Thiamine	5 mg/L
Nicotinic acid	5 mg/L
Pantothenic acid	5 mg/L
B-12	0.1 mg/L
p-aminobenzoic acid	5 mg/L
Thioctic acid	5 mg/L

Mineral Mix	
NTA	1.5 g/L
$MgSO_4$	3.0 g/L
$MnSO_4 \cdot H_2O$	0.5 g/L
NaCl	1.0 g/L
$FeSO_4 \cdot 7H_2O$	0.1 g/L
$CaCl_2 \cdot 2H_2O$	0.1 g/L
$CoCl_2 \cdot 6H_2O$	0.1 g/L
$ZnCl_2$	0.13 g/L
$CuSO_4 \cdot 5H_2O$	0.01 g/L
$AlK(SO_4) \cdot 12H_2O$	0.01 g/L
H_3BO_3	0.01 g/L
Na_2MoO_4	0.025 g/L
$NiCl_2 \cdot 6H_2O$	0.024 g/L
$Na_2WO_4 \cdot 2H_2O$	0.025 g/L

Appendix D

Gel Probe Field Data

Gel probes deployed in July 2003, October 2003, October 2004, August 2005, and May 2006 were analyzed according to the methods described in Chapter 3. In July 2003, October 2003, and October 2004, As, Fe, Mn, and P were measured. In August 2005 and May 2006, gel probes were analyzed for P, Cr, Mn, Ni, Cu, As, Se, Sr, Mo, Sb, Ba, W, Pb, and U. Any elements not reported in the tables below were not detected.

Table D1. July 2003 field deployment, clear gels only

Depth (cm)	As (µM)	Fe (µM)	Mn (µM)	P (µM)
-13.44	0.02	5.57	0.08	3.32
-12.80	0.04	6.22	0.13	3.97
-12.16	0.03	6.07	0.15	4.47
-11.52	0.02	5.11	0.09	4.21
-10.88	0.02	6.19	0.10	4.38
-10.24	0.03	5.10	0.08	2.20
-9.60	0.03	6.83	0.16	3.38
-8.96	0.04	9.33	0.27	2.80
-8.32	0.02	2.54	0.07	2.10
-7.68	0.01	2.61	0.08	2.25
-7.04	0.02	4.74	0.12	3.47
-6.40	0.02	2.59	0.29	4.46
-5.76	0.07	8.97	0.35	6.17
-5.12	0.04	3.27	0.31	5.30
-4.48	0.02	1.23	0.28	5.62
-3.84	0.01	0.45	0.24	4.85
-3.20	0.02	1.75	0.27	5.58
-2.56	0.00	2.16	0.24	3.72
-1.92	0.02	1.68	0.25	5.36
-1.28	0.03	3.85	0.29	5.79
-0.64	0.02	2.89	0.29	4.80
0.00	0.03	2.63	0.30	4.87
0.64	0.03	5.24	0.29	4.47
1.28	0.02	2.65	0.29	4.18
1.92	0.02	1.95	0.26	4.33
2.56	0.03	2.49	0.26	5.58
3.20	0.04	2.77	0.29	6.05
3.84	0.07	8.36	0.30	7.05
4.48	0.04	2.39	0.29	5.79
5.12	0.03	3.18	0.33	4.25
5.76	0.04	3.49	0.34	4.31
6.40	0.04	2.92	0.29	3.76
7.04	0.03	5.08	0.35	4.67
7.68	0.02	6.28	0.27	3.68
8.32	0.03	1.64	0.25	4.78
8.96	0.04	0.85	0.26	4.63
9.60	0.02	2.24	0.29	5.45
10.24	0.04	4.89	0.37	5.11
10.88	0.04	4.25	0.39	5.80
11.52	0.03	3.01	0.33	5.35
12.16	0.05	5.42	0.53	6.18
12.80	0.29	13.22	1.10	4.40
13.44	0.45	22.41	2.25	4.51
14.08	0.38	27.07	2.82	5.02
14.72	0.57	105.04	5.38	5.70
15.36	0.52	117.05	9.86	5.82
16.00	0.68	215.09	7.97	6.18
16.64	1.47	246.76	7.41	8.22
17.28	3.48	533.91	9.04	18.14
17.92	6.22	618.46	7.46	32.95
18.56	5.73	724.34	12.05	34.42

Table D2. October 2003 probe 1, clear gels only

Depth (cm)	As (μM)	Fe (μM)	P (μM)	Mn (μM)
-9.60	0.07	0.00	3.01	0.00
-8.96	0.08	0.00	2.83	0.00
-8.32	0.04	0.00	3.02	0.00
-7.68	0.09	0.00	2.85	0.00
-7.04	0.05	0.00	2.21	0.00
-6.40	0.07	0.00	1.74	0.00
-5.76	0.03	0.00	2.60	0.00
-5.12	0.03	0.00	2.09	0.00
-4.48	0.08	0.00	1.58	0.00
-3.84	0.02	0.00	1.93	0.00
-3.20	0.02	0.00	1.75	0.00
-2.56	0.07	0.00	1.02	0.00
-1.92	0.04	0.00	3.36	0.00
-1.28	0.05	0.00	1.39	0.00
-0.64	0.11	0.00	1.09	0.00
0.00	0.11	0.00	0.96	0.00
0.64	0.12	0.00	0.47	0.00
1.28	0.01	0.00	1.28	0.00
1.92	0.01	0.00	1.09	0.00
2.56	0.08	0.00	0.15	0.00
3.20	0.08	0.00	0.89	0.48
3.84	0.19	3.94	1.10	1.45
4.48	0.41	13.81	1.21	3.37
5.12	0.47	24.14	1.32	2.26
5.76	0.48	14.19	0.62	5.06
6.40	0.51	9.76	0.10	6.48
7.04	0.55	24.84	0.80	7.52
7.68	0.51	25.65	0.47	6.63
8.32	0.54	28.18	0.43	7.88
8.96	0.68	38.68	0.19	8.89
9.60	0.78	60.83	0.47	6.39
10.24	0.84	70.91	1.78	8.04
10.88	0.86	72.41	0.40	8.12
11.52	0.63	64.39	1.01	7.86
12.16	1.47	214.28	1.17	15.39
12.80	1.91	223.12	1.40	11.76
13.44	2.81	427.90	1.40	18.60
14.08	4.94	375.79	4.07	16.19
14.72	3.91	432.97	2.42	15.99
15.36	3.70	515.62	3.42	13.19
16.64	6.55	866.02	6.53	16.04
17.28	7.07	898.07	2.77	17.25
17.92	7.99	774.94	5.47	17.24
18.56	8.27	726.76	3.40	18.35
19.20	9.37	690.46	18.31	18.52
19.84	7.69	571.18	8.57	18.12
21.12	9.32	709.74	19.63	19.70
21.76	11.06	820.70	21.80	21.78
22.40	11.51	847.65	23.70	21.37
23.04	12.02	880.89	34.18	21.35
23.68	7.98	613.00	12.23	19.06
24.32	11.75	990.33	13.78	24.94
24.96	9.47	820.14	17.32	18.26
25.60	9.87	746.46	21.32	15.52

Table D3. October 2003 probe 2, clear gels only

Depth (cm)	As (µM)	Fe (µM)	P (µM)	Mn (µM)
2.56	0.62	62.24	0.96	5.12
3.20	0.85	83.40	3.10	5.07
3.84	0.94	101.07	2.15	5.31
4.48	0.87	90.71	1.83	5.32
5.12	0.89	99.27	1.34	5.51
5.76	0.81	101.01	0.84	5.31
6.40	0.99	91.12	4.65	6.62
7.04	1.36	125.10	1.55	9.12
7.68	1.39	136.06	1.83	9.58
8.32	1.59	136.67	2.32	11.92
8.96	1.48	190.09	1.07	10.31
9.60	2.25	192.87	0.63	10.20
10.24	1.88	205.54	0.19	12.02
10.88	2.03	196.75	1.96	12.74
11.52	1.90	199.35	3.11	7.71
12.16	2.33	221.34	1.86	11.77
12.80	2.57	276.78	1.74	12.98
13.44	3.58	292.76	2.58	15.49
14.08	3.91	321.00	2.25	15.22
14.72	3.32	378.33	6.22	12.15
15.36	2.79	278.93	2.76	11.45
16.00	3.97	353.20	3.83	12.91
16.64	4.11	427.73	8.86	15.87
17.28	5.21	479.22	8.59	15.45
17.92	4.11	387.73	8.86	15.87
18.56	8.17	410.92	21.77	15.87
19.20	8.28	416.30	16.95	16.00
19.84	7.35	459.28	17.68	16.53
20.48	8.69	464.74	19.55	16.20
21.12	8.33	492.56	15.39	19.20
21.76	7.38	492.85	13.64	18.87
22.40	9.10	493.67	15.24	17.90
23.04	10.48	501.78	22.38	16.82
23.68	9.58	589.85	29.03	18.77
24.32	7.05	610.31	12.77	16.53
24.96	8.02	670.75	5.34	14.39
25.60	7.01	644.02	13.44	22.10
26.24	10.76	666.08	16.95	16.00
26.88	7.01	792.64	10.34	17.00
27.52	6.78	702.75	8.59	15.45
28.16	9.56	734.85	17.68	16.53
28.80	13.62	802.85	22.38	16.82
29.44	9.59	788.55	13.64	18.87
30.08	11.30	743.59	19.55	16.20
30.72	10.83	788.09	15.39	19.20
31.36	12.19	890.53	14.43	13.86
32.00	7.93	666.41	13.66	22.81
32.64	11.30	743.59	19.55	16.20
33.28	9.76	752.51	9.62	15.22
33.92	8.30	795.83	15.56	12.15
34.56	12.45	943.76	19.03	18.77
35.20	9.16	976.50	12.77	16.53

Table D4. October 2003 probe 3, clear gels only

Depth (cm)	As (µM)	Fe (µM)	P (µM)	Mn (µM)
-9.60	0.09	0.00	4.85	0.00
-8.96	0.10	0.00	3.91	0.00
-8.32	0.07	0.00	2.98	0.00
-7.68	0.07	0.00	5.30	0.00
-7.04	0.08	0.00	2.09	0.00
-6.40	0.11	0.00	1.58	0.00
-5.76	0.13	0.00	1.93	0.00
-5.12	0.16	0.00	4.79	0.00
-4.48	0.03	0.00	3.91	0.00
-3.84	0.12	0.00	3.54	0.00
-3.20	0.07	0.00	3.31	0.00
-2.56	0.10	0.00	3.93	0.00
-1.92	0.11	0.00	4.02	0.00
-1.28	0.17	0.00	5.66	0.00
-0.64	0.21	0.00	4.51	0.00
0.00	0.23	0.00	5.10	0.00
0.64	0.14	0.00	5.47	0.00
1.28	0.32	0.00	5.01	0.00
1.92	0.24	0.00	6.12	0.00
2.56	0.22	0.00	4.75	0.00
3.20	0.11	0.00	4.30	0.00
3.84	0.24	0.00	4.69	0.00
4.48	0.21	0.00	4.43	0.00
5.12	0.37	0.00	4.92	0.00
5.76	0.27	0.00	3.99	0.00
6.40	0.19	0.00	4.86	0.00
7.04	0.15	0.00	4.19	0.00
7.68	0.13	0.00	3.94	0.32
8.32	0.27	0.00	5.05	0.48
8.96	0.12	5.82	4.61	0.40
9.60	0.21	14.18	4.24	0.43
10.24	0.16	8.17	4.11	0.33
10.88	0.13	7.74	3.73	0.32
11.52	0.13	8.72	4.07	0.28
12.16	0.20	15.26	3.95	0.45
12.80	0.20	29.53	3.66	0.39
13.44	0.45	55.78	5.09	0.61
14.08	0.10	10.81	3.43	0.23
14.72	0.39	33.02	3.42	0.58
15.36	0.23	19.73	3.44	0.43
16.00	0.36	35.47	4.33	0.58
16.64	0.37	33.04	4.05	0.64
17.28	0.49	52.51	4.76	0.73
17.92	0.79	97.32	6.85	1.04
18.56	0.61	67.25	5.30	0.82
19.20	0.69	52.47	2.24	1.28
19.84	0.97	79.59	2.67	2.02
20.48	0.99	78.32	3.81	1.88
21.12	1.36	98.17	6.68	2.80
21.76	1.36	126.39	4.36	2.32
22.40	1.54	103.83	9.04	3.64
23.04	1.28	64.89	2.92	3.02
23.68	2.14	134.85	7.36	3.35

(Table D4 continued)

Depth (cm)	As (µM)	Fe (µM)	P (µM)	Mn (µM)
24.32	2.84	169.10	12.05	3.85
25.60	2.91	135.72	6.59	4.30
26.24	4.24	186.58	8.74	5.53
26.88	3.76	183.98	10.53	4.74
27.52	2.37	138.65	6.74	5.54
28.16	2.51	144.59	5.03	5.50
28.80	2.22	132.67	4.19	5.87
29.44	2.57	123.57	4.39	6.97
30.08	2.53	94.82	3.48	6.57
31.36	3.06	108.30	10.83	5.20
32.00	3.66	127.18	11.37	5.44
32.64	2.64	78.69	4.03	4.83
33.28	4.89	168.56	9.69	7.90
33.92	4.31	179.39	11.11	5.94
34.56	5.24	179.92	16.09	6.04
35.20	5.06	204.31	14.44	7.09
35.84	7.52	279.76	15.48	7.90
36.48	6.70	263.94	15.43	7.36
37.12	6.48	268.65	22.80	6.20
37.76	8.17	293.10	17.87	8.33
38.40	7.77	291.28	18.46	6.58
39.04	7.69	271.18	18.57	7.12
39.68	7.32	265.74	17.63	6.70
40.32	7.03	305.70	16.63	8.28

Table D5. October 2003 probe 4, clear gels only

Depth (cm)	As (µM)	Fe (µM)	P (µM)	Mn (µM)
-8.96	0.16	0.00	0.15	0.00
-8.32	0.03	0.00	0.16	0.00
-7.68	0.12	0.00	0.16	0.00
-7.04	0.07	0.00	0.13	0.00
-6.40	0.20	0.00	0.20	0.00
-5.76	0.10	0.00	0.14	0.00
-5.12	0.15	0.00	0.13	0.00
-4.48	0.10	0.00	0.20	0.00
-3.84	0.07	0.00	0.12	0.00
-3.20	0.06	0.00	0.16	0.00
-2.56	0.06	0.00	0.13	0.00
-1.92	0.07	0.00	0.15	0.00
-1.28	0.09	0.00	0.18	0.00
-0.64	0.10	0.00	0.13	0.00
0.00	0.17	0.00	0.23	0.00
0.64	0.11	0.00	0.19	0.00
1.28	0.09	0.00	0.12	0.00
1.92	0.12	0.00	0.16	0.00
2.56	0.22	0.00	0.14	0.00
3.20	0.33	0.00	0.26	0.00
3.84	0.11	0.00	0.16	1.10
4.48	0.21	0.00	0.17	2.79
5.12	0.17	5.88	0.12	3.55
5.76	0.28	22.40	0.23	5.23
6.40	0.36	38.87	0.21	7.09
7.04	0.29	27.30	0.16	6.67
7.68	0.78	79.35	0.17	7.20
8.32	0.55	50.37	0.13	6.36
8.96	1.10	112.91	0.22	9.22
9.60	1.23	93.79	0.17	9.63
10.24	1.82	142.86	0.37	9.64
10.88	3.10	146.95	0.70	13.44
11.52	3.12	143.25	0.93	9.93
12.16	3.45	146.87	0.81	12.02
12.80	3.25	116.69	0.72	13.42
13.44	3.08	125.38	0.64	12.72
14.08	3.13	118.14	0.55	14.17
14.72	2.73	78.10	0.38	15.77
15.36	2.95	108.60	0.35	17.86
16.00	3.21	151.35	0.58	19.64
16.64	3.35	125.69	0.51	25.31
17.28	2.33	90.39	0.37	17.93
17.92	2.48	89.86	0.36	18.87
18.56	2.86	126.71	0.40	20.98
19.20	2.42	117.72	0.44	16.98
19.84	3.28	160.61	0.45	20.34
20.48	2.02	78.29	0.40	13.07
21.12	1.85	66.81	0.19	11.80
21.76	1.75	69.61	0.30	9.67
22.40	1.93	106.61	0.28	13.43
23.04	2.10	128.14	0.34	13.11
23.68	2.50	179.84	0.36	18.18
24.32	2.60	196.89	0.46	17.75
24.96	2.16	191.98	0.48	15.77

Table D6. October 2003 probe 5, clear gels only

Depth (cm)	As (µM)	Fe (µM)	P (µM)	Mn (µM)
-8.96	0.02	0.00	1.98	0.00
-8.32	0.08	0.00	2.65	0.00
-7.68	0.04	0.00	3.12	0.00
-7.04	0.07	0.00	2.97	0.00
-6.40	0.07	0.00	2.78	0.00
-5.76	0.05	0.00	3.22	0.00
-5.12	0.02	0.00	1.75	0.00
-4.48	0.01	0.00	2.29	0.00
-3.84	0.04	0.00	2.04	0.00
-3.20	0.08	0.00	2.21	0.00
-2.56	0.05	0.00	1.55	0.00
-1.92	0.08	0.00	2.88	0.00
-1.28	0.08	0.00	2.32	0.00
-0.64	0.12	0.00	1.76	0.00
0.00	0.16	0.00	3.44	0.00
0.64	0.09	0.00	1.84	0.00
1.28	0.12	0.00	3.22	0.00
1.92	0.07	0.00	1.70	0.00
2.56	0.17	10.02	3.07	0.00
3.20	0.11	9.67	2.47	0.00
3.84	0.21	15.07	3.91	0.34
4.48	0.34	33.19	5.16	0.58
5.12	0.87	31.30	4.06	2.61
5.76	0.38	57.51	5.44	0.68
6.40	0.31	30.27	4.91	0.58
7.04	0.62	68.31	9.08	1.02
7.68	0.62	88.73	11.62	0.94
8.32	0.17	25.73	4.77	0.35
8.96	0.60	74.73	10.40	0.99
9.60	0.55	59.46	8.10	1.05
10.24	0.88	69.21	6.61	2.35
10.88	1.02	57.25	5.09	3.38
11.52	1.37	96.24	8.51	3.46
12.16	0.53	24.24	3.77	1.93
12.80	0.59	41.05	4.35	2.14
13.44	1.10	76.28	7.24	3.59
14.08	1.10	65.40	7.04	3.85
14.72	2.13	96.75	10.14	5.75
15.36	3.47	173.42	6.71	0.70
16.00	3.60	144.88	14.75	6.78
16.64	2.91	111.49	12.67	6.59
17.28	3.65	145.48	12.64	8.72
17.92	3.37	143.78	10.79	6.90
18.56	2.81	100.41	8.90	7.35
19.20	4.00	115.73	11.45	8.23
19.84	4.70	120.26	10.35	9.20
20.48	4.72	135.73	17.16	7.59
21.12	4.59	140.72	21.30	6.13
21.76	4.77	165.01	21.05	7.29
22.40	4.35	125.52	20.26	9.35
23.04	3.77	122.42	17.12	7.66
23.68	3.10	129.66	12.98	7.66
24.32	4.12	146.89	18.46	8.75
24.96	4.23	151.98	15.48	9.77

Table D7. October 2003 probe 6, clear gels only

Depth (cm)	As (µM)	Fe (µM)	P (µM)	Mn (µM)
-16.00	0.07	0.00	2.60	0.00
-15.36	0.02	0.00	2.09	0.00
-14.72	0.09	0.00	2.85	0.00
-14.08	0.04	0.00	3.36	0.00
-13.44	0.05	0.00	2.92	0.00
-12.80	0.03	0.00	2.36	0.00
-12.16	0.07	0.00	3.12	0.00
-11.52	0.06	0.00	2.70	0.00
-10.88	0.09	0.00	1.96	0.00
-10.24	0.09	0.00	3.25	0.00
-9.60	0.08	0.00	2.65	0.00
-8.96	0.07	0.00	1.73	0.00
-8.32	0.09	0.00	3.22	0.00
-7.68	0.10	0.00	2.06	0.00
-7.04	0.10	0.00	1.60	0.00
-6.40	0.06	0.00	2.59	0.00
-5.76	0.09	0.00	2.21	0.00
-5.12	0.12	0.00	3.28	0.00
-4.48	0.09	0.00	3.27	0.00
-3.84	0.07	0.00	2.68	0.00
-3.20	0.11	0.00	3.19	0.00
-2.56	0.08	0.00	3.49	0.00
-1.92	0.06	0.00	2.19	0.00
-1.28	0.09	0.00	3.79	0.00
-0.64	0.10	0.00	3.07	0.00
0.00	0.20	0.00	3.09	0.00
0.64	0.12	0.00	3.13	0.00
1.28	0.14	0.00	1.80	0.00
1.92	0.26	13.66	3.74	1.34
2.56	0.31	23.66	3.14	0.00
3.20	0.41	34.66	2.84	0.00
3.84	0.38	35.79	4.50	1.21
4.48	0.31	24.86	3.86	1.12
5.12	0.49	54.58	4.06	4.81
5.76	0.60	72.04	9.10	1.97
6.40	0.54	75.45	5.40	5.26
7.04	0.81	106.58	7.04	4.86
7.68	1.57	119.51	7.98	7.91
8.32	1.00	135.44	5.82	8.15
8.96	0.85	108.96	5.36	7.52
9.60	0.48	121.32	4.58	3.58
10.24	1.26	115.89	7.60	10.57
10.88	1.14	79.70	6.70	8.92
11.52	1.53	81.65	5.89	9.33
12.16	0.64	72.47	8.43	3.90
12.80	1.59	79.05	6.50	9.82
13.44	2.27	100.82	8.07	8.90
14.08	2.90	109.48	10.82	11.26
14.72	1.86	130.37	8.97	10.13
15.36	2.59	81.90	10.01	11.32
16.00	1.62	57.89	4.42	9.28
16.64	2.17	86.70	7.83	11.63
17.28	1.52	63.11	10.18	9.91
17.92	1.91	81.01	6.75	10.51

(Table D7 continued)

Depth (cm)	As (µM)	Fe (µM)	P (µM)	Mn (µM)
18.56	0.47	57.08	6.61	2.46
19.20	1.52	63.11	10.18	9.91
19.84	2.01	61.75	11.36	10.60
20.48	2.66	104.09	12.33	12.93
21.12	2.86	90.83	10.53	13.07
21.76	2.67	111.23	15.51	12.12
22.40	2.56	151.09	14.02	12.43
23.04	3.09	143.02	13.89	14.41
23.68	1.44	131.54	9.06	8.92
24.32	3.56	161.88	16.08	13.76
25.60	2.79	95.64	10.37	11.78
26.24	2.40	76.11	8.35	12.52
26.88	2.07	74.28	7.39	9.76
27.52	2.10	74.62	7.72	8.86
28.16	2.56	105.54	8.96	11.64
28.80	1.96	167.84	10.71	12.37
29.44	2.04	109.92	10.35	9.88
30.08	1.90	108.86	21.37	9.78
31.36	2.99	100.30	11.89	11.66
32.00	2.33	137.73	11.39	12.70
32.64	2.28	84.21	10.74	10.52
33.28	2.37	132.26	11.13	10.42
33.92	1.57	174.77	11.67	9.08
34.56	2.81	205.22	11.25	15.41
35.20	2.55	199.74	10.86	11.67

Table D8. October 2004, single probe with HFO and clear gels, probe 1

Clear gels

Depth (cm)	As (µM)	Fe (µM)	P (µM)	Mn (µM)
0.69	0.00	154.95	1.83	1.01
2.06	0.00	47.80	1.78	9.02
3.43	0.00	56.12	0.58	13.82
4.80	0.00	43.95	0.44	14.32
6.17	0.33	175.82	0.32	21.29
7.54	0.08	162.48	0.00	17.04
8.91	0.06	179.12	0.00	18.59
10.28	0.00	155.99	0.00	17.32
11.65	0.09	164.48	0.00	17.88
13.02	0.11	217.80	0.00	19.57
14.39	0.27	283.38	0.58	21.59
15.76	0.09	226.63	0.00	20.10
17.13	0.27	282.55	0.04	22.41
18.50	0.35	317.39	0.00	25.69
19.87	0.19	229.18	0.15	17.09
21.24	0.26	272.80	3.35	21.48
22.61	0.33	282.91	3.48	21.44
23.98	0.75	327.83	6.18	26.21
25.35	1.19	411.27	5.35	24.29
26.72	1.13	428.75	5.54	24.64
28.09	2.00	510.05	11.23	29.51
29.46	1.39	524.74	4.56	28.32
30.83	1.20	499.85	4.14	28.81
32.20	0.69	349.76	2.69	17.53
33.57	1.02	361.08	7.74	20.13
34.94	1.70	425.87	3.57	19.31
36.31	1.73	495.14	2.81	23.97
37.68	1.92	549.05	3.42	24.93
39.05	1.77	520.30	2.70	23.42
40.42	1.84	542.69	2.57	26.03
41.79	1.62	476.44	2.25	21.15
43.16	3.45	528.22	22.23	18.65
44.53	4.24	584.24	16.06	19.01
45.90	6.65	659.37	29.36	19.52
47.27	5.21	615.02	48.00	17.86
48.64	9.05	860.08	60.89	21.66
50.01	6.93	655.56	78.44	17.95
51.38	11.86	945.84	91.83	23.23
52.75	9.67	844.92	65.59	21.86
54.12	7.63	845.09	37.93	25.05

HFO-doped gels

Depth (cm)	mol As/mol Fe	mol P/mol Fe
1.37	0.0002	0.0020
2.74	0.0008	0.0023
4.11	0.0005	0.0014
5.48	0.0007	0.0015
6.85	0.0023	0.0024
8.22	0.0010	0.0013
9.59	0.0009	0.0015
10.96	0.0012	0.0017
12.33	0.0011	0.0018
13.70	0.0017	0.0018
15.07	0.0011	0.0019
16.44	0.0013	0.0017
17.81	0.0017	0.0020
19.18	0.0012	0.0014
20.55	0.0012	0.0014
21.92	0.0017	0.0017
23.29	0.0014	0.0015
24.66	0.0042	0.0044
26.03	0.0027	0.0022
27.40	0.0028	0.0028
28.77	0.0032	0.0023
30.14	0.0032	0.0028
31.51	0.0029	0.0021
32.88	0.0028	0.0026
34.25	0.0038	0.0037
35.62	0.0031	0.0023
36.99	0.0047	0.0047
38.36	0.0028	0.0022
39.73	0.0033	0.0025
41.10	0.0027	0.0023
42.47	0.0032	0.0037
43.84	0.0070	0.0080
45.21	0.0086	0.0101
46.58	0.0099	0.0131
47.95	0.0115	0.0225
49.32	0.0140	0.0324
50.69	0.0159	0.0341
52.06	0.0106	0.0199
53.43	0.0124	0.0193
54.80	0.0081	0.0115

Table D9. October 2004, single probe with HFO and clear gels, probe 2

Clear gels

Depth (cm)	As (µM)	Fe (µM)	P (µM)	Mn (µM)
-2.74	0.08	35.68	4.59	0.07
-1.37	0.08	17.06	2.66	0.00
0.00	0.06	12.60	2.41	0.00
1.37	0.03	8.62	1.94	0.00
2.74	0.03	11.47	2.05	0.00
4.11	0.14	22.85	4.29	1.10
5.48	0.15	42.15	2.50	4.25
6.85	0.14	31.09	1.68	5.86
8.22	0.28	56.23	2.28	8.37
9.59	0.76	149.28	3.22	8.91
10.96	1.22	284.67	2.53	14.66
12.33	1.48	359.36	2.47	14.95
13.70	2.04	429.40	2.35	11.98
15.07	1.77	360.91	2.77	7.85
16.44	1.53	432.14	2.35	13.19
17.81	1.95	530.76	3.78	12.93
19.18	3.04	658.36	5.09	14.91
20.55	4.43	686.82	14.96	12.29
21.92	5.90	907.69	13.90	17.48
23.29	4.00	693.31	12.08	16.16
24.66	4.21	662.63	23.84	28.68
26.03	5.11	619.60	35.80	64.06
27.40	6.23	733.15	47.14	76.62
28.77	4.78	563.94	50.54	50.83
30.14	6.61	753.16	39.06	63.64
31.51	6.62	831.16	53.66	51.74
32.88	6.29	814.67	41.37	47.75

HFO-doped gels

Depth (cm)	mol As/mol Fe	mol P/mol Fe
-2.06	0.0001	0.0015
-0.69	0.0001	0.0014
0.69	0.0001	0.0014
2.06	0.0001	0.0013
3.43	0.0002	0.0013
4.80	0.0004	0.0015
6.17	0.0005	0.0012
7.54	0.0006	0.0013
8.91	0.0012	0.0018
10.28	0.0018	0.0015
11.65	0.0022	0.0017
13.02	0.0036	0.0022
14.39	0.0027	0.0015
15.76	0.0039	0.0022
17.13	0.0032	0.0023
18.50	0.0044	0.0033
19.87	0.0061	0.0044
21.24	0.0073	0.0066
22.61	0.0062	0.0047
23.98	0.0073	0.0081
25.35	0.0072	0.0098
26.72	0.0089	0.0173
28.09	0.0089	0.0225
29.46	0.0092	0.0216
30.83	0.0090	0.0199
32.20	0.0090	0.0202
33.57	0.0051	0.0070

Table D.10a. August 2005, double probe 1, clear gels

Depth (cm)	As (µM)	P (µM)	Mn (µM)	Cu (µM)	Sr (µM)	Mo (µM)	Ba (µM)	W (µM)
-4.80	--	--	--	--	--	--	--	--
-2.74	-0.04	1.23	-0.09	0.00	0.63	0.12	0.07	0.36
-0.69	-0.08	3.79	-0.13	0.00	0.69	0.13	0.06	0.29
1.37	-0.09	0.92	-0.14	0.00	0.75	0.13	0.06	0.23
3.43	0.10	2.22	0.63	0.05	0.64	0.14	0.07	0.23
5.48	0.54	3.28	1.21	0.00	0.63	0.14	0.08	0.26
7.54	1.58	15.43	2.85	0.00	0.83	0.13	0.18	0.46
9.59	2.15	35.21	3.54	0.24	0.95	0.12	0.27	0.68
11.65	1.34	11.97	3.84	0.15	1.07	0.17	0.19	0.47
13.70	3.37	39.19	9.12	0.53	1.27	0.24	0.85	0.64
15.76	1.18	6.66	4.57	0.01	1.08	0.23	0.14	0.41
17.81	1.46	9.61	5.12	0.01	1.01	0.22	0.17	0.45
19.87	4.90	62.47	7.85	0.16	1.49	0.20	0.65	1.13
21.92	4.16	37.88	5.86	0.18	1.07	0.18	0.47	1.09
23.98	5.12	86.23	6.59	0.12	1.10	0.15	0.70	1.11
26.03	5.36	62.50	6.24	0.03	1.07	0.19	0.50	1.37
28.09	2.98	22.13	4.50	0.02	0.84	0.18	0.22	0.74
30.14	2.81	19.94	5.96	0.31	0.99	0.21	0.40	0.75

Depth (cm)	Fe (µM)
-3.43	5.59
-1.37	2.96
0.69	4.70
2.74	9.15
4.80	72.97
6.85	126.56
8.91	162.08
10.96	162.08
13.02	232.05
15.07	176.42
17.13	349.07
19.18	391.37
21.24	317.08
23.29	261.11
25.35	421.68
27.40	255.55

Table D.10b. August 2005, double probe 1, HFO-doped gels

Depth (cm)	mol As/mol Fe	mol P/mol Fe	mol Mn/mol Fe	mol Sr/mol Fe	mol Mo/mol Fe	mol W/mol Fe
-4.80	0.0038	0.0003	0.0001	0.0002	0.0001	0.0004
-2.74	0.0027	0.0006	0.0001	0.0002	0.0001	0.0003
-0.69	0.0026	0.0007	0.0001	0.0001	0.0002	0.0003
1.37	0.0029	0.0004	0.0000	0.0001	0.0003	0.0002
3.43	0.0030	0.0002	0.0001	0.0001	0.0003	0.0002
5.48	0.0025	0.0009	0.0006	0.0001	0.0002	0.0002
7.54	0.0028	0.0004	0.0010	0.0002	0.0002	0.0001
9.59	0.0030	0.0009	0.0007	0.0001	0.0003	0.0002
11.65	0.0033	0.0025	0.0008	0.0002	0.0002	0.0003
13.70	0.0032	0.0040	0.0009	0.0002	0.0001	0.0004
15.76	0.0043	0.0068	0.0009	0.0002	0.0001	0.0007
17.81	0.0035	0.0045	0.0009	0.0001	0.0001	0.0005
19.87	0.0039	0.0048	0.0012	0.0002	0.0001	0.0006
21.92	0.0041	0.0065	0.0011	0.0002	0.0001	0.0006
23.98	0.0067	0.0130	0.0014	0.0002	0.0001	0.0010
26.03	0.0078	0.0214	0.0018	0.0002	0.0001	0.0013
28.09	0.0070	0.0191	0.0016	0.0002	0.0001	0.0013
30.14	0.0050	0.0088	0.0015	0.0002	0.0001	0.0007

Table D.11a. August 2005, double probe 2, clear gels

Depth (cm)	As (µM)	P (µM)	Mn (µM)	Cu (µM)	Sr (µM)	W (µM)
-2.06	4.00	0.00	8.53	0.22	1.08	0.15
0.00	2.23	2.41	6.23	0.05	1.03	0.19
2.06	5.56	28.93	4.49	0.00	1.61	0.58
4.11	3.22	10.94	4.44	0.00	1.29	0.45
6.17	2.48	10.00	5.30	0.01	1.32	0.38
8.22	3.39	3.94	4.88	0.03	1.26	0.40
10.28	4.26	42.78	3.17	0.00	0.99	0.51
12.33	4.69	41.83	2.50	0.02	0.98	0.82
14.39	4.95	27.90	2.72	0.00	1.07	0.89
16.44	6.55	37.59	2.93	4.95	1.12	1.26
18.50	7.33	46.01	2.68	0.06	1.11	1.46
20.55	7.47	43.87	3.03	0.01	1.14	1.74
22.61	5.91	47.11	2.51	0.02	0.95	1.31
24.66	7.55	82.24	3.96	0.10	1.15	1.48
26.72	7.93	64.38	3.17	0.24	1.30	1.79
28.77	5.55	44.29	3.13	0.05	1.07	1.53
30.83	5.77	38.64	3.70	0.09	1.13	1.59
32.88	6.97	85.85	3.69	0.01	1.24	1.91

Depth (cm)	Fe (µM)
0.00	59.73
1.37	270.70
2.06	144.89
3.43	240.49
4.11	235.57
6.17	273.04
8.22	217.87
9.59	226.70
10.28	203.40
12.33	227.21
13.70	267.18
14.39	263.15
16.44	311.94
17.81	273.42
18.50	358.44
20.55	289.41
21.92	301.17
22.61	311.05
24.66	279.91
26.03	316.44
26.72	353.94
28.77	339.95
30.14	343.34
30.83	303.29
32.88	277.45
34.25	269.34
34.94	262.89

Table D.11b. August 2005, double probe 2, HFO-doped gels

Depth (cm)	mol P/ mol Fe	mol Cr/ mol Fe	mol Mn/ mol Fe	mol As/ mol Fe	mol Sr/ mol Fe	mol Mo/ mol Fe	mol Ba/ mol Fe	mol W/ mol Fe
-2.06	0.0000	0.0002	0.0024	0.0023	0.0001	0.0003	0.0001	0.0001
0.00	0.0000	0.0001	0.0017	0.0020	0.0001	0.0002	0.0001	0.0001
2.06	0.0000	0.0001	0.0017	0.0024	0.0001	0.0003	0.0001	0.0001
4.11	0.0000	0.0001	0.0013	0.0021	0.0001	0.0002	0.0001	0.0001
6.17	0.0000	0.0002	0.0014	0.0027	0.0002	0.0002	0.0001	0.0001
8.22	0.0028	0.0001	0.0014	0.0034	0.0002	0.0002	0.0001	0.0003
10.28	0.0022	0.0002	0.0015	0.0033	0.0002	0.0002	0.0001	0.0002
12.33	0.0015	0.0002	0.0013	0.0032	0.0002	0.0001	0.0001	0.0003
14.39	0.0081	0.0001	0.0012	0.0045	0.0002	0.0001	0.0001	0.0006
16.44	0.0133	0.0001	0.0010	0.0059	0.0002	0.0001	0.0002	0.0013
18.50	0.0106	0.0002	0.0010	0.0064	0.0002	0.0001	0.0002	0.0012
20.55	0.0058	0.0001	0.0011	0.0047	0.0002	0.0001	0.0001	0.0008
22.61	0.0151	0.0002	0.0011	0.0079	0.0002	0.0001	0.0002	0.0015
24.66	0.0222	0.0002	0.0010	0.0087	0.0002	0.0001	0.0002	0.0020
26.72	0.0225	0.0002	0.0011	0.0085	0.0003	0.0000	0.0002	0.0016
28.77	0.0195	0.0001	0.0010	0.0084	0.0002	0.0000	0.0002	0.0016
30.83	--	--	--	--	--	--	--	--
32.88	0.0158	0.0002	0.0012	0.0082	0.0003	0.0001	0.0002	0.0016

Table D.12. August 2005, double probe 3, clear gels

Depth (cm)	As (µM)	P (µM)	Mn (µM)	Cu (µM)	Sr (µM)	Mo (µM)	Ba (µM)	W (µM)
-4.80	-0.04	51.89	0.00	0.00	0.72	0.10	0.07	0.24
-2.06	-0.05	6.11	0.00	0.00	0.83	0.11	0.05	0.22
0.69	0.00	1.92	1.27	0.00	0.83	0.11	0.07	0.17
3.43	1.75	6.87	7.35	0.01	1.48	0.25	0.10	0.43
6.17	3.41	16.76	6.59	0.23	1.02	0.22	0.08	0.40
8.91	5.31	62.03	9.33	0.82	1.27	0.27	0.47	0.73
11.65	7.97	53.89	13.38	0.75	1.83	0.37	0.50	0.69
13.70	2.07	118.90	10.03	0.77	1.60	0.39	0.29	0.40
17.13	0.78	--	8.54	6.40	1.27	0.27	0.25	0.23
19.87	0.36	102.98	8.84	0.44	1.43	0.27	0.19	0.19
22.61	0.70	11.12	7.74	1.72	1.16	0.16	0.47	0.22
25.35	0.36	7.77	9.30	0.84	1.68	0.23	0.42	0.16
28.09	0.21	5.05	6.55	0.10	1.64	0.24	0.11	0.16

Depth (cm)	Fe (µM)
-5.48	11.27
-2.74	4.68
0.00	33.34
2.74	72.16
5.48	71.65
8.22	94.42
10.96	134.43
13.70	126.24
16.44	65.25
19.18	110.10
21.92	56.29
24.66	24.79
27.40	23.09

Table D.13. LC-ICP-MS As speciation data from August 2005 double probes 1, 2, and 3

Double Probe 1		
depth (cm)	**As(III) (µM)**	**As(V) (µM)**
-4.11	0.28	0.43
-2.06	0.28	0.37
0.00	0.28	0.33
2.06	0.28	0.44
4.11	0.32	0.62
6.17	0.47	0.89
8.22	0.87	0.90
10.28	1.60	1.14
12.33	0.72	0.76
14.39	0.86	1.19
16.44	0.91	1.13
18.50	1.22	0.99
20.55	2.65	1.44
22.61	3.22	1.59
24.66	2.78	2.03
26.72	3.43	1.74
28.77	1.95	1.42
30.83	1.21	1.17

Double Probe 2		
depth (cm)	**As(III) (µM)**	**As(V) (µM)**
0.69	2.50	0.97
4.80	2.20	1.55
8.91	3.29	1.77
13.02	4.13	1.94
17.13	4.14	1.66
21.24	3.46	1.83
25.35	5.61	2.45
29.46	3.94	2.10
33.57	4.26	1.79

Double Probe 3		
depth (cm)	**As(III) (µM)**	**As(V) (µM)**
-4.80	0.06	0.18
-2.06	0.27	0.16
0.69	0.68	1.05
3.43	3.58	0.97
6.17	5.25	0.77
8.91	7.82	1.18
11.65	7.38	1.64
14.39	6.67	1.19
17.13	6.82	1.32
19.87	5.22	1.64
22.61	1.22	0.76
25.35	0.73	0.58
28.09	0.85	0.65

Table D.14a. May 2006 clear gels

Depth (cm)	As (µM)	P (µM)	Mn (µM)	Sr (µM)	W (µM)	Fe (µM)
-0.69	0.45	18.74	2.57	1.33	1.03	79.86
0.00	0.49	5.29	1.54	1.18	0.49	81.91
0.69	0.31	0.00	1.28	0.97	0.37	27.66
1.37	0.44	0.41	2.07	1.07	0.36	55.71
2.74	0.60	8.08	2.77	1.04	0.38	72.16
3.43	1.07	13.23	4.10	1.20	0.41	80.93
4.11	1.19	5.34	4.77	1.34	0.46	89.31
4.80	1.15	4.20	5.35	1.44	0.42	108.90
6.17	0.96	5.15	4.32	1.12	0.38	156.18
6.85	1.43	5.31	7.78	1.74	0.56	73.41
7.54	0.93	7.30	4.20	1.07	0.41	139.97
8.22	1.10	33.57	4.98	1.29	0.40	82.70
9.59	1.23	9.52	5.25	1.34	0.35	79.91
10.28	1.11	6.95	4.98	1.27	0.39	106.69
10.96	1.68	10.33	6.93	1.73	0.49	99.06
11.65	1.92	9.52	7.68	1.69	0.48	97.29
13.02	2.10	9.94	7.26	1.61	0.50	133.36
13.70	2.00	8.94	7.94	1.68	0.54	124.16
14.39	1.60	8.28	6.08	1.39	0.49	114.60
15.07	1.70	8.33	7.20	1.61	0.43	110.35
16.44	1.61	13.33	6.34	1.50	0.45	103.58
17.13	1.60	8.60	7.21	1.60	0.44	94.62
17.81	1.64	10.64	7.13	1.64	0.45	104.73
18.50	1.96	9.83	10.93	2.15	0.49	111.81
19.87	1.44	34.08	8.13	1.71	0.44	96.90
20.55	1.96	5.78	13.36	2.58	0.48	146.98
21.24	1.92	9.68	10.29	2.10	0.46	187.26
21.92	1.76	8.13	8.52	1.83	0.42	137.02
23.29	2.37	17.77	7.25	1.65	0.55	138.91
23.98	1.78	9.98	6.81	1.58	0.58	155.31
24.66	2.26	11.72	6.30	1.37	0.74	120.11
25.35	3.53	24.79	5.16	1.33	0.87	106.14
26.72	4.04	150.36	5.02	1.48	0.97	166.76
27.40	--	--	--	--	--	--
28.09	5.40	53.26	4.11	1.42	1.10	159.29
28.77	3.96	65.66	3.97	1.24	0.82	140.68
30.14	--	--	3.91	1.23	0.90	158.34
30.83	4.67	28.11	5.09	1.52	1.76	156.06
31.51	5.05	47.61	4.35	1.40	1.18	199.14
32.20	4.86	79.18	4.25	1.37	1.10	184.46
33.57	6.05	55.60	4.52	1.48	1.22	211.29
34.25	4.79	35.19	4.60	1.43	1.10	157.87
34.94	3.51	11.87	6.81	1.52	0.81	100.87
35.62	2.09	5.93	7.29	1.52	0.52	115.86

Table D.14b. May 2006, HFO-doped gels

Depth (cm)	mol As/mol Fe	mol P/mol Fe	mol Sr/mol Fe	mol W/mol Fe
-0.69	0.0008	0.0139	0.0002	0.0003
0.00	0.0008	0.0000	0.0002	0.0002
0.69	0.0019	0.0036	0.0002	0.0004
1.37	0.0020	0.0230	0.0003	0.0004
2.74	0.0018	0.0016	0.0003	0.0003
3.43	0.0012	0.0000	0.0003	0.0002
4.11	0.0013	0.0000	0.0003	0.0002
4.80	0.0009	0.0000	0.0002	0.0002
6.17	0.0018	0.0000	0.0003	0.0002
6.85	0.0012	0.0000	0.0002	0.0002
7.54	0.0018	0.0055	0.0003	0.0002
8.22	0.0028	0.0064	0.0005	0.0004
9.59	0.0022	0.0057	0.0003	0.0003
10.28	0.0021	0.0017	0.0003	0.0002
10.96	0.0036	0.0045	0.0004	0.0004
11.65	0.0027	0.0023	0.0004	0.0003
13.02	0.0028	0.0035	0.0004	0.0003
13.70	0.0021	0.0008	0.0003	0.0003
14.39	0.0022	0.0141	0.0003	0.0003
15.07	0.0018	0.0019	0.0004	0.0002
16.44	0.0022	0.0012	0.0004	0.0002
17.13	0.0023	0.0039	0.0004	0.0003
17.81	0.0025	0.0046	0.0003	0.0003
18.50	0.0024	0.0030	0.0004	0.0003
19.87	0.0020	0.0010	0.0004	0.0002
20.55	0.0023	0.0082	0.0004	0.0002
21.24	0.0016	0.0008	0.0003	0.0002
21.92	0.0011	0.0000	0.0003	0.0001
23.29	0.0037	0.0090	0.0003	0.0005
23.98	0.0034	0.0075	0.0004	0.0007
24.66	0.0035	0.0086	0.0004	0.0005
25.35	0.0051	0.0163	0.0004	0.0006
26.72	0.0044	0.0108	0.0004	0.0006
27.40	0.0045	0.0156	0.0004	0.0006
28.09	0.0044	0.0138	0.0004	0.0006
28.77	0.0050	0.0164	0.0004	0.0006
30.14	0.0058	0.0184	0.0004	0.0007
30.83	0.0058	0.0190	0.0004	0.0008
31.51	0.0048	0.0141	0.0004	0.0006
32.20	0.0076	0.0189	0.0004	0.0007
33.57	0.0097	0.0275	0.0004	0.0009
34.25	0.0078	0.0221	0.0004	0.0008
34.94	0.0049	0.0115	0.0004	0.0005
35.62	0.0009	0.0000	0.0003	0.0002

Table D.15. LC-ICP-MS arsenic speciation data for May 2006

Depth (cm)	As(III) (µM)	As(V) (µM)
0.69	0.24	0.27
4.11	0.64	0.35
7.54	0.69	0.36
10.96	1.17	0.59
14.39	0.89	0.49
17.81	1.01	0.35
21.24	1.23	0.56
24.66	2.63	0.72
28.09	3.14	0.82
31.51	3.84	1.13

Appendix E

Core Analysis and Microcosm Results

E1. A 600 mL container of sediment was defrosted under N_2 in an anaerobic chamber. At each time point, the sediment was homogenized and a 20 mL aliquot was centrifuged to separate the bulk solids from the porewater. The porewater was syringe filtered (0.2 µm) and analyzed for dissolved total Fe and Fe(II) by a colorometric method and As by ICP-MS.

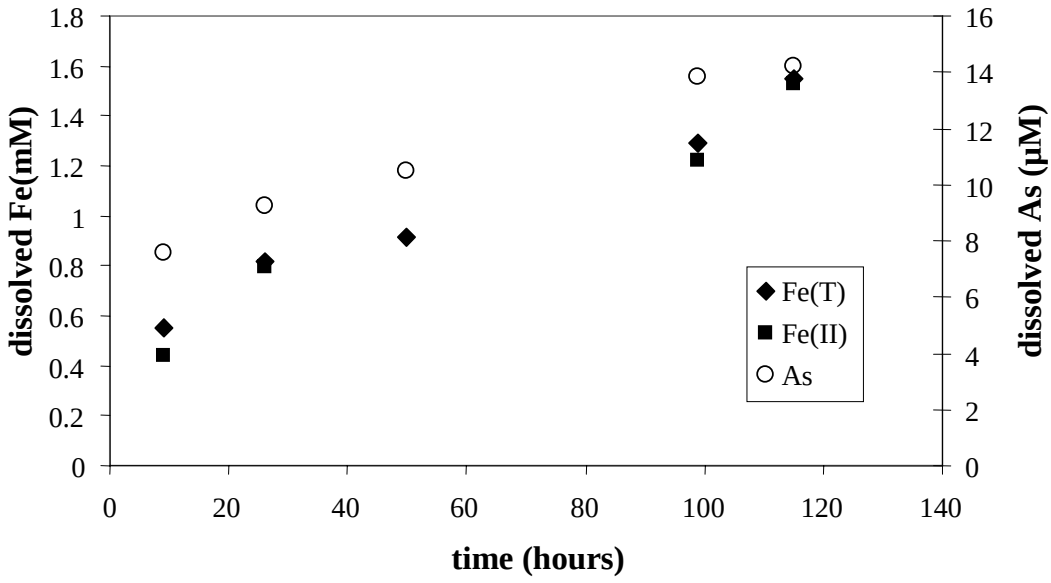

E2. Sediment core sections from May 2006 were extracted with 25 mM H_3PO_4 under N_2 in an anaerobic chamber. The slurry was centrifuged, the supernatant was syringe filtered (0.2 µm) and analyzed by LC-ICP-MS.

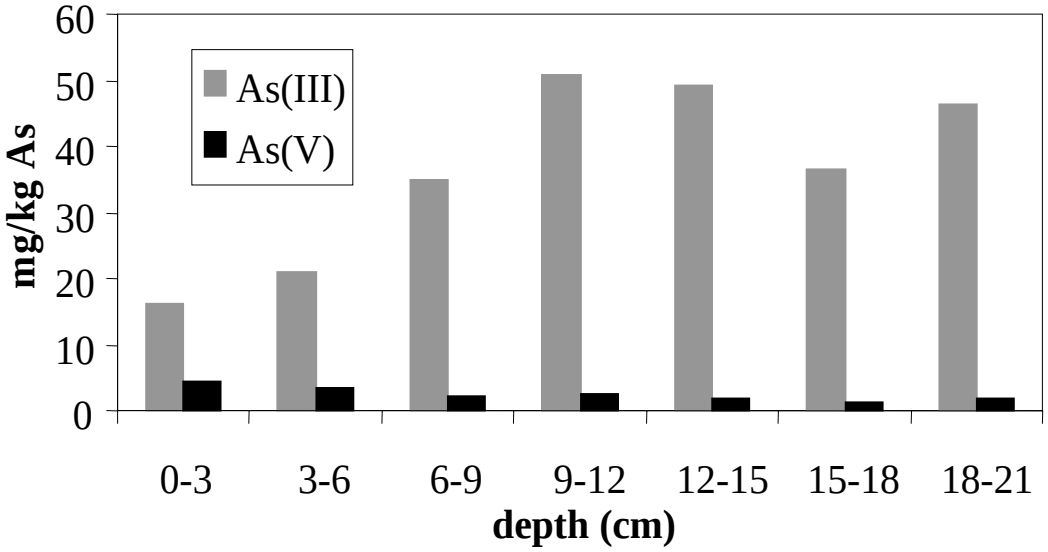

E3. The solid-to-solution ratio was measured by weighing a core section, drying it at 60°C, and reweighing the sample. The core was taken in May 2006 prior to the gel probe deployment when the sediment was soft.

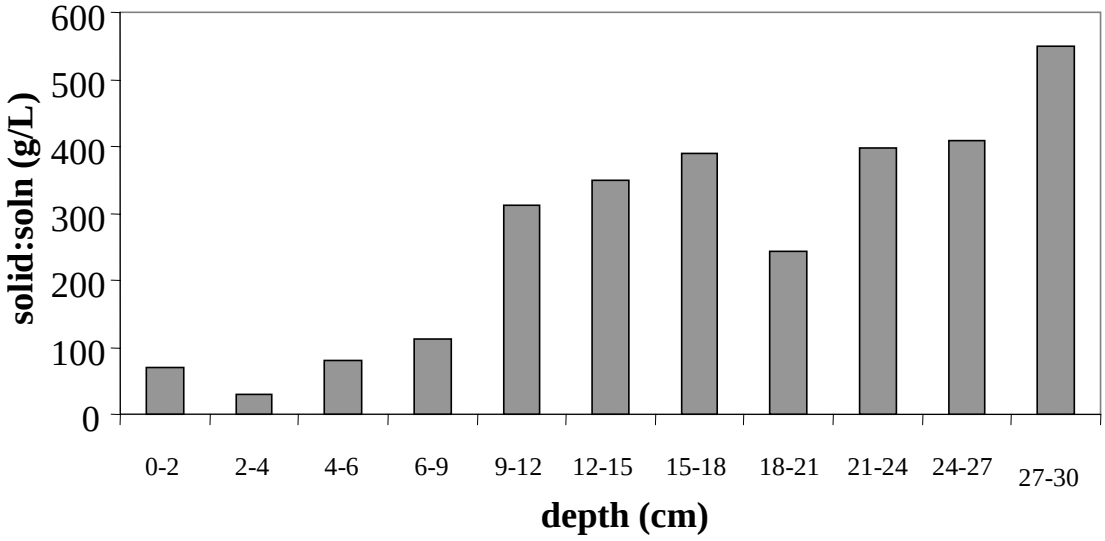

E4. The solid-to-solution ratio was measured by weighing a core section, drying it at 60°C, and reweighing the sample. The core was taken in May 2006 at the time of gel probe deployment, when the sediment was hard.

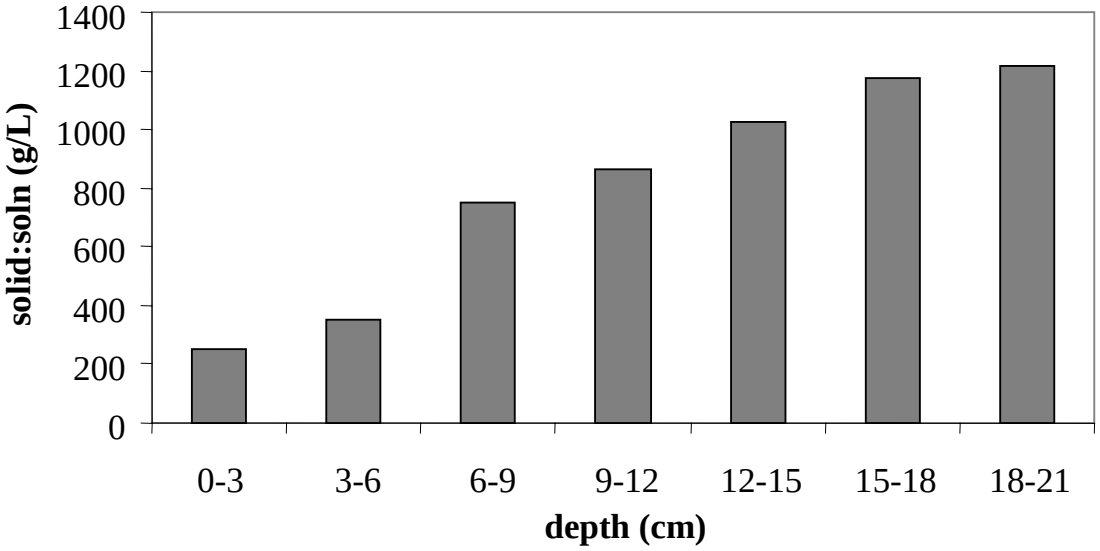

References

Acharyya, S. K. (2002). "Arsenic contamination in groundwater affecting major parts of southern West Bengal and parts of western Chhattisgarh: Source and mobilization processes." Current Science **82**(6): 740-744.

Afonso, M. D. S., P. J. Morando, M. A. Blesa, S. Banwart and W. Stumm (1990). "The reductive dissolution of iron oxides by ascorbate." Journal of Colloid and Interface Science **138**(1): 74-82.

Aggett, J. and G. A. O'Brien (1985). "Detailed Model for the Mobility of Arsenic in the Lacustrine Sediments Based on Measurements in Lake Ohakuri." Environmental Science and Technology **19**(3): 231-238.

Ahmann, D., L. R. Krumholz, H. F. Hemond, D. R. Lovley and F. M. Morel (1997). "Microbial Mobilization of Arsenic from Sediments of the Aberjona Watershed." Environmental Science and Technology **31**(10): 2923-2930.

Akai, J., K. Izumi, H. Fukuhara, H. Masuda, S. Nakano, T. Yoshimura, H. Ohfuji, H. M. Anawar and K. Akai (2004). "Mineralogical and geomicrobiological investigations on groundwater arsenic enrichment in Bangladesh." Applied Geochemistry **19**: 215-230.

Amirbahman, A., D. Kent, G. Curtis and J. Davis (2006). "Kinetics of abiotic arsenic(III) oxidation by aquifer materials." Geochimica et Cosmochimica Acta ***in press***.

Anawar, H. M., J. Akai and H. Sakugawa (2004). "Mobilization of arsenic from subsurface sediments by effect of bicarbonate ions in groundwater." Chemosphere **54**: 753-762.

Anderson, L. C. and K. W. Bruland (1991). "Biogeochemistry of arsenic in natural waters: The importance of Methylated Species." Environmental Science and Technology **25**: 420-424.

Antelo, J., M. Avena, S. Fiol, R. Lopez and F. Arce (2005). "Effects of pH and ionic strength on the adsorption of phosphate and arsenate at the goethite-water interface." Journal of Colloid and Interface Science **285**: 476-486.

Appelo, C. A. J., M. J. J. Van der Weiden, C. Tournassat and L. Charlet (2002). "Surface Complexation of Ferrous Iron and Carbonate on Ferrihydrite and the Mobilization of Arsenic." Environmental Science and Technology **36**(14): 3096-3103.

Arai, Y., D. L. Sparks and J. A. Davis (2004). "Effects of Dissolved Carbonate on Arsenate Adsorption and Surface Speciation at the Hematite-Water Interface." environmental Science and Technology **38**: 817-824.

Azcue, J. M. and J. O. Nriagu (1994). "Role of sediment porewater in the cycling of arsenic in a mine-polluted lake." Environment International **20**(4): 517-527.

Baltpurvins, K. A., R. C. Burns and G. A. Lawrance (1996). "Effect of pH and Anion Type on the Aging of Freshly Precipitated Iron(III) Hydroxide Sludges." Environmental Science and Technology **30**: 939-944.

Bargar, J. R., J. D. Kubicki, R. Reitmeyer and J. A. Davis (2005). "ATR-FTIR spectroscopic characterization of coexisiting carbonate surface complexes on hematite." Geochimica et Cosmochimica Acta **69**(6): 1527-1542.

Bauer, M. and C. Blodau (2006). "Mobilization of arsenic by dissolved organic matter from iron oxides, soils, and sediments." The Science of the Total Environment **354**: 179-190.

Benner, S. C., C. M. Hansel, B. W. Wielinga, T. M. Barber and S. Fendorf (2002). "Reductive dissolution and biomineralization of iron hydroxide under dynamic flow conditions." Environmental Science and Technology **36**(8): 1705-1711.

Bhattacharyya, R., D. Chatterjee, B. Nath, J. Jana, G. Jacks and M. Vahter (2003). "High arsenic groundwater: Mobilization, metabolism, and mitigation - an overview in the Bengal Delta Plain." Molecular and Cellular Biochemistry **253**: 347-355.

Biber, M. V., M. d. S. Afonso and W. Stumm (1994). "The coordination chemistry of weathering: IV. Inhibition of the dissolution of oxide minerals." Geochimica et Cosmochimica Acta **58**(9): 1999-2010.

Bocher, F., A. Gehin, C. Ruby, J. Ghanbaja, M. Abdelmoula and J.-M. R. Genin (2004). "Coprecipitation of Fe(II-III) hydroxycarbonate green rust stabilized by phosphate adsorption." Solid State Sciences **6**(1): 117-124.

Bondietti, G., J. Sinniger and W. Stumm (1993). "The reactivity of Fe(III) (hydr)oxides: effects of ligands in inhibiting the dissolution." Colloids and Surfaces A: Physiochemical and Engineering Aspects **79**: 157-167.

Bonneville, S., P. V. Cappellen and T. Behrends (2004). "Microbial reduction of iron(III) oxyhydroxides: effects of mineral solubility and availability." Chemical Geology **212**: 255-268.

Bose, P. and A. Sharma (2002). "Role of iron in controlling speciation and mobilization of arsenic in subsurface environment." Water Research **36**: 4916-4926.

Bowell, R. J. (1994). "Sorption of arsenic by iron oxides and oxyhydroxides in soils." Applied Geochemistry **9**: 279-268.

Brown, G. E., G. Calas, G. A. Waychunas and J. Petiau (1988). X-ray absorption spectroscopy: Applications in mineralogy and geochemistry. Spectroscopic Methods in Mineralogy and Geology. F. C. Hawthorne. Washington, DC, Mineralogical Society of America. **18:** 431-512.

Buschmann, J., A. Kappeler, U. Lindauer, D. Kistler, M. Berg and L. Sigg (2006). "Arsenite and Arsenate Binding to Dissolved Humic Acids: Influence of pH, Type of Humic Acid, and Aluminum." Environmental Science and Technology **40**(19): 6015-6020.

Campbell, K. M., D. Malasarn, C. W. Saltikov, D. K. Newman and J. G. Hering (2006). "Simultaneous Microbial Reduction of Iron(III) and Arsenic(V) in Suspensions of Hydrous Ferric Oxide." Environmental Science and Technology **40**(19): 5950 - 5955.

Cervantes, C., G. Ji, J. L. Ramirez and S. Silver (1994). "Resistance to arsenic compounds in microorganisms." FEMS Microbiology Reviews **15**: 355-367.

Chiu, V. Q. and J. G. Hering (2000). "Arsenic Adsorption and Oxidation at Manganite Surfaces. 1. Method for Simultaneous Determination of Adsorbed and Dissolved Arsenic Species." Environmental Science and Technology **34**(10): 2029-2034.

Cooper, D. C., A. L. Neal, R. K.Kukkadapu, D. Brewe, A. Coby and F. W. Picardal (2005). "Effects of sediment iron mineral composition on microbially mediated changes in divalent metal speciation: Importance of ferrihydrite." Geochimica et Cosmochimica Acta **69**(7): 1739-1754.

Cornell, R. M. and U. Schwertmann (1996). The Iron Oxides: Structure, Properties, Reactions, Occurrence and Uses. Weinheim, VCH.

Cullen, W. R. and K. J. Reimer (1989). "Arsenic Speciation in the Environment." Chemical Reviews **89**: 713-764.

Cummings, D. E., A. W. March, B. Bostick, S. Spring, J. Frank Caccavo, S. Fendorf and R. F. Rosenzweig (2000). "Evidence for Microbial Fe(III) Reduction in Anoxic, Mining-Impacted Lake Sediments (Lake Coeur d'Alene, Idaho)." Applied and Environmental Microbiology **66**(1): 154-162.

Davison, W., G. W. Grime, J. A. W. Morgan and K. Clarke (1991). "Distribution of dissolved iron in sediment pore waters at submillimetre resolution." Nature **352**: 323-324.

Davison, W., H. Zhang and G. W. Grime (1994). "Performance Characteristics of Gel Probes Used for Measuring the Chemistry of Pore Waters." Environmental Science and Technology **28**(9): 1623-1632.

Dixit, S. and J. G. Hering (2003). "Comparison of Arsenic(V) and Arsenic(III) Sorption onto Iron Oxide Minerals: Implications for Arsenic Mobility." Environmental Science and Technology **37**(18): 4182-4189.

Docekalova, H., O. Clarisse, S. Salomon and M. Wartel (2002). "Use of constrained DET probe for a high-resolution determination of metals and anions distribution in the sediment pore water." Talanta **57**: 145-155.

Dowdle, P. R., A. M. Laverman and R. S. Oremland (1996). "Bacterial Dissimilatory Reduction of Arsenic(V) to Arsenic(III) in Anoxic Sediments." Applied and Environmental Microbiology **62**(5): 1664-1669.

Dzombak, D. A. and F. M. M. Morel (1990). Surface Complexation Modeling: Hydrous Ferric Oxide. New York, John Wiley & Sons.

Edenborn, H. M., and L.A. Brickett (2002). "Determination of Manganese Stability in a Constructed Wetland Sediment Using Redox Gel Probes." Geomicrobiology Journal **19**: 485-504.

Edenborn, H. M. and L. A. Brickett (2002). "Determination of Trace Element Stability in Sediments Using Redox Gel Probes: Probe Construction and Theoretical Performance." Geomicrobiology Journal **19**: 465-483.

Eggleton, R. A. and R. W. Fitzpatrick (1988). "New Data and a revised structural model for ferrihydrite." Clays and Clay Minerals **36**(2): 111-124.

Eick, M. J., J. D. Peak and W. D. Brady (1999). "The Effect of Oxyanions on the Oxalate-Promoted Dissolution of Goethite." Soil Science Society of America Journal **62**: 1133-1141.

Ford, R. G. (2002). "Rates of Hydrous Ferric Oxide Crystallization and the Influence on Coprecipitated Arsenate." Environmental Science and Technology **36**(11): 2459-2463.

Ford, R. G., P. M. Bertsch and K. J. Farley (1997). "Changes in Transition and Heavy Metal Partitioning during Hydrous Iron Oxide Aging." Environmental Science and Technology **31**(7): 2028-2033.

Fredrickson, J. K., J. M. Zachara, D. W. Kennedy, H. Dong, T. C. Onstott, N. W. Hinman and S.-M. Li (1998). "Biogenic iron mineralization accompanying the dissimilatory reduction of hydrous ferric oxide by a groundwater bacterium." Geochimica et Cosmochimica Acta **62**(19/20): 3239-3257.

Fujii, M., A. L. Rose, T. D. Waite and T. Omura (2006). "Superoxide-mediated Dissolution of Amorphous Oxyhydroxide in Seawater." Environmental Science and Technology **40**(3): 880-887.

Fuller, C. C., J. A. Davis and G. A. Waychunas (1993). "Surface chemistry of ferrihydrite: Part 2. Kinetics of arsenate adsorption and coprecipitation." Geochimica et Cosmochimica Acta **57**: 2271-2282.

Goldberg, S. (2002). "Competitive Adsorption of Arsenate and Arsenite on Oxides and Clay Minerals." Soil Science Society of America Journal **66**: 413-421.

Goldberg, S. and C. T. Johnston (2001). "Mechanisms of Arsenic Adsorption on Amorphous Oxides Evaluated Using Macroscopic Measurements, Vibrational Spectroscopy, and Surface Complexation Modeling." Journal of Colloid and Interface Science **234**: 204-216.

Grafe, M., M. J. Eick and P. R. Grossl (2001). "Adsorption of Arsenate (V) and Arsenite (III) on Goethite in the Presence and Absence of Dissolved Organic Carbon." Soil Science Society of America Journal **65**: 1680-1687.

Grafe, M., M. J. Eick, P. R. Grossl and A. M. Saunders (2002). "Adsorption of Arsenate and Arsenite of Ferrihydrite in the Presence and Absence of Dissolved Organic Carbon." Journal of Environmental Quality **31**: 1115-1123.

Gu, C. and K. G. Karthikeyan (2005). "Interaction of Tetracycline with Aluminum and Iron Hydrous Oxides." Environmental Science and Technology **39**(8): 2660-2667.

Hansel, C. M., S. G. Benner and S. Fendorf (2005). "Competing Fe(II)-induced mineralization pathways of ferrihydrite." Environmental Science and Technology **39**(18): 7147-7153.

Hansel, C. M., S. G. Benner, J. Ness, A. Dohnalkova, R. K. Kukkadapu and S. Fendorf (2003). "Secondary mineralization pathways induced by dissimilatory iron reduction of ferrihydrite under advective flow." Geochimica et Cosmochimica Acta **67**(16): 2977-2992.

Hansel, C. M., S. G. Benner, P. Nica and S. Fendorf (2004). "Structural constraints of ferric (hydr)oxides on dissimilatory iron reduction and the fate of Fe(II)." Geochimica et Cosmochimica Acta **68**(15): 3217-3229.

Harrington, J. M., S. Fendorf and R. F. Rosenzweig (1998). "Biotic Generation of Arsenic(III) in Metal(loid)-contaminated freshwater lake sediments." Environmental Science and Technology **32**(16): 2425-2430.

Herbel, M.; Fendorf, S. Transformation and transport of arsenic within ferric hydroxide coated sands upon dissimilatory reducing bacterial activity. In *Advances in*

Arsenic Research; O'Day, P. A., Vlassopoulos, D., Meng, X., and Benning, L., Ed.; ACS Symposium Series 915; American Chemical Society: Washington, DC, 2005; pp 77-90.

Hering, J. and P. Kneebone (2001). Biogeochemical Controls on Arsenic Occurrence and Mobility in Water Supplies. Environmental Chemistry of Arsenic. J. William T. Frankenberger. New York, Marcel Dekker, Inc.**:** 155-181.

Hering, J. G. and W. Stumm (1990). Oxidative and Reductive Dissolution of Minerals. Reviews in Mineralogy: Mineral-Water Interface Chemistry. J. Michael F. Hochella and A. F. White. Washington, D.C., Mineralogical Society of America. **23:** 427-465.

Hiemstra, T., R. Rahnemaie and W. H. van Riemsdijk (2004). "Surface complexation of carbonate on goethite: IR spectroscopy, structure and charge distribution." Journal of Colloid and Interface Science **278**: 282-290.

Holm, T. R. (2002). "Effects of CO_3^{2-}/bicarbonate, Si, and PO_4^{3-} on Arsenic sorption to HFO." Journal of American Water Works Association **94**(4): 174-181.

Hongshao, Z. and R. Stanforth (2001). "Competitive Adsorption of Phosphate and Arsenate on Goethite." Environmental Science and Technology **35**: 4753-4757.

Hsia, T.-H., S.-L. Lo, C.-F. Lin and D.-Y. Lee (1994). "Characterization of arsenate adsorption on hydrous iron oxide using chemical and physical methods." Colloids and Surfaces A: Physiochemical and Engineering Aspects **85**: 1-7.

Islam, F. S., A. G. Gault, C. Boothman, D. A. Polya, J. M. Charnock, D. Chatterjee and J. R. Lloyd (2004). "Role of metal-reducing bacteria in arsenic release from Bengal delta sediments." Nature **430**: 68-71.

Jain, A. and R. H. Loeppert (2000). "Effect of Competing Anions on the Adsorption of Arsenate and Arsenite by Ferrihydrite." Journal of Environmental Quality **29**: 1422-1430.

Jain, A., K. P. Raven and R. H. Loeppert (1999). "Arsenite and Arsenate Adsorption on Ferrihydrite: Surface Charge Reduction and Net OH- Release Stoichiometry." Environmental Science and Technology **33**(8): 1179-1184.

Janney, D. E., J. M. Cowley and P. R. Buseck (2000). "Structure of synthetic 2-line ferrihydrite by electron nanodiffraction." American Mineralogist **85**: 1180-1187.

Jia, Y., L. Xu, Z. Fang and G. P. Demopoulos (2006). "Observation of Surface Precipitation of Arsenate on Ferrihydrite." Environmental Science and Technology **40**: 3248-3253.

Jones, C. A., H. W. Langner, K. Anderson, T. R. McDermott and W. P. Inskeep (2000). "Rates of Microbially Mediated Arsenate Reduction and Solubilization." Soil Science Society of America Journal **64**: 600-608.

Kaiser, K., G. Guggenberger, L. Haumaier and W. Zech (1997). "Dissolved organic matter sorption on subsoils and minerals studied by ^{13}C-NMR and DRIFT spectroscopy." European Journal of Soil Science **48**: 301-310.

Kim, M. J., J. Nriagu and S. Haack (2000). "Carbonate Ions and arsenic dissolution by groundwater." Environmental Science and Technology **34**(15): 3094-3100.

Kneebone, P.E. (2000). Arsenic geochemistry in a geothermally impacted system: The Los Angeles Aqueduct. Ph.D. Thesis, California Institute of Technology**,** Pasadena, CA.

Kneebone, P. E., P. A. O'Day, N. Jones and J. G. Hering (2002). "Deposition and Fate of Arsenic in Iron- and Arsenic-Enriched Reservoir Sediments." Environmental Science and Technology **36**(3): 381-386.

Ko, I., J.-Y. Kim and K.-W. Kim (2004). "Arsenic speciation and sorption kinetics in the As-hematite-humic acid system." Colloids and Surfaces A: Physiochemical and Engineering Aspects **234**: 43-50.

Kraemer, S. M., V. Q. Chiu and J. G. Hering (1998). "Influence of pH and competitive adsorption on the kinetics of ligand-promoted dissolution of aluminum oxide." Environmental Science and Technology **32**(19): 2876-2882.

Krafft, T. and J. M. Macy (1998). "Purification and characterization of the respiratory arsenate reductase of *Chrysiogenes arsenatis*." European Journal of Biochemistry **255**: 647-653.

Krom, M. D., P. Davison, H. Zhang and W. Davison (1994). "High Resolution pore water sampling with a gel sampler." Limnol. Oceanogr. **39**(8): 1967-1972.

Langmuir, D., J. Mahoney and J. Rowson (2006). "Solubility products of amorphous ferric arsenate and crystalline scorodite ($FeAsO_4 \cdot 2H_2O$) and their application to arsenic behavior in buried mine tailings." Geochimica et Cosmochimica Acta **70**: 2942-2956.

Langner, W. and W. P. Inskeep (2000). "Microbial Reduction of Arsenate in the Presence of Ferrihydrite." Environmental Science and Technology **34**(15): 3131-3136.

Larsen, O. and D. Postma (2001). "Kinetics of reductive bulk dissolution of lepidocrocite, ferrihydrite, and goethite." Geochimica et Cosmochimica Acta **65**: 1367-1379.

Latimer, W. M. (1952). The Oxidation States of the Elements and their Potentials in Aqueous Solutions. Englewood Cliffs, Prentice-Hall.

Laverman, A. M., J. S. Blum, J. K. Schaefer, E. J. P. Phillips, D. R. Lovley and R. S. Oremland (1995). "Growth of Strain SES-3 with Arsenate and other diverse electron acceptors." Applied and Environmental Microbiology **61**(10): 3556-3561.

Lin, H.-T., M. C. Wang and G.-C. Li (2004). "Complexation of arsenate with humic substance in water extract of compost." Chemosphere **56**: 1105-1112.

Liu, F., A. D. Cristofaro and A. Violante (2001). "Effect of pH, phosphate and oxalate on the adsorption/desorption of arsenate on/from goethite." Soil Science **166**(3): 197-208.

Lovley, D. R., E. J. P. Phillips and D. J. Lonergan (1991). "Enzymatic versus nonenzymatic mechanisms for Fe(III) reduction in aquatic sediments." Environmental Science and Technology **25**: 1062-1067.

Macur, R. E., C. R. Jackson, L. M. Botero, T. R. McDermott and W. P. Inskeep (2004). "Bacterial Populations Associated with the Oxidation and Reduction of Arsenic in an Unsaturated Soil." Environmental Science and Technology **38**(1): 104-111.

Makris, K. C., W. G. Harris, G. A. O'Connor and H. El-Shall (2005). "Long-term phosphorous effects on evolving physicochemical properties of iron and aluminum hydroxides." Journal of Colloid and Interface Science **287**: 552-560.

Malasarn, D., C. W. Saltikov, K. M. Campbell, J. Santini, J. G. Hering and D. K. Newman (2004). "arrA is a reliable marker for As(V) respiration." Science **306**(5695): 455.

Manceau, A. (1995). "The mechanism of anion adsorption in iron oxides: Evidence for the bonding of arsenate tetrahedra on free $Fe(O,OH)_6$ edges." Geochimica et Cosmochimica Acta **59**(17): 3647-3653.

Manning, B. A., S. Fendorf, B. C. Bostick and D. L. Suarez (2002). "Arsenic (III) oxidation and arsenic (V) adsorption reactions on synthetic birnessite." Environmental Science and Technology **36**(5): 976-981.

Manning, B. A., S. E. Fendorf and S. Goldberg (1998). "Surface Structures and Stability of Arsenic(III) on Goethite: Spectroscopic Evidence for Inner-Sphere Complexes." Environmental Science and Technology **32**(16): 2383-2388.

Manning, B. A. and S. Goldberg (1996). "Modeling Competitive Adsorption of Arsenate with Phosphate and Molybdate on Oxide Minerals." Soil Science Society of America Journal **60**: 121-131.

Manning, B. A. and S. Goldberg (1997). "Adsorption and Stability of Arsenic(III) at the Clay Mineral-Water interface." Environmental Science and Technology **31**: 2005-2011.

Martell, A. E. and R. M. Smith (2001). NIST Critically Selected Stability Constants of Metal Complexes, Texas A&M University.

McArthur, J. M., D. M. Banerjee, K. A. Hudson-Edwards, R. Mishra, R. Purohit, P. Ravenscroft, A. Cronin, R. J. Howarth, A. Chatterjee, T. Talukder, D. Lowry, S. Houghton and D. K. Chadha (2004). "Natural organic matter in sedimentary basins and its relation to arsenic in anoxic ground water: the example of West Bengal and its worldwide implications." Applied Geochemistry **19**: 1255-1293.

McGeehan, S. L. and D. V. Naylor (1994). "Sorption and Redox Transformation of Arsenite and Arsenate in Two Flooded Soils." Soil Science Society of America Journal **58**: 337-342.

Meng, X., S. Bang and G. P. Korfiatis (2000). "Effects of Silicate, Sulfate, and Carbonate on Arsenic Removal by Ferric Chloride." Water Research **34**(4): 1255-1261.

Neuberger, C. S. and G. R. Helz (2005). "Arsenic(III) carbonate complexation." Applied Geochemistry **20**: 1218-1225.

Newman, D. K. (2000). Arsenic. Encyclopedia of Microbiology, Academic Press. **1:** 332-338.

Newman, D. K., D. Ahmann and F. M. Morel (1998). "A Brief Review of Microbial Arsenate Respiration." Geomicrobiology Journal **15**: 255-268.

Newman, D. K., B. T.J. and F. M. Morel (1997). "Precipitation of arsenic trisulfide by *Desulfotomaculum auripigmentum*." Applied and Environmental Microbiology **63**(5): 2022-2028.

Ng, J. C., J. Wang and A. Shraim (2003). "A global health problem caused by arsenic from natural sources." Chemosphere **52**: 1353-1359.

Nickson, R., J. McArthur, W. Burgess, K. M. Ahmed, P. Ravenscroft and M. Rahman (1998). "Arsenic Poisoning of Bangladesh Groundwater." Nature **395**: 338.

Nickson, R. T., J. M. McArthur, P. Ravencroft, W. G. Burgess and K. M. Ahmed (2000). "Mechanism of arsenic release to groundwater, Bangladesh and West Bengal." Applied Geochemistry **15**: 403-413.

Nordstrom, D. K. (2002). "Worldwide Occurrences of Arsenic in Groundwater." Science **296**.

Nordstrom, D. K. and D. G. Archer (2003). Arsenic thermodynamic data and environmental geochemistry. Arsenic in Groundwater: Geochemistry and Occurrence. A. H. Welch and K. G. Stollenwerk. Norwell, Kluwer Academic Press**:** 1-25.

NRC (1999). Arsenic in Drinking Water. Washington, DC, National Academy Press.

NRC (2001). Arsenic in Drinking Water Update. Washington, DC, National Academy Press.

Ona-Nguema, G., C. Careret, O. Benali, M. Abdelmoula, J. M. Genin and F. Jorand (2004). "Competitive formation of hydroxycarbonate green rust 1 versus hydroxysulfate green rust 2 in *Shewanella putrefaciens* cultures." Geomicrobiology Journal **21**(2): 79-90.

Ona-Nguema, G., G. Morin, F. Juillot, G. Calas and G. B. Jr. (2005). "EXAFS Analysis of Arsenite Adsorption onto Two-Line Ferrihydrite, Hematite, Goethite, and Lepidocrocite." Environmental Science and Technology **39**: 9147-9155.

Oremland, R., S. Hoeft, J. Santini, N. Bano, R. Hollibaugh and J. Hollibaugh (2002). "Anaerobic Oxidation of Arsenite in Mono Lake Water and by a Facultative, Arsenite-Oxidizing Chemoautotroph, Strain MLHE-1." Applied and Environmental Microbiology **68**(10): 4795-4802.

Oremland, R. S., P. R. Dowdle, S. Hoeft, J. O. Sharp, J. K. Schaefer, L. G. Miller, J. S. Blum, R. L. Smith, N. S. Bloom and D. Wallschlaeger (2000). "Bacterial dissimilatory reduction of arsenate and sulfate in meromictic Mono Lake, California." Geochimica et Cosmochimica Acta **64**(18): 3073-3084.

Oremland, R. S. and J. F. Stolz (2003). "The Ecology of Arsenic." Science **300**: 393-944.

Pedersen, H. D., D. Postma and R. Jakobsen (2006). "Release of arsenic associated with the reduction and transformation of iron oxides." Geochimica et Cosmochimica Acta **70**: 4116-4129.

Pedersen, H. D., D. Postma, R. Jakobsen and O. Larsen (2005). "Fast transformation of iron oxyhydroxides by the catalytic action of aqueous Fe(II)." Geochimica et Cosmochimica Acta **69**(16): 3967-3977.

Peterson, M. L. and R. Carpenter (1986). "Arsenic distributions in porewaters and sediments of Puget Sound, Lake Washington, the Washington coast and Saanich Inlet, B.C." Geochimica et Cosmochimica Acta **50**: 353-369.

Pierce, M. L. and C. B. Moore (1980). "Adsorption of arsenite on amorphous iron hydroxide from dilute aqueous solution." Environmental Science and Technology **14**(2): 214-216.

Pierce, M. L. and C. B. Moore (1982). "Adsorption of arsenite and arsenate on amorphous iron hydroxide." Water Research **16**: 1247-1253.

Radu, T., J. L. Subacz, J. M. Phillippi and M. O. Barnett (2005). "Effects of Dissolved Carbonate on Arsenic Adsorption and Mobility." Environmental science and Technology **39**(20): 7875-7882.

Randall, S. R., D. M. Sherman and K. V. Ragnarsdottir (2001). "Sorption of As(V) on green rust (Fe4(II)Fe2(III)(OH)12SO4. 3H2O) and lepidocrocite ([gamma]-FeOOH): Surface complexes from EXAFS spectroscopy." Geochimica et Cosmochimica Acta **65**(7): 1015-1023.

Raven, K. P., A. Jain and R. H. Leoppert (1998). "Arsenite and Arsenate Adsorption on Ferrihydrite: Kinetics, Equilibrium, and Adsorption Envelopes." Environmental Science and Technology **32**(3): 344-349.

Redman, A. D., D. L. Macalady and D. Ahmann (2002). "Natural Organic Matter Affects Arsenic Speciation and Sorption onto Hematite." Environmental Science and Technology **36**: 2889-2896.

Reeburgh, W. S. and R. E. Ericson (1982). "A "dipstick" measurement for rapid, continuous chemical profiles in sediments." Limnol. Oceanogr. **27**(3): 556-559.

Ritter, K., G. R. Aiken, J. F. Ranville, M. Bauer and D. L. Macalady (2006). "Evidence for the Aquatic Binding of Arsenate by Natural Organic Matter-Suspended Fe(III)." Environmental Science and Technology **40**: 5380-5387.

Rochette, E. A., B. C. Bostick, G. Li and S. Fendorf (2000). "Kinetics of Arsenate Reduction by dissolved sulfide." Environmental Science and Technology **34**(22): 4714-4720.

Roden, E. E. (2003). "Fe(III) Oxide Reactivity Toward Biological versus Chemical Reduction." Environmental Science and Technology **37**: 1319-1324.

Roden, E. E. (2004). "Analysis of long-term bacterial vs. chemical Fe(III) oxide reduction kinetics." Geochimica et Cosmochimica Acta **68**(15): 3205-3216.

Roden, E. E. and J. M. Zachara (1996). "Microbial Reduction of Crystalline Iron (III) Oxides: Influence of Oxide Surface Area and Potential for Cell Growth." Environmental Science and Technology **30**(5): 1618-1628.

Root, R., S. Dixit, K. M. Campbell, A. Jew, J. G. Hering and P. A. O'Day (2006). "Arsenic sequestration by sorption processes in high-iron sediments." *In preparation.*

Rosen, B. P. (1996). "Bacterial Resistance to heavy metals and metalloids." JBIC **1**: 273-277.

Royer, R. A., W. D. Burgos, A. S. Fisher, B.-H. Jeon and B. A. Dempsey (2002). "Enhancement of Hematite Bioreduction by Natural Organic Matter." Environmental Science and Technology **36**(13): 2897-2904.

Royer, R. A., B. A. Dempsey, B.-H. Jeon and W. Burgos (2004). "Inhibition of Biological Reductive Dissolution of Hematite by Ferrous Iron." Environmental Science and Technology **38**(1): 187-193.

Ruby, C., C. Upadhyay, A. Gehin, G. Ona-Nguema and J.-M. R. Genin (2006). "In Situ redox flexibility of Fe(II)-(III) oxyhydroxycarbonate green rust and fougerite." Environmental Science and Technology **40**(15): 4696-4702.

Saltikov, C. W., A. Cifuentes, K. Vankateswaran and D. K. Newman (2003). "The *ars* Detoxification System is Advantageous but not Required for As(V) Respiration by the Genetically Tractable *Shewanella* Species Strain ANA-3." Applied and Environmental Microbiology **69**(5): 2800-2809.

Saltikov, C. W. and D. K. Newman (2003). "Genetic identification of a respiratory arsenate reductase." PNAS.

Saltikov, C. W., R. Wildman and D. K. Newman (2005). "Expression Dynamics of Arsenic Respiration and Detoxification in *Shewanella* sp. Strain ANA-3." Journal of Bacteriology **187**(21): 7390-7395.

Schecher, W. D. and D. C. McAvoy (1998). MINEQL+. Hallowell, Environmental Research Software.

Schwertmann, U. (1991). "Solubility and dissolution of iron oxides." Plant and Soil **130**: 1-25.

Schwertmann, U. and R. M. Cornell (1991). Iron Oxides in the Laboratory. Weinheim, Wiley-VCH.

Scott, M. J. and J. J. Morgan (1995). "Reactions at Oxide Surfaces. 1. Oxidation of As(III) by Synthetic Birnessite." Environmental Science and Technology **29**(8): 1898-1905.

Sherman, D. M. and S. R. Randall (2003). "Surface Complexation of arsenic(V) to iron(III) (hydr)oxides: Structural mechanism from ab initio molecular geometries

and EXAFS spectroscopy." Geochimica et Cosmochimica Acta **67**(22): 4223-4230.

Smedley, P. L. and D. G. Kinniburgh (2002). "A review of the source, behavior and distribution of arsenic in natural waters." Applied Geochemistry **17**: 517-568.

Song, Y. and G. Muller (1999). Sediment-Water Interactions in Anoxic Freshwater Sediments: Mobility of Heavy Metals and Nutrients. Berlin, Springer-Verlag.

Standard Methods for the Examination of Water and Wastewater (1995). Washington, D.C., American Public Health Association.

Stolarik, G. and J. D. Christie (1999). Interim Arsenic Management Plan for Los Angeles. Proceedings of the 1999 American Water Works Association Annual Conference, Chicago, Illinois.

Stookey, L. L. (1970). "Ferrozine-A new spectophotometric reagent for iron." Analytical Chemistry **42**(7): 779-781.

Stumm, W. and J. J. Morgan (1996). Aquatic Chemistry. New York, John Wiley & Sons, Inc.

Su, C. and D. L. Suarez (1997). "*In situ* infrared speciation of adsorbed carbonate on aluminum and iron oxides." Clays and Clay Minerals **45**(6): 814-825.

Su, C. and R. W. Puls (2004). "Significance of iron(II,III) hydroxycarbonate green rust in arsenic remediation using zerovalent iron in laboratory column tests." Environmental Science and Technology **38**(19): 5224-5231.

Su, C. and R. T. Wilkin (2005). Arsenate and Arsenite Sorption on and Arsenite Oxidation by Iron(II,III) Hydroxycarbonate Green Rust. Advances in Arsenic Research: Integration of Experimental and Observational Studies and Implications for Mitigation. P. A. O'Day, D. Vlassopoulos, X. Meng and L. G. Benning. Washington, DC, American Chemical Society. **915:** 25-40.

Sun, X. and H. E. Doner (1996). "An Investigation of Arsenate and Arsenite Bonding Structures on Goethite by FTIR." Soil Science **161**(12): 865-872.

Suter, D., S. Banwart and W. Stumm (1991). "Dissolution of Hydrous Iron(III) Oxides by Reductive Mechanisms." Langmuir **7**: 809-813.

Swartz, C. H., N. K. Blute, B. Badruzzman, A. Ali, D. Brabander, J. Jay, J. Besancon, S. Islam, H. F. Hemond and C. F. Harvey (2004). "Mobility of arsenic in a Bangladesh aquifer: Inferences from geochemical profiles, leaching data, and mineralogical characterization." Geochimica et Cosmochimica Acta **68**(22): 4539-4557.

Swedlund, P. J. and J. G. Webster (1999). "Adsorption and polymerization of silicic acid on ferrihydrite and its effect on arsenic adsorption." Water Research **33**(16): 3413-3422.

Tamaki, S. and J. W.T. Frankenberger (1992). "Environmental Biogeochemistry of Arsenic." Reviews of Environmental Contamination and Toxicology **124**: 79-110.

Tanaka, T. (1981). "Gels." Scientific American **244**(1): 124-138.

Tadanier, C. J., M. E. Schreiber and J. W. Roller (2005). "Arsenic Mobilization through Microbially Mediated Deflocculation of Ferrihydrite." Environmental Science and Technology **39**: 3061-3068.

Teal, T. K., D. P. Lies, B. J. Wold and D. K. Newman (2006). "Spatiometabolic Stratification of *Shewanella oneidensis* Biofilms." Applied and Environmental Microbiology **72**(11): 7324-7330.

Thamdrup, B. (2000). "Bacterial Manganese and Iron Reduction in Aquatic Systems." Advances in Microbial Ecology **16**: 41-84.

Thanabalasingam, P. and W. F. Pickering (1986). "Arsenic Sorption by Humic Acids." Environmental Pollution (Series B) **12**: 233-246.

Tucker, M. D., L. L. Barton and B. M. Thomson (1998). "Reduction of Cr, Mo, Se, and U by *Desulfovibrio desulfuricans* immobilized in polyacrylamide gels." Journal of Industrial Microbiology and Biotechnology **20**: 13-19.

Urrutia, M. M. and E. E. Roden (1998). "Microbial and Surface Chemistry Controls on Reduction of Synthetic Fe(III) Oxide Minerals by the Dissimilatory Iron-Reducing Bacterium *Shewanella alga*." Geomicrobiolgy **15**: 269-291.

Urrutia, M. M., E. E. Roden and J. M. Zachara (1999). "Influence of Aqueous and Solid-Phase Fe(II) Complexants on Microbial Reduction of Crystalline Iron(III) Oxides." Environmental Science and Technology **33**: 4022-4028.

van Geen, A., A. P. Robertson and J. O. Leckie (1994). "Complexation of carbonate species at the goethite surface: Implications for adsorption of metal ions in natural waters." Geochimica et Cosmochimica Acta **58**(9): 2073-2086.

van Geen, A., J. Rose, S. Thoral, J. M. Garnier, Y. Zheng and J. Y. Bottero (2004). "Decoupling of As and Fe Release to Bangladesh groundwater under reducing conditions. Part II: Evidence from sediment incubations." Geochimica et Cosmochimica Acta **68**(17): 3475-3486.

Villalobos, M. and J. O. Leckie (2000). "Carbonate adsorption on goethite under closed and open CO_2 conditions." Geochimica et Cosmochimica Acta **64**(22): 3787-3802.

Villalobos, M. and J. O. Leckie (2001). "Surface Complexation Modeling and FTIR study of carbonate adsorption to goethite." Journal of Colloid and Interface Science **235**: 15-32.

Violante, A. and M. Pigna (2002). "Competitive sorption of arsenate and phosphate on different clay minerals and soils." Soil Science Society of America Journal **66**: 1788-1796.

Warwick, P., E. Inam and N. Evans (2005). "Arsenic's Interaction with Humic Acid." Environmental Chemistry **2**: 119-124.

Waychunas, G. A., J. A. Davis and C. C. Fuller (1995). "Geometry of sorbed arsenate on ferrihydrite and crystalline FeOOH: Re-evaluation of EXAFS results and topological factors in predicting sorbate geometry, and evidence for monodentate complexes." Geochimica et Cosmochimica Acta **59**(17): 3655-3661.

Waychunas, G. A., B. A. Rea, C. C. Fuller and J. A. Davis (1993). "Surface Chemistry of ferrihydrite: Part 1. EXAFS studies of the geometry of coprecipitated and adsorbed arsenate." Geochimica et Cosmochimica Acta **57**: 2251-2269.

Welch, A. H. and M. S. Lico (1998). "Factors controlling As and U in shallow groundwater, southern Carson Desert, Nevada." Applied Geochemistry **13**(4): 521-539.

Welch, A. H., D. B. Westjohn, D. R. Helsel and R. B. Wanty (2000). "Arsenic in Ground Water of the United States: Occurrence and Geochemistry." Groundwater **38**(4): 589-604.

Wilkie, J. and J. G. Hering (1996). "Adsorption of arsenic onto hydrous ferric oxide: effects of adsorbate/adsorbent ratios and co-occurring solutes." Colloids and Surfaces A: Physiochemical and Engineering Aspects **107**: 97-110.

Wilkie, J. and J. G. Hering (1998). "Rapid Oxidation of Geothermal Arsenic(III) in streamwaters of the eastern Sierra Nevada." Environmental Science and Technology **32**(5): 657-662.

Willets, D. B., R. C. Fox, S. L. Werner, M. Mukae, A. Schiffman, R. L. Blodnikar and J. F. LoBue (1967). Investigation of geothermal waters in the Long Valley area, Mono County. S. o. C. D. o. W. Resources**:** 141.

Williams, A. G. B. and M. M. Scherer (2004). "Spectroscopic evidence for Fe(II)-Fe(III) electron transfer at the Fe oxide-water interface." Environmental Science and Technology **38**: 4782-4790.

Xu, H., B. Allard and A. Grimvall (1991). "Effects of acidification and natural organic materials on the mobility of arsenic in the environment." Water, Air, and Soil Pollution **57-58**: 269-278.

Zachara, J. M., R. K. Kukkadupu, J. K. Fredrickson, Y. A. Gorby and S. C. Smith (2002). "Biomineralization of Poorly Crystalline Fe(III) Oxides by Dissimilatory Metal Reducing Bacteria (DMRB)." Geomicrobiology Journal **19**: 179-207.

Zhang, H. and W. Davison (1995). "Performance Characteristics of Diffusion Gradients in Thin Films for the in Situ Measurement of Trace Metals in Aqueous Solution." Analytical Chemistry **67**(19): 3391-3400.

Zhang, H., W. Davison, b. Knight and S. McGrath (1998). "*In Situ* Measurements of Solution Concentrations and Fluxes of Trace Metals in soils using DGT." Environmental Science and Technology **32**(5): 704-710.

Zhang, H., W. Davison, S. Miller and W. Tych (1995). "In situ high resolution measurements of fluxes of Ni, Cu, Fe, and Mn and concentration of Zn and Cd in porewaters by DGT." Geochimica et Cosmochimica Acta **59**(20): 4181-4192.

Zinder, B., G. Furrer and W. Stumm (1986). "The coordination chemistry of weathering: II. Dissolution of Fe(III) oxides." Geochimica et Cosmochimica Acta **50**: 1861-1869.

Zobrist, J., P. R. Dowdle, J. A. Davis and R. S. Oremland (2000). "Mobilization of Arsenite by dissimilatory reduction of adsorbed arsenate." Environmental Science and Technology **34**(22): 4747-4753.